

Computationally Modeled Cellular Response to the Extracellular Mechanical
Environment

Dissertation

Presented in Partial Fulfillment of the Requirements for the Degree Doctor of Philosophy
in the Graduate School of The Ohio State University

By

Benjamin William Scandling, M.S.

Graduate Program in Biomedical Engineering

The Ohio State University

2021

Dissertation Committee

Dr. Keith Gooch, Advisor

Dr. Thomas Hund

Dr. Aaron Trask

Dr. Seth Weinberg

Copyrighted by
Benjamin William Scandling
2021

Abstract

The human body is a complex mechanical environment that exposes cells to variations in both passive and active forces, where forces vary depending on tissue type, location, and function. Recent work has been done to analyze how the mechanical environment changes in different disease states and the effects of these changes on organ and cellular function. As a result, there are several well-known changes in in vitro cellular behavior in response to perturbations in the mechanical environment including: cell shape, size, phenotype, and differentiation. While other groups have begun to distinguish key components related to cell sensing of the mechanical environment, the exact mechanism remains poorly understood.

The motor-clutch biophysical model describes cytoskeletal dynamics as a balance between substrate adhesion, myosin contractility, and actin polymerization. Initially, the model was hypothesized as a mechanism to explain cellular traction force generation and resultant actin flow. An initial computational formulation of the motor-clutch system demonstrated that it accurately predicts changes in neuronal cell behavior as a function of changes in extracellular substrate stiffness.

Here we adapt the computational motor-clutch model to include external substrate motion as a means of simulating cyclic substrate deformation. We then use this adapted model to study the combined effect of cyclic substrate deformation and substrate stiffness

on actin cytoskeleton organization and dynamics. The goal of this work was to demonstrate that the motor-clutch model can be used to predict and explain distinct cellular responses to applied cyclic strain. Furthermore, the adapted model allows for the study of experimental parameter spaces that are otherwise difficult to re-create experimentally. We found that the model predicts that applied cyclic stretch significantly impacts actin traction force generation and adhesion dynamics. Importantly, adhesion dynamics are finely controlled by substrate motion and control a cell's ability to generate traction along its substrate. We also found that the model precisely re-creates the distinct cellular reorientation response to cyclic stretch. Therefore, we propose the motor-clutch model as a mechanism for changes in cell morphology in response to the mechanical environment. The development of the adapted motor-clutch model not only reveals potentially novel cellular responses to changes in substrate compliance and deformation but can also be used to more closely study specific disease states that significantly alter the extracellular mechanical environment.

Dedication

To my parents. For their unconditional love, their push for me to be the best I can be, and their constant support. I would not be who I am, or where I am, without you.

Acknowledgments

First, I am incredibly grateful for my advisor, Dr. Keith Gooch. Your mentorship has made me a better scientist, communicator, thinker, and most importantly, person. I am incredibly fortunate to have you as a role-model in my life.

I would like to thank each of the mentors and collaborators that I have worked with during my time at Ohio State. Dr. Orlando Simonetti and Dr. David Gross for introducing me to scientific research and the commitment required to achieve excellence in your work. Dr. Aaron Trask and Dr. Patricia McCallinhart for not only including me in their work and assisting me with mine, but for providing opportunities to de-stress. Dr. Thomas Hund for his guidance through candidacy and proposal submissions. Dr. Seth Weinberg for his thoughtful collaboration and assistance in developing MATLAB code and our computational models. Dr. Chuan Xue and Dr. Jia Gou for their assistance with the mathematical formulations of our models. I am also thankful for classmates and members of Dr. Gooch's lab that assisted with all aspects of my research: Dr. Rachel Childers, Dr. Jessica Thomas, Dr. Nehal Patel, Jackie Xuan, Ben DiFranco, Zachary Osborn, and Ketan Fernandes.

Lastly, I would like to thank friends and family from outside of my work that have contributed to where I am today. My brother, Jonathan, for showing me what it takes to truly be great. Your examples of work ethic and passion constantly push me to be better.

Finally, I would like to thank Sarah, for your love and support. I would not have been able to accomplish this goal without you standing there with me. I cannot wait for the next part of our adventure.

Vita

May 2012.....Olentangy Liberty High School
May 2016.....B.S. Biomedical Engineering, The Ohio State University
December 2018.....M.S. Biomedical Engineering, The Ohio State University
August 2016 – August 2019.....Graduate Research Associate,
Department of Biomedical Engineering,
The Ohio State University
August 2019 – Present.....Graduate Teaching Assistant,
Department of Biomedical Engineering,
The Ohio State University

Publications

1. Gooch KJ, Firstenberg MS, Shrefler BS, & **Scandling BW** (2018). Biomechanics and mechanobiology of saphenous vein grafts. *J Biomech Eng*, 140(2).
2. Patel NJ, Nassal DM, Greer-Short AD, Unudurthi SD, **Scandling BW**, Gratz D, Xu X, Kalyanasundaram A, Fedorov VV, Accornero F, Mohler PJ, Gooch KJ, Hund TJ. (2019). β IV-Spectrin/STAT3 complex regulates fibroblast phenotype, fibrosis, and cardiac function. *JCI Insight*, 4(20).
3. McCallinhart P, **Scandling BW**, & Trask AJ (2020). Coronary Remodeling and Biomechanics: Are We Going with the Flow in 2020?. *Am J Physiol Heart Circ Physiol*.

Fields of Study

Major Field: Biomedical Engineering

Table of Contents

Abstract	ii
Dedication	iv
Acknowledgments.....	v
Vita.....	vii
List of Tables	xii
List of Figures	xiii
Chapter 1 Introduction	1
1.1 Components of the Active and Passive Mechanical Environment	1
1.2 Impacts of the Mechanical Environment on Cellular Form and Function.....	3
1.3 Proposed Mechanisms for how Cells Respond to their Mechanical Environment...	7
1.4 The Motor Clutch Model as a Mechanism for Cellular Tension Generation and Overall Substrate Sensing	9
1.5 Summary of Dissertation Focus.....	11
1.6 Summary of Contributions.....	12
Chapter 2 Methods	13
2.1 Biomechanical description of the motor-Clutch model	13
2.2 Stochastic mathematical formulation of the motor-clutch model.....	14
2.3 Modifications to the motor-clutch model	17
2.4 Further modifications to the motor-clutch model to study action reorientation	20
Chapter 3 The Motor-Clutch Model as a Mechanism for Cellular Traction Force Generation as a Function of the Mechanical Environment.....	23
3.1 Introduction.....	23
3.2 Methods.....	25
3.3 Results.....	25
3.3.1 Cyclic stretch differentially alters traction force generation.....	25

3.3.2 Combined effects of amplitude and frequency on traction force generation... 27	27
3.3.3 Clutch engagement dynamics are a function of substrate stiffness and cyclic stretch..... 30	30
3.3.4 Differences between actin flow and substrate motion describe clutch engagement dynamics..... 34	34
3.3.5 Inclusion of catch-bond behavior accounts for experimentally observed cell spreading as a function of substrate stiffness and cyclic stretch..... 39	39
3.4 Discussion..... 41	41
3.5 Conclusion 43	43
Chapter 4 The Motor Clutch Model as a Mechanism for the Cellular Morphological Response to Cyclic Force..... 44	44
4.1 Introduction..... 44	44
4.1.1 Cell alignment in response to cyclic stretch 44	44
4.1.2 Biophysical processes that could potentially lead to cytoskeletal alignment .. 45	45
4.1.3 Existing mathematical models of fiber and cell alignment..... 47	47
4.2 Methods..... 48	48
4.2.1 Cyclic stretch of in vitro cell cultures 48	48
4.2.2 Motor-clutch model of cell substrate interactions 50	50
4.3 Results and Discussion 51	51
4.3.1 In vitro cell and actin fiber orientation as a function of the amplitude of simple cyclic elongation 51	51
4.3.2 Experimental data informs biophysical processes that could potentially lead to actin reorientation. 53	53
4.3.3 Type of cyclic stretch and actin reorientation..... 53	53
4.3.4 Amplitude of stretch and actin reorientation. 58	58
4.3.5 Frequency of stretch and actin reorientation..... 60	60
4.3.6 Substrate stiffness and actin reorientation. 62	62
4.3.7 Myosin motor function is required for actin bundle reorientation response.... 65	65
4.3.8 Mechanism by which cyclic stretch causes changes in actin bundle orientation. 66	66
4.3.9 Model capabilities, limitations, and opportunities for improvements. 72	72
4.4 Conclusions..... 73	73
Chapter 5 Discussion and Future Directions 75	75
5.1 Volume overload heart failure mechanics and impacts on cell function 75	75

5.2 Utilizing the adapted motor-clutch model to further study CF function in the VO HF environment.	79
5.2.1 Why the adapted motor-clutch model is useful to study the VO HF environment.	79
5.2.3 How does cyclic stretch impact CF behavior, and can the adapted motor-clutch model provide insight into the initial insult that fuels the cascade into VO HF?	81
5.2.4 Why does cyclic stretch not revert fibroblasts back quiescent phenotype following initial structural changes?	83
5.2.5 What are the effects of changes in heart rate and contractility waveform on CF function?	84
5.3 Future Directions	87
Chapter 6 Summary and Concluding Remarks.....	90
Bibliography	92
Appendix A: Adapted motor-clutch model MATLAB function	103

List of Tables

Table 2-1: Motor-clutch model parameters. 16
Table 2-2: Motor-clutch catch bond model parameters. 20
Table 4-1: Comparison of simulation predictions and in vitro experimental observations.
..... 56

List of Figures

Figure 1-1: Human Tissue Stiffness	2
Figure 1-2: Cell and actin organization as a function of substrate stiffness.	4
Figure 1-3: Motor-clutch model dynamics as a function of substrate stiffness.	10
Figure 2-1: The motor-clutch model and cyclic stretch.	14
Figure 3-1: Actin traction force generation as a function of cyclic stretch and substrate stiffness.	27
Figure 3-2: Traction force generation as a function of cyclic stretch amplitude and frequency.	29
Figure 3-3: Clutch dynamics as a function of substrate stiffness.	31
Figure 3-4: Clutch binding dynamics as a function of cyclic stretch.	33
Figure 3-5: Substrate motion, actin motion, and total number of engaged clutches over time.	36
Figure 3-6: Comparison of substrate motion and actin motion for special case of high k_{sub} and low cyclic stretch amplitude.	38
Figure 3-7: Actin spreading speed as a function of substrate stiffness and cyclic stretch amplitude.	40
Figure 4-1: Cellular morphological response to applied mechanical stretch.	46
Figure 4-2: Experimental application of mechanical cyclic stretch to culture cells.	50
Figure 4-3: In vitro cellular morphology changes as a function of applied cyclic stretch.	52
Figure 4-4: Simulated and in vitro maximum reported actin fiber and/or cell orientation.	54
Figure 4-5: Simulated actin bundle reorientation.	57
Figure 4-6: Actin bundle reorientation as a function of cyclic stretch amplitude.	59
Figure 4-7: Actin bundle reorientation as a function of cyclic stretch frequency.	61
Figure 4-8: Actin bundle reorientation as a function of both substrate stiffness and cyclic stretch type.	64
Figure 4-9: Simulated actin bundle reorientation as a function of motor-clutch model myosin motor function.	66
Figure 4-10: Clutch bond failure timing.	68
Figure 4-11: Proposed mechanism for changes in actin bundle orientation.	70
Figure 5-1: Myocardial stiffness in various HF disease states.	76
Figure 5-2: Fibroblast classification.	77
Figure 5-3: Hypofibrotic CF phenotype associated with VO HF.	78
Figure 5-4: Force generation and kinetics in normal and failing hearts.	87
Figure 5-5: CF morphology as a function of substrate stiffness.	89

Chapter 1 Introduction

1.1 Components of the Active and Passive Mechanical Environment

The human body is a complex mechanical environment that exposes cells to variations in both passive and active forces, where forces vary depending on tissue type, location, and function. Tissue material properties vary both in terms of elastic nature (such as linear elastic vs. non-linear viscoelastic) and in stiffness, or modulus, magnitude ranging from as low as less than 1 kPa in brain tissue to as high as 10 GPa in bone (Figure 1-1) [1], [2]. Similarly, several tissue types are exposed to mechanical loading, either derived within the tissue itself or applied from external sources. For instance, cells within the heart are exposed to cyclic contractile and compressive forces as the myocardium contracts and relaxes with each heartbeat. Similarly, blood vessels experience cyclic force through the pulsatile nature of blood flow, but also expose cells within vessels to shear derived from blood flow. Bone and cartilage is also differentially loaded as a function of applied force and exposes cells to forces that vary in both magnitude and in time.

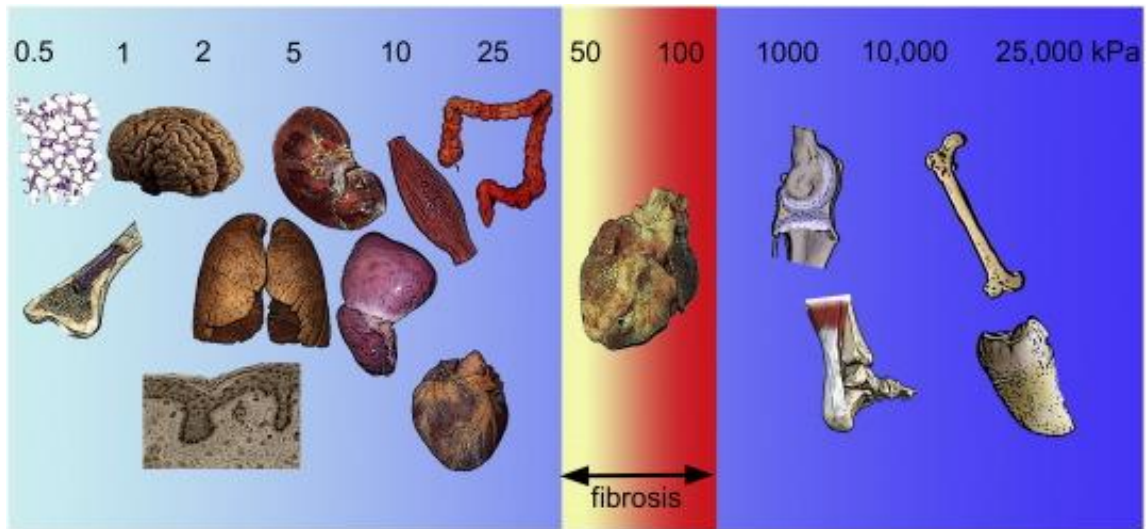


Figure 1-1: Human Tissue Stiffness

Typical stiffness values of several human tissues, and how fibrosis can alter stiffness. Reproduced with permission from Hinz 2013 [2].

Recent work has been done to analyze how the mechanical environment changes in different disease states and the effects of these changes on organ and cellular function. A common emphasis is the effect of fibrosis on tissue stiffening as it occurs in several diseases and processes. Often, fibrosis begins as a wound-healing or structural maintenance process, where deposition of additional matrix proteins stiffens the tissue to maintain proper organ function (Figure 1-1) [3], [4]. However, continual increases in stiffness result in changes in cell structure and function associated with diseases such as tumor development, liver and pulmonary fibrosis, heart failure, and arterial stiffening [5]–[10]. Similarly, alterations in mechanical loading of tissues can contribute to progression of disease states. For instance, over-loading bone and cartilage can result in changes to overall structure and organization of the tissue itself [11]–[14]. Often disease progression involves changes to both the active and passive mechanical environment that have profound impacts

on cell function. For instance, others have indicated that initial aortic injury may result in increased inflammation and stenosis in the valve [15]–[17]. In response to changes in force and inflammation, valve interstitial cells (VICs) lay down extracellular matrix at a high rate [18], [19] signaling a fibrosis cascade which stiffens the valve and further alters blood hemodynamics. Example such as valve stenosis has made it increasingly more clear that tissue function is finely tuned by changes in cell function in response to alterations in the mechanical environment.

1.2 Impacts of the Mechanical Environment on Cellular Form and Function

The effects of the mechanical environment on cellular morphology have been studied extensively for many years. Perhaps the most widely recognized cellular response to the passive mechanical environment is cell shape as a function of extracellular substrate stiffness. Using a novel technique for varying polyacrylamide (PA) hydrogel stiffness and cellular adhesion, Pelham and Wang demonstrated changes in cell shape with varying substrate stiffness, where both normal rat kidney cells and 3T3 fibroblasts increased their observed cell area with increases in gel stiffness [20]. Many other cell types including fibroblasts, endothelial cells, macrophages, stellate cells, and myocytes have since been shown to exhibit similar behaviors, where cell spread area increases with increasing substrate stiffness (Figure 1-2) [21]. Guo et al. recently found that cell volume decreases with increasing substrate stiffness [22], providing quantified verification of the observation that cells spread and flatten on stiff substrates such as cell culture plastic and exist in rounded ball-like shapes on softer, more compliant substrates.

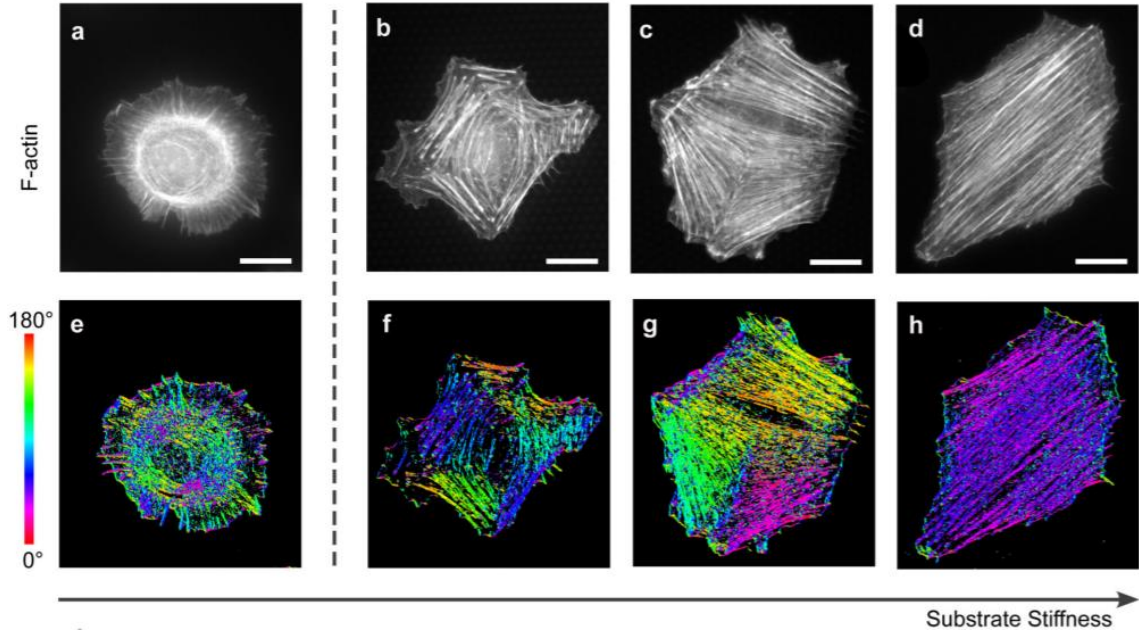


Figure 1-2: Cell and actin organization as a function of substrate stiffness. Cells spread and generate well-defined and organized actin stress fibers with increasing substrate stiffness. Reproduced with permission from Gupta et al. 2015 [23].

Similar to the study of substrate stiffness as a regulator of cell morphology, the effects of cyclic stretch on cell cultures have been thoroughly investigated. The initial use of cell binding proteins such as collagen and fibronectin in substrate stiffness studies extended to elastic silicone substrates such as polydimethylsiloxane (PDMS) to allow for culture of cells on silicone deformable substrates. In an early cyclic stretch study, Ives et al. demonstrated for perhaps the first time that cultured cells alter their orientation in response to cyclic substrate deformation, where human umbilical vein endothelial cells (HUVECs) aligned perpendicular to the direction of stretch [24]. Soon thereafter, Dartsch and Betz demonstrated this same phenomenon in aortic endothelial cells [25]. Both groups also noted that intracellular actin filaments noticeably reorient perpendicular to the

direction of stretch. Since the conclusion of these studies, many groups have demonstrated this same perpendicular reorientation response with various cell types and stretch apparatuses [26]–[33], suggesting the response is mostly cell type independent. An interesting development out of more recent work has more specifically noted that cells typically align along an axis of minimal strain, which develops as a result of the unique combination of stretch parameters and substrate material properties, in an attempt to minimize the amount of strain within the cell. For instance, Wang et al. reports that endothelial cells align in distinct patterns depending on whether they are exposed to purely uniaxial stretch (i.e., no substrate compression along the axis perpendicular to the stretching axis) or a simple elongation stretch (i.e., the substrate is free to compress along the perpendicular axis during stretching) [34]. In the purely uniaxial stretch case, the axis of minimal strain is perfectly perpendicular to the direction of applied stretch, and cells align along this axis. In the simple elongation case, the axis of minimal strain exists along some oblique angle, and cells align around an angle of 60-70 degrees with respect to the direction of stretch.

Beyond altering shape and orientation, the mechanics of the extracellular substrate have a profound impact on overall cell function. On a micro-cellular scale, organization and function of the cytoskeleton is heavily dependent on both substrate stiffness and stretch. In their stiffness work, Pelham and Wang reported changes in cell motility and distributions of focal adhesion sites as a function of stiffness [20], suggesting that there are cytoskeletal changes associated with changes in substrate stiffness. Since then, numerous groups have reported increases in actin stress fiber development and organization with

increasing stiffness [23], [35]–[38]. Extension of this analysis to include cyclic stretch shows a similar effect, where stretching cultured cells results in highly developed and organized stress fibers [39]–[41]. On the macro-cellular scale, there exists a wealth of knowledge on the impacts of stiffness and stretch on several cell functions such as proliferation, migration, differentiation, ECM production and maintenance, and survival [26], [42]–[47].

There are some interesting contradictions to well-known cell responses to the mechanical environment that have recently fueled closer analysis. For instance, while Pelham and Wang report optimal cell motility occurs with decreased substrate stiffness [20], others have observed decreases in cell migration with further decreases in substrate stiffness [48], [49]. Similarly, neuronal cells are known to spread and extend processes most effectively on soft substrates [50], [51], while other cell types both derived from the central nervous system (such as glial cells, astrocytes, and fibroblasts) and other tissues increase their spread area on stiff substrates [21], [52], [53]. Recently, in an attempt to investigate the additive effects of substrate stiffness and cyclic stretch, Quinlan et al. show that applying cyclic stretch to cells on soft substrates increases their spread area but stretching cells on already stiff substrates actually decreases their spread area [54]. While these observations appear contradictory, the differences in cell response to different extracellular mechanics are likely a result of the existence of an optimal mechanical environment for proper cell function. This idea will be discussed in detail in subsequent chapters, as it is becoming more and more apparent that distinct combinations of mechanical parameters have a profound impact on cell form and function.

1.3 Proposed Mechanisms for how Cells Respond to their Mechanical Environment

Cells sense their mechanical environment by adhering and pulling on their substrate. Tension is generated within the cytoskeletal framework and is transmitted to the extracellular substrates through transmembrane binding protein clusters (integrin groups known as focal adhesions). A popular model of cytoskeletal tension, known as the cellular tensegrity model, is often invoked as a description of how cells maintain cytoskeletal structure and integrity as a function of their mechanical environment. Cellular tensegrity was originally proposed by Ingber in his original commentary on the topic, where he argues that cells exist as prestressed tensegrity structures [55]. Specifically, he describes the cytoskeleton as a network of interconnected components under tension that resist compression. Perhaps most important for the context of cell-substrate sensing, he also suggests cellular tensegrity is integral in a cell's ability to alter its motility in response to perturbations in the mechanical environment. In short, the tensegrity model describes a constant adhesion tension cycle, where actin polymerizes in cell extensions, adheres to the substrate, and generates additional tension all as means for maintaining proper stress within the cytoskeletal framework. Recent experimental evidence supports the idea that tension generation within a cell is critical to cellular morphological changes in response to the mechanical environment. For instance, cellular prestress is critically important for maintenance of cell shape and stability [56], [57] and that cell stiffness is a function of initial prestress [58].

Others have proposed mechanisms for how cells feel and respond to their mechanical environment, each typically associated with the cytoskeletal framework and

cell adhesion. Like the idea of cellular tensegrity structure and prestress, the maintenance of tension generation has been indicated as a key component of cell force sensing. Several groups have demonstrated the importance of actomyosin contraction in proper cell response to the mechanical environment by studying the impacts of non-muscle myosin. In an important study, Engler et al. demonstrated that stem cell differentiation fate is controlled by substrate stiffness but inhibition of non-muscle myosin II (nmII) blocks all substrate directed differentiation [59]. Similarly, several other groups have demonstrated that proper nmII function is essential in several substrate sensing processes such as: cell spreading, formation of actin stress fibers, migration and motility, and re-orientation in response to cyclic stretch [39], [60]–[62].

Beyond the importance of cell tension maintenance in substrate sensing, other groups have focused on identifying key pathways for mechanical signal transduction. Following the action of cells pulling on their substrate through the generation of cytoskeletal tension, several signaling pathways are postulated to transmit signals for alterations in overall cell function. In in vitro studies, Sheetz and his group have indicated several pathways as potential mechanical signal transducers [63]–[66]. Specifically, they focus on tyrosine phosphorylation resulting from structural changes in cytoskeletal organization [64]. Interestingly, others have demonstrated the dependence of tyrosine kinase activity on substrate stiffness [20] and that members of the Src family are involved with cell processes known to be controlled by substrate mechanics such as survival, migration, and transformation/differentiation [67]. Similarly, Sheetz's group has more recently demonstrated localized phosphorylation of the Src family kinase substrate Cas

(Crk associated substrate) in areas of increased cytoskeletal tension [68]. Studies demonstrating the importance of certain proteins in mechanical signal transduction have indicated key players involved in cell substrate sensing and continue to reinforce the idea that cellular tension generation is key for proper cell function.

1.4 The Motor Clutch Model as a Mechanism for Cellular Tension Generation and Overall Substrate Sensing

While important specific molecular components have been identified, the overall mechanism for tension generation and subsequent cellular sensing of the mechanical environment is less well understood. As discussed in section 1.3 the cellular tensegrity model portrays the importance of cellular prestress, and how it impacts cell function, but it does not provide a mechanism for the origin of stress within individual filaments. In an initial study of how neuronal cells extend processes along their substrates, Mitchison and Kirschner propose a method for cellular traction generation that is a function of adhesion and actin flow [69]. In their proposed process, an actin filament first mechanically couples to its substrate by binding to it through integrin-talin adhesion complexes. Bound adhesion complexes counteract myosin motor forces that pull on the filament toward the center of the cell, therefore generating tension within the filament. Polymerization of actin extends the leading edge of the filament and pushes on the cell membrane. Therefore, tension generation is a result of a balance between adhesion complex binding, myosin derived retrograde flow, and actin polymerization derived leading edge extension.

In their now seminal work, Chan and Odde developed a stochastic simulation of Mitchison and Kirschner's motor-clutch model to test the effects of substrate stiffness on the system [70]. Chan and Odde model adhesion complexes as simple Hookean springs

which stochastically bind and unbind from the compliant substrate as a function of applied force. They report that actin flow, traction generation, and adhesion dynamics are all a function of substrate compliance (Figure 1-3). They define adhesion binding dynamics as falling into one of two categories, load and fail or frictional slippage. Load and fail occurs on soft, compliant substrates where retrograde flow is low and force generation is high. Frictional slippage occurs on stiff substrates, where flow is high, and force is low. Importantly, their model observations are all reproduced in vitro experiments of neuronal cell actin dynamics.

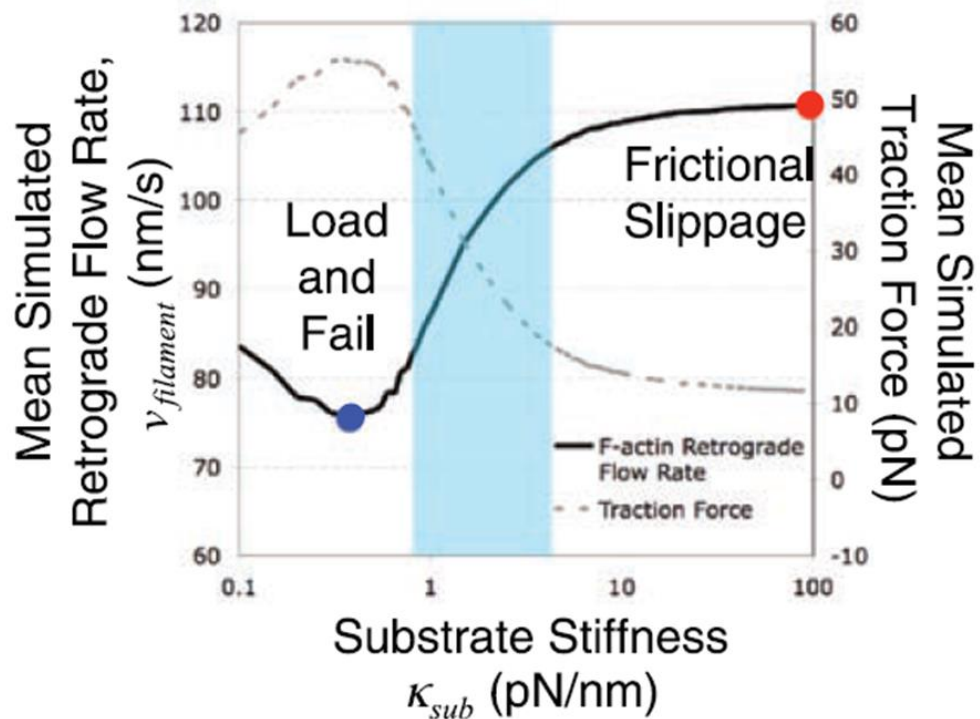


Figure 1-3: Motor-clutch model dynamics as a function of substrate stiffness.

Actin retrograde velocity and traction force generation as a function of substrate stiffness. Load and fail dynamics are associated with low flow rates and high traction force, while frictional slippage dynamics are associated with increased flow rates and low traction force. Reproduced from Chan and Odde 2008 [70] with permission from AAAS.

1.5 Summary of Dissertation Focus

While recent advances in experimental techniques allow for control of the extracellular mechanical environment, questions about the combined effects of the active and passive environment still exist. The focus of this research involves adapting Chan and Odde's computational motor-clutch model to study the combined effect of cyclic substrate deformation and substrate stiffness on actin cytoskeleton organization and dynamics. This work also provides a means for comparing the impacts of cyclic stretch and substrate stiffness on cell function, and whether the two alter cell function in similar ways. The work summarized here concludes that the motor-clutch model is a potential mechanism for cellular sensing of the mechanical environment. Chapter 3 presents the adapted motor-clutch model as means for exploring the combined effects of stretch and stiffness on cytoskeleton derived traction force. Next, chapter 4 utilizes the adapted model as a mechanism for exploring cell morphological alterations in response to changes in the mechanical environment. Specifically, the adapted motor-clutch model is used to accurately predict experimentally observed cell and cytoskeleton reorganization as a function of applied cyclic stretch. Lastly, chapter 5 discusses future directions and use of the adapted motor clutch model to study the role of the mechanical environment in the progression of a heart failure disease model.

1.6 Summary of Contributions

Much of the work here is the result of collaborative efforts. Major contributions by other individuals are summarized here and, in some cases, how the work of others interacted with my own. Dr. Jessica Thomas conducted endothelial cell cyclic stretch experiments and imaged representative cells. I conducted quantitative image analysis of these images with the help of Jackie Xuan to assess properties of cell and matrix morphology (Figure 4-3). Drs. Chuan Xue and Jia Guo implemented in MATLAB the equations for the original motor-clutch model and extended the model to include 2-D actin fiber movement and cyclic substrate movement. I expanded upon this model and utilized it for all data collection associated with Chapter 4. For studies of the effect of cyclic stretch on actin traction force generation, I modified MATLAB code originally developed by Dr. Seth Weinberg to account for cyclic substrate movement. Ben DiFranco assisted with ideas and data collection presented in Chapter 3.

Chapter 2 Methods

2.1 Biomechanical description of the motor-Clutch model

The motor-clutch model describes the motion of a singular actin bundle within a cell (Figure 2-1). Myosin motors permanently couple with the actin bundle and pull it away from the cell membrane (i.e., retrograde motion). Molecular clutches (e.g., individual integrin complexes) link the intracellular actin bundle to the extracellular substrate. Multiple clutches can independently form (bind) and dissociate (unbind) to and from the substrate. The clutches apply a force to the actin bundle resisting myosin motor force thereby decreasing the speed of the retrograde motion. Actin subunits are continuously added to the leading edge of the actin bundle. This addition of new subunits tends to extend the end of the actin fiber away from center of the cell while individual subunits within the fiber move towards the center of the cell. If the rate of fiber elongation is greater than the rate of retrograde motion, the actin fiber can push against the plasma membrane thereby elongating the cell in that direction.

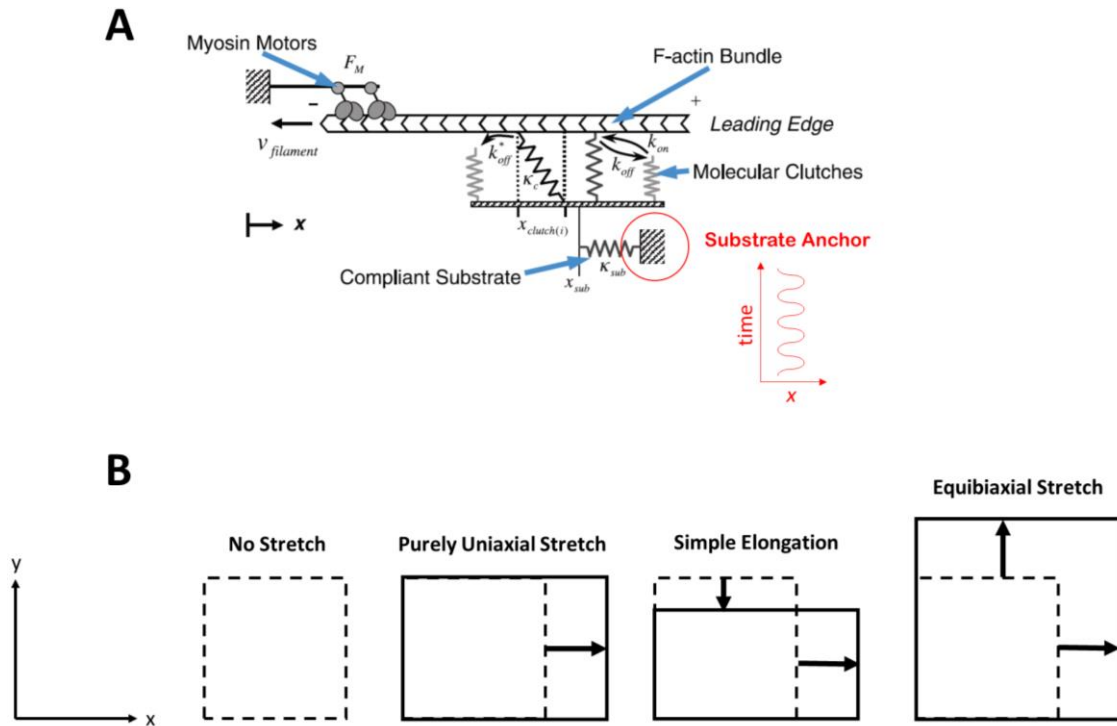


Figure 2-1: The motor-clutch model and cyclic stretch.

(A) Schematic of the motor-clutch model, reproduced from Chan and Odde 2008 [70] with permission from AAAS, with the adaptation to include cyclic stretch of the substrate anchor. (B) Graphical representation of different types of simulated cyclic stretch that the adapted motor-clutch model is capable of reproducing. Dashed outline represents the original substrate dimensions, solid lines represent substrate dimensions during extension portion of cyclic stretch cycle. Black arrows demonstrate the direction of substrate deformation.

2.2 Stochastic mathematical formulation of the motor-clutch model

Chan and Odde developed a set of equations that embody the concepts of the motor clutch model and applied it to a cell on a deformable substrate [70]–[72]. The model consists of an F-actin bundle, molecular clutches, and a compliant substrate. The actin bundle is treated as a rigid rod. The velocity of the actin (v_{actin}) is a linear function of the sum of the forces applied by all of the clutches ($\sum F_{\text{clutch}(i)}$). Specifically,

$$V_{\text{actin}} = V_u (1 + \sum F_{\text{clutch}(i)} / F_{\text{stall}}) \quad \langle \text{Equation 1} \rangle$$

where V_u is the unloaded velocity of the bundle and F_{stall} is the force that would prevent bundle motion. The stall force is the stall force of one motor (F_m) times the number of motors (n_m). Thus, when $\sum F_{\text{clutch}(i)}$ is equal and opposite to the stall force, $v_{\text{actin}} = 0$. The velocity of actin polymerization at the leading edge is a function of available free actin. While addition of new actin monomers to the leading edge impacts bundle length, it does not impact bundle velocity directly. Each individual clutch bond is treated as a single, Hookean spring with the magnitude of the force it exerts ($F_{\text{clutch}(i)}$) proportional to its deformation. Specifically,

$$F_{\text{clutch}(i)} = K_{\text{clutch}(i)} (x_i - x_{\text{sub}}) \quad \langle \text{Equation 2} \rangle$$

where x_i is the position of the clutch, x_{sub} is the position of the substrate, and $K_{\text{clutch}(i)}$ is the clutch spring constant. The sum of the forces for all the clutches ($\sum F_{\text{clutch}(i)}$) is applied to and deforms the substrate, which is treated as a single, Hookean spring with a spring constant K_{sub} . Specifically,

$$\sum F_{\text{clutch}(i)} = K_{\text{sub}} x_{\text{sub}} \quad \langle \text{Equation 3} \rangle$$

K_{sub} is related to the modulus of the substrate with 1pN/nm corresponding to 1 kPa [70]. Clutch binding and unbinding are stochastic, with a forward rate constant (k_{on}) and a reverse rate constant (k_{off}^*). To account for the fact that mechanically loading the clutch bond can increase the probability that it breaks, the Bell relationship is used. Specifically,

$$k_{\text{off}}^* = k_{\text{off}} e^{(\text{abs}(F_{\text{clutch}} / F_b))} \quad \langle \text{Equation 4} \rangle$$

Where k_{off} is the unloaded off-rate and F_b is a characteristic rupture force.

Values for the free parameters were obtained by Chan and Odde from the literature or their own experimental work (Table 2-1, [70]).

Model Parameter	Description	Value
n_m	Number of myosin motors	50
F_m	Single myosin motor stall force	-2 pN
v_u	Unloaded bundle velocity	-120 nm/s
n_c	Number of molecular clutches	50
k_{on}	Pseudo first-order on-rate constant of clutch binding	1 s^{-1}
k_{off}	Pseudo first-order unloaded off-rate constant of clutch unbinding	0.1 s^{-1}
F_b	Characteristic bond rupture force	-2 pN
K_c	Molecular clutch spring constant	5 pN/nm

Table 2-1: Motor-clutch model parameters.

Values reproduced from Chan and Odde 2008 [70].

2.3 Modifications to the motor-clutch model

The Chan and Odde computational motor-clutch model was adapted to include cyclic movement of the substrate anchor to simulate cyclic stretch (Figure 2-1A). Cyclic stretch of the substrate in the x-direction (the direction parallel to the orientation of the actin fiber) is modeled through movement of the substrate anchor (X_{anchor}) according to a sinusoidal function,

$$X_{\text{anchor}} = X * \frac{1}{2} * (1 - \cos(2\pi * t / P)) * \epsilon_{\text{rtx}} \quad \langle \text{Equation 5} \rangle$$

where X is the Lagrangian x-coordinate of the actin bundle tip at time of the first clutch binding in relation to the stretch cycle, P is the period of stretch, and ϵ_{rtx} is the applied cyclic stretch ratio in the direction parallel (x-) to applied stretch. The functional form $1 - \cos(\text{constant} * t)$ was chosen so that at the beginning of the simulation (i.e., time = 0) there would be no applied stretch on the bundle, which matches the conditions of our experiments and those of most others.

The position of the substrate following movement of the anchor is then updated utilizing an adapted form of the substrate position equation derived by Chan and Odde,

$$X_{\text{sub}} = (k_{\text{clutch}} * \sum_{i=1}^{n_{\text{eng}}} x_i + k_{\text{sub}} * X_{\text{anchor}}) / (k_{\text{sub}} + k_{\text{clutch}} * n_{\text{eng}}) \quad \langle \text{equation 6} \rangle$$

where n_{eng} is the number of engaged clutches. The velocity of the actin bundle (V_{actin}) is then also updated to include movement of the substrate anchor,

$$V_{\text{actin}} = V_u (1 - k_{\text{sub}} * (X_{\text{sub}} - X_{\text{anchor}}) / F_{\text{stall}}). \quad \text{<equation 7>}$$

The length of the actin bundle (L) is influenced both by depolymerization on the nuclear edge, or minus end, and polymerization on the leading edge, or plus end. Depolymerization of the minus end is assumed to be equal to V_{actin} . v_p is allowed to increase as L decreases, which is consistent with the notion that as the bundle shortens there would be more globular (G-actin), or free, actin, which could increase polymerization rate. We captured this behavior with the equation,

$$v_p = v_p^* (L_{\text{max}} - L) / L \quad \text{<Equation 8>}$$

where v_p^* is the maximum actin polymerization rate and L_{max} is the maximum allowable bundle length.

Catch-bond behavior was then included in the adapted model to re-create true in vitro cell spreading behavior. The clutch off-rate (k_{off}^*) was altered to include both catch and slip behavior,

$$k_{\text{off}}^* = k_{\text{off}} e^{(\text{abs}(F_{\text{clutch}} / F_b))} + k_{\text{offc}} e^{(\text{abs}(F_{\text{clutch}} / F_c))} \quad \text{<Equation 9>}$$

where k_{offc} is the specific catch-bond unloaded off-rate and F_c is the characteristic clutch catch force.

To compare with in vitro experimental observations of cell spreading as a function of the mechanical environment, cell spreading speed is calculated as a function of retrograde velocity and a constant polymerization rate. Specifically,

$$V_{spread} = V_{poly} - V_{actin} \quad \text{<equation 10>}$$

where V_{spread} is the initial cell spreading speed and V_{poly} is the constant polymerization rate (for this instance only).

The specific model parameter values used for catch-bond simulations are presented in Table 2-2.

Model Parameter	Description	Value
n_m	Number of myosin motors	75
F_m	Single myosin motor stall force	-2 pN
v_u	Unloaded bundle velocity	-120 nm/s
n_c	Number of molecular clutches	75
k_{on}	Pseudo first-order on-rate constant of clutch binding	0.1 s^{-1}
k_{off}	Pseudo first-order unloaded off-rate constant of clutch unbinding	0.004 s^{-1}
F_b	Characteristic bond rupture force	-8 pN
K_c	Molecular clutch spring constant	5 pN/nm
F_c	Clutch catch force	2 pN
k_{offc}	Pseudo first-order unloaded off-rate constant of clutch catch unbinding	10 s^{-1}

Table 2-2: Motor-clutch catch bond model parameters.

Values reproduced from Bangasser et al. 2013. [71]

2.4 Further modifications to the motor-clutch model to study action reorientation

The adapted cyclic stretch motor-clutch model was further modified to account for rotation of the actin fiber to study actin reorientation as a function of cyclic stretch. First the y-coordinate of the fiber tip is defined as the Lagrangian y-coordinate in relation to the substrate position, similarly to how the x-coordinate is defined. When the fiber is bound, it is stretched and compressed with cyclic movement of the substrate, allowing for both the

x- and y-coordinate to change with time. The final orientation of the actin fiber is then calculated as a function of the x- and y-coordinate of the fiber tip.

To compare with several experimental systems, the adapted motor-clutch model can recreate three types of cyclic stretch (Figure 2-1B): true uniaxial stretch (stretch in only the direction parallel to the actin fiber), simple elongation (stretch in the parallel direction and compression in the perpendicular direction), and equibiaxial stretch (equal stretch in both directions). True uniaxial stretch utilizes only Equation 5 for all substrate anchor movement. To incorporate strain in the y-direction, which is perpendicular to the direction of applied stretch (modeling simple elongation), the y-coordinate of the substrate anchor (Y_{anchor}) was moved,

$$Y_{\text{anchor}} = Y * \frac{1}{2} * (1 + \cos(2\pi * t/P)) * \epsilon_{\text{rty}} \quad \langle \text{Equation 9} \rangle$$

where Y is the Lagrangian y-coordinate of the actin bundle tip at time of the first clutch binding in relation to the stretch cycle, P is the period of stretch, and ϵ_{rty} is the applied cyclic compression ratio in the direction perpendicular (y-) to applied stretch as a result of elongation in the parallel direction (x-). The compression ratio was calculated as a function of stretch applied in the parallel (x-) direction and the estimated poisson's ratio of the modeled substrate. Our in vitro experimental system applied stretch in the x-direction and the substrate was not confined in the y-direction. By recording the motion of fiduciary markers placed on our in vitro PDMS deformable substrate, we determined the Poisson's

ratio to be 0.52, similar to that reported for elastomers (specifically silicone rubbers) [73], which we approximated as 0.5 in simulations of simple elongation.

In simulations of cyclic equibiaxial stretch, stretch was applied equally in both the parallel (x-) and perpendicular (y-) directions by moving the x- and y-coordinate of the substrate anchor equally in space and time,

$$X_{\text{anchor}} = Y_{\text{anchor}} = L_{xy} * \frac{1}{2} * (1 - \cos(2\pi * t/P)) * \epsilon_{rxy} \quad \langle \text{Equation 10} \rangle$$

where L_{xy} is the Lagrangian tip of the actin bundle at time of the first clutch binding in relation to the stretch cycle, and ϵ_{rxy} is the applied cyclic stretch ratio.

Chapter 3 The Motor-Clutch Model as a Mechanism for Cellular Traction Force Generation as a Function of the Mechanical Environment

3.1 Introduction

The generation and maintenance of tension within the actin cytoskeleton is critical for cell function. Proper tension generation is known to play a role in several cellular processes such as: cell motility, migration, changes in cell morphology, differentiation, survival, and extracellular matrix organization in development, wound healing, and tissue maintenance [38], [61], [74]–[79]. Others have also demonstrated that cytoskeletal tension is likely a part of cellular mechanobiological responses, where cells alter their form and function in response to perturbations in the mechanical environment, such as extracellular substrate stiffness [52], [53], [59], [80]–[86]. In his early cell geometry model, Ingber describes cells as tensegrity structures, comprised of many prestressed intracellular filaments that are vital for proper cell structure [55]. He also describes how the cell tensegrity model can be used to describe cell motility, potentially one of the first proposed mechanisms for how cells respond to their mechanical environment through cytoskeletal changes.

Evidence now strongly suggests that cytoskeletal tension originates from the interplay between substrate adhesion and actomyosin contraction. In their initial description of neuronal cell extension and protrusion, Mitchison and Kirschner propose the motor-clutch model as a mechanism for traction force generation [69]. In their model, actin reversibly

binds to the extracellular substrate through molecular clutches, which resist myosin motor derived retrograde flow. As myosin motors pull on the actin filament, traction is transmitted through bound molecular clutches to the extracellular substrate. Recent studies further demonstrate the importance of proper actomyosin contraction in responding to the mechanical environment. For instance, cellular prestress within the cytoskeleton is crucial for the maintenance of cell stability and morphology, and overall cell stiffness is a function of initial cell prestress [57], [58]. Others have demonstrated that cells without properly functioning non-muscle myosin lost their ability to both control their morphology [60], [61] and differentiate in response to substrate stiffness [59], further reinforcing the importance of actomyosin contractile function in cell sensing of the mechanical environment. To further analyze cytoskeletal tension and cellular mechanobiology, Chan and Odde developed a computational simulation of Mitchison and Kirschner's motor-clutch model [70]. They use their stochastic simulation to initially demonstrate how tension and traction force is a function of substrate stiffness. In more recent work, they report an optimal stiffness for traction force generation which is sensitive to changes in clutch and motor strength [71], [72].

In addition to intracellular forces derived from actomyosin contraction, forces arise outside a cell from motion of the extracellular substrate and are transmitted to the actin cytoskeleton through substrate adhesions. For example, cells in vivo are exposed to cyclic stretching of their substrates through beating of the heart, blood pulse wave propagation through the arterial system, and peristalsis in the digestive system. In vitro studies have revealed that cyclic stretch impacts cell morphology and several diverse cell functions [26],

[30], [31], [39], [42]–[47] similar to those impacted by changes to extracellular substrate stiffness [21], [38], [53], [81], [81]–[85]. Since cytoskeletal tension is frequently proposed as a mechanism by which cells respond to their mechanical environment, we adapted the stochastic motor clutch model originally proposed by Chan and Odde to study the impacts of cyclic stretch on cytoskeletal tension and traction force generation.

3.2 Methods

Computational simulations utilized the adapted motor-clutch model described in Chapter 2. All simulations were run for a total time of 500 seconds unless otherwise noted. Simulation data is presented as an average of 10 individual simulations.

3.3 Results

3.3.1 Cyclic stretch differentially alters traction force generation.

The application of cyclic stretch to the motor-clutch model significantly impacts actin traction force generation and is dependent on the value of k_{sub} . At low values of k_{sub} (0.1 pN/nm), cyclic stretch has no impact on force generation, where force remains constant over a wide range of stretch amplitudes (Figure 3-1B, Blue). At moderate k_{sub} values (1.0 pN/nm), there is a clear, constituent trend with increasing stretch amplitude leading to decreasing traction force (Figure 3-1B, Orange). At high values of k_{sub} (10 pN/nm), however, there is a non-monotonic relationship. Initial increases in stretch amplitude increase force generation, followed by a decrease in force with further increases in stretch amplitude (Figure 3-1B, Yellow).

As reported by Chan and Odde and others [70]–[72], original motor-clutch model (no cyclic stretch) behavior is heavily dependent on the value of k_{sub} . Over a wide range

of k_{sub} values, traction force initially increases until reaching an optimal stiffness, where further increases in substrate stiffness decreases traction force generation (Figure 3-1A, No Stretch case). The application of cyclic stretch results in force generation that follows this same general trend, with slight shifts in the resultant force vs. k_{sub} curve (Figure 3-1A, all lines). For most stretch amplitudes ($>3\%$), traction force is decreased for all values of k_{sub} . However, stretch amplitudes ranging from 1-3% increase force generation above that for the no stretch condition at certain substrate thresholds (~ 2 pN/nm for 1%, ~ 4 pN/nm for 2%, and ~ 11 pN/nm for 3%).

In addition to impacting the magnitude of traction force generation, cyclic stretch also changes substrate stiffness value at which traction force is maximized (termed optimal stiffness) (Figure 3-1C). Specifically, for moderate stretch amplitudes (1-6%) optimal stiffness decreases steadily with increasing stretch amplitude. Optimal stiffness remains constant, however, with further increases in stretch amplitude.

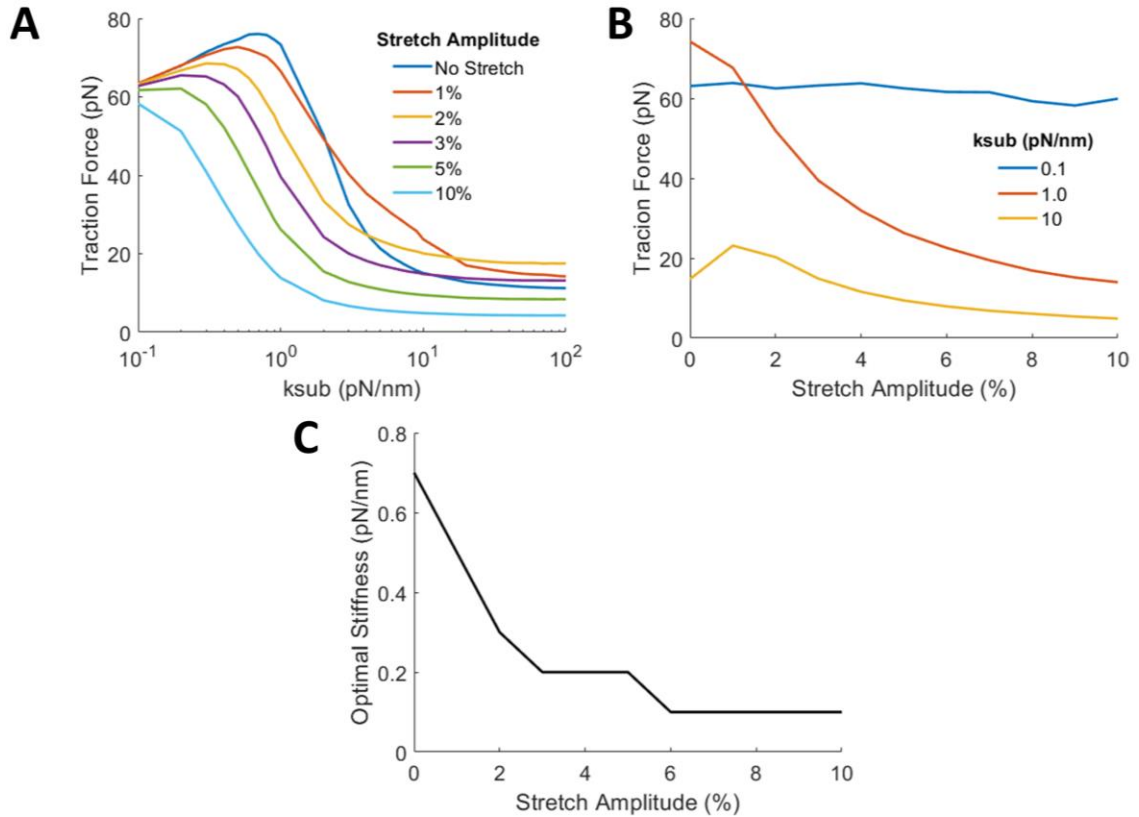


Figure 3-1: Actin traction force generation as a function of cyclic stretch and substrate stiffness.

Simulated traction force generation as a function of variable cyclic stretch amplitude and values of k_{sub} . (A) Traction force vs. k_{sub} with different values of cyclic stretch amplitude. (B) Traction force vs. stretch amplitude with different values of k_{sub} . (C) Optimal stiffness (k_{sub} for which traction force is maximized) vs. cyclic stretch amplitude.

3.3.2 Combined effects of amplitude and frequency on traction force generation.

Next, we varied both stretch amplitude and stretch frequency to analyze the effects of cyclic stretch more closely on motor-clutch dynamics. We expected that altering amplitude or frequency of stretch would have some impact on traction force as both parameters contribute to substrate motion, and therefore force application to bound clutches.

Interestingly, general changes to amplitude and frequency have similar effects where increasing amplitude or frequency typically decreases traction force generation (Figure 3-2).

As previously noted, the distinct model response to cyclic stretch is heavily dependent on the value of k_{sub} . Even over a wide range of stretch amplitudes and frequencies, there is still little to no change in traction force generation or retrograde velocity for low k_{sub} values (Figure 3-2, 0.1 pN/nm (top)). For moderate values of k_{sub} , traction force and retrograde velocity change monotonically with increases in amplitude and frequency (Figure 3-2 1.0 pN/nm (middle)) and changes to the parameters appear to have equal effects on both force and velocity. Specifically, force decreases similarly with equal increases in frequency or amplitude. The amplitude frequency contour plot for high values of k_{sub} shows a similar response to stretch, where initial increases in both stretch amplitude and frequency increases traction force generation and decreases retrograde velocity and subsequent increases in stretch decrease force and increase velocity (Figure 3-1B and 3-2 10 pN/nm (bottom)). The contour plot reveals a window of specific stretch parameters, typically combinations that include low amplitude or low frequency.

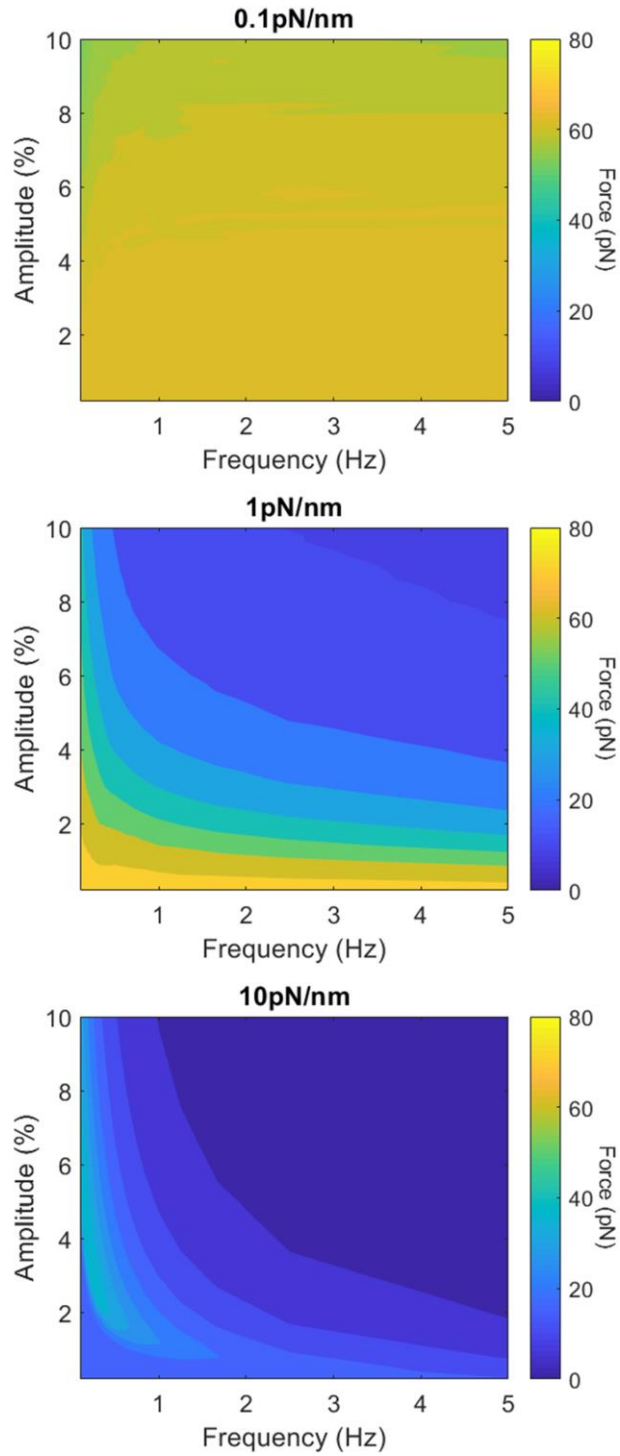


Figure 3-2: Traction force generation as a function of cyclic stretch amplitude and frequency.

Contours of simulated traction force generation as a function of both stretch amplitude and frequency. Combined effects are also heavily dependent on the value of k_{sub} .

3.3.3 Clutch engagement dynamics are a function of substrate stiffness and cyclic stretch.

Changes in traction force and actin flow as a function of substrate coincide with changes in clutch engagement dynamics (i.e., load and fail vs. frictional slippage) (Figure 1-3) [70]. To quantify the differences between load and fail and frictional slippage behavior as a function of both substrate stiffness and cyclic stretch, we calculate average number of engaged clutches and average clutch lifespan (Figure 3-3). For cases with no cyclic stretch, load and fail clutch dynamics (associated with lower values of k_{sub} , 0.1-1.0 pN/nm) are characterized by long average bond lifespans and high number of engaged clutches (Figure 3-3A,B). As k_{sub} is increased beyond 1.0 pN/nm and clutch dynamics shift toward frictional slippage like behavior, bond lifespan and number of engaged clutches decrease (Figure 3-3A,B). Interestingly, maximum clutch lifespan and engaged clutch number is not correlated with optimal stiffness for traction force generation. This suggests that even though bond lifespan and number decrease with substrate stiffness, force generation is a balance between the value of k_{sub} and clutch behavior. Therefore, while clutch engagement metrics are excellent predictors of bonding profile, they do not singly predict traction force generation.

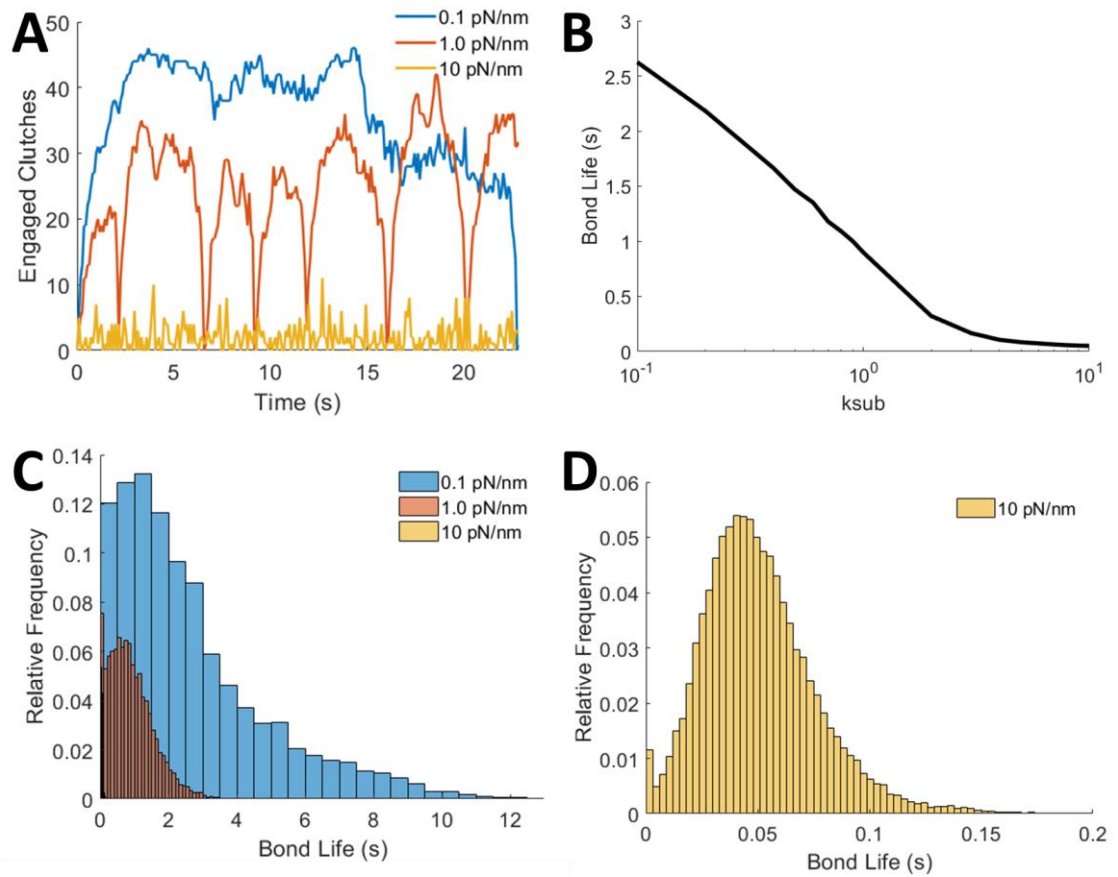


Figure 3-3: Clutch dynamics as a function of substrate stiffness.

(A) Clutch binding profiles for different values of k_{sub} . Binding profiles display the total number of engaged clutches over time. (B) Average bond life for a single clutch as a function of k_{sub} . (C) Relative frequency histograms of average bond life for different values of k_{sub} . (D) Close-up histogram of 10 pN/nm case.

We then applied the characterization of clutch dynamics and quantification of bonding profile to cyclic stretch cases. The effects of cyclic stretch on model behavior are most apparent for moderate values of k_{sub} (~ 1.0 pN/nm) where increases in stretch amplitude steadily decrease traction force generation. Expectedly, analysis of clutch behavior for moderate k_{sub} demonstrates that the introduction of stretch shifts the clutch binding profile from a load and fail like behavior to frictional slippage (Figure 3-4A middle). This

transformation is characterized by a decrease in average number of engaged clutches and average bond lifespan (Figure 3-4B orange line). For lower values of k_{sub} (e.g., 0.1 pN/nm) where cyclic stretch has little to no effect on traction force generation, there are no changes in clutch engagement behaviors. Specifically, a load and fail binding profile remains load and fail like after the introduction of stretch and there are no significant changes in average bond lifespan or number of engaged clutches.

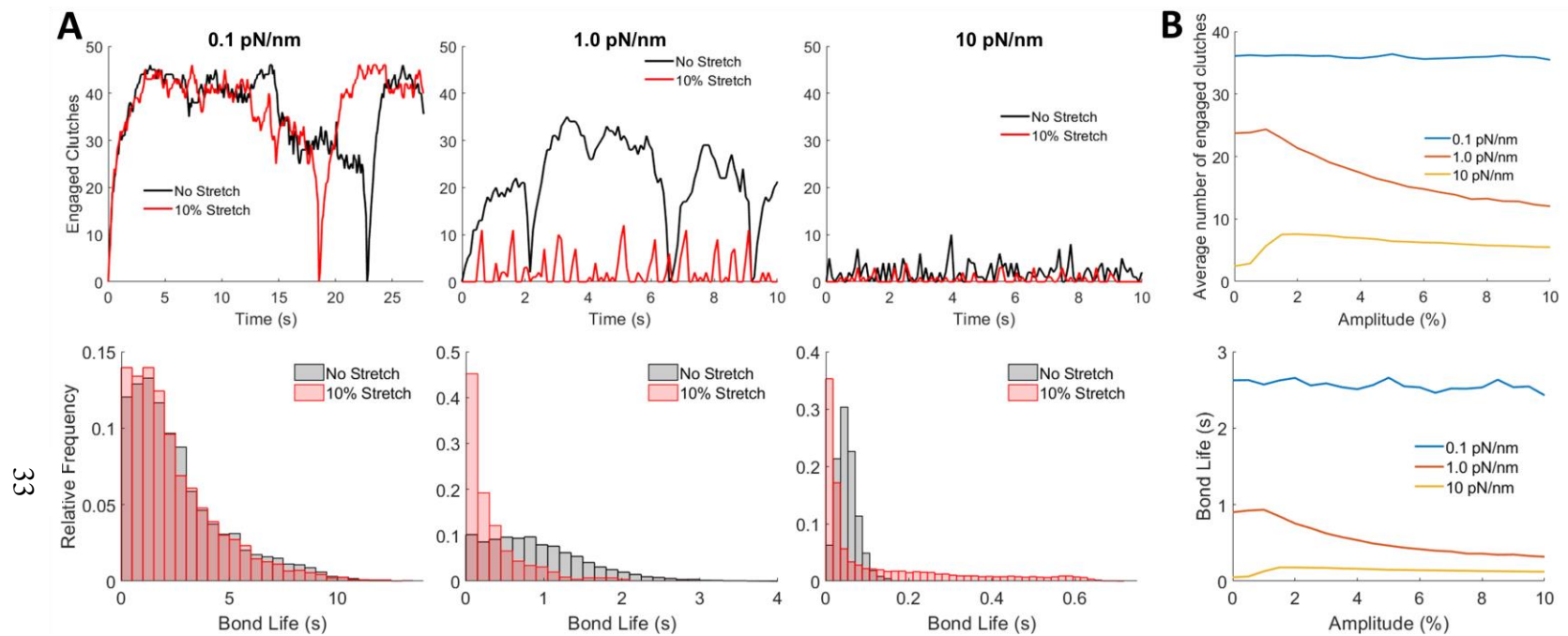


Figure 3-4: Clutch binding dynamics as a function of cyclic stretch.

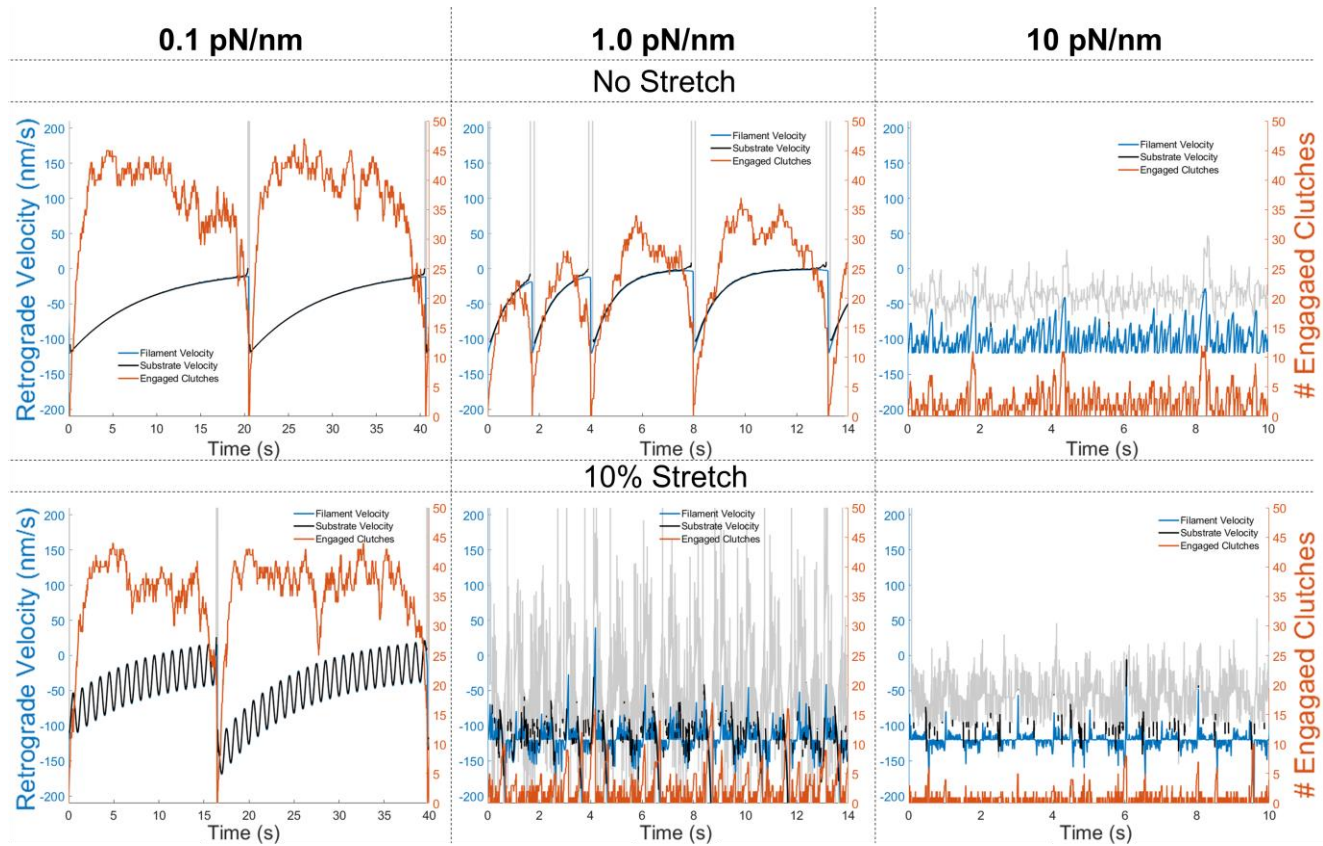
(A) Clutch binding profiles (top) and bond life histograms (bottom) for no stretch and 10% stretch conditions for different values of k_{sub} . (B) Average number of engaged clutches (top) and average bond life (bottom) as a function of cyclic stretch amplitude for different values of k_{sub} .

Changes in clutch binding dynamics also explain the differential response to cyclic stretch associated with high values of k_{sub} (e.g., 10 pN/nm). As noted previously, traction force generation initially increases with low levels of stretch. This increase in force corresponds with a shift in binding profile from frictional slippage to load and fail like, characterized by increases in both average number of engaged clutches and average bond life span (Figure 3-4B yellow line). Further increases in stretch amplitude slowly decrease number of engaged clutches and bond lifespan, as the binding profile returns to a frictional slippage like behavior. Further increases in stretch amplitude progressively decrease engaged clutch numbers and bond lifespan, but not to the same levels as the no stretch case. This is also apparent in the frequency distribution histogram for the stretch cases for high substrate stiffnesses. Specifically, for the 10% stretch case, most bond lifespans are short (<0.1 s) but there are more cases of bonds with longer lifespans (>0.2 s).

3.3.4 Differences between actin flow and substrate motion describe clutch engagement dynamics.

Next, we set out to determine what dictates changes in clutch engagement dynamics associated with changes in substrate stiffness and cyclic stretch. Knowing that cyclic stretch of the substrate will introduce additional substrate motion that directly impacts clutch engagement behavior, we hypothesized that changes in clutch dynamics can be described by comparing substrate motion with filament motion. First, examining the no stretch case demonstrates a strong correlation between the matching of actin retrograde velocity and substrate velocity and total number of engaged clutches (Figure 3-5 top). For the case of low substrate stiffness ($k_{\text{sub}} = 0.1$ pN/nm), the substrate and actin filament move with equal velocities for an extended period (roughly 20 seconds) during which clutches

bind and remained engaged. The velocities diverge only during the failure portion of the load and fail cycle, and quickly converge upon re-engagement of clutches. Similarly, for the case of moderate substrate stiffness ($k_{\text{sub}} = 1.0 \text{ pN/nm}$), substrate and actin velocities are matched for extended periods of time which correspond with clutches binding and remaining engaged. However, the duration of matched velocities before the two diverge is significantly shorter than the low stiffness case, explaining the lower maximum number of engaged clutches and shorter load and fail cycle times. As expected, increasing stiffness further ($k_{\text{sub}} = 10 \text{ pN/nm}$) results in permanently mismatched substrate and actin velocity. For this reason, total engaged clutch numbers remain low, individual clutch lifespan is short, and distinct load and fail cycles are not apparent.



36

Figure 3-5: Substrate motion, actin motion, and total number of engaged clutches over time.

Substrate velocity (black) and actin velocity (blue) plotted vs. time with corresponding clutch binding profile (orange) for no stretch (top) and 10% stretch (bottom conditions). Substrate velocity is plotted as a solid, black line while substrate velocity and actin velocity are within 10% of each other. Once the difference between the velocities reaches higher than 10%, substrate velocity is plotted as a gray line.

As expected, the changes in clutch binding dynamics associated with the introduction of cyclic stretch are explained by changes in substrate and filament velocity matching. At low values of k_{sub} (0.1 pN/nm), substrate and filament motion remain in unison resulting in no changes in clutch binding compared to the no stretch case. (Figure 3-5 bottom, left). At moderate values of k_{sub} (1.0 pN/nm), however, the filament and substrate no longer move in unison (Figure 3-5 bottom, middle). The difference between substrate and filament velocity is high, resulting in a transition from load and fail behavior associated with the no stretch case to frictional slippage. While there are occasional instantaneous moments of matched velocities (transition from gray line to short black lines), velocities remain mismatched for the majority of each stretch cycle.

Increasing k_{sub} higher (10 pN/nm) introduces an unexpected behavior. As mentioned previously, while cyclic stretch on high substrate stiffnesses still results in a frictional slippage binding profile, number of engaged clutches and clutch lifespan increases slightly. Analysis of instantaneous filament and substrate velocity reveals periods of matched velocities that were not apparent for the no stretch condition. Certain stretch parameter combinations magnify these observations even further. Specifically, for the case of 1% stretch at a frequency of 1 Hz, there are extended periods of both load and fail and frictional slippage behavior (Figure 3-6). Each cycle begins in a frictional slippage regime with actin retrograde velocity nearing the unloaded actin velocity, v_u . As substrate velocity decreases and nears actin retrograde velocity, the total number of engaged clutches increases and a load and fail cycle begins. Clutches continue to engage and remain engaged

as the substrate and filament begin to move in total unison. The velocities near 0 (representing the inflection point of substrate motion, where the substrate begins moving in the opposite direction it was previously moving) and clutches begin disengaging leading to an eventual catastrophic failure event. The periodic matching of velocities associated with the load and fail cycles explain the increases in average number of engaged clutches and average clutch life span (Figure 3-4). These changes for the specific parameter combination of 1% stretch and 1 Hz also explain the initial increase in traction force generation for high values of k_{sub} (Figure 3-1).

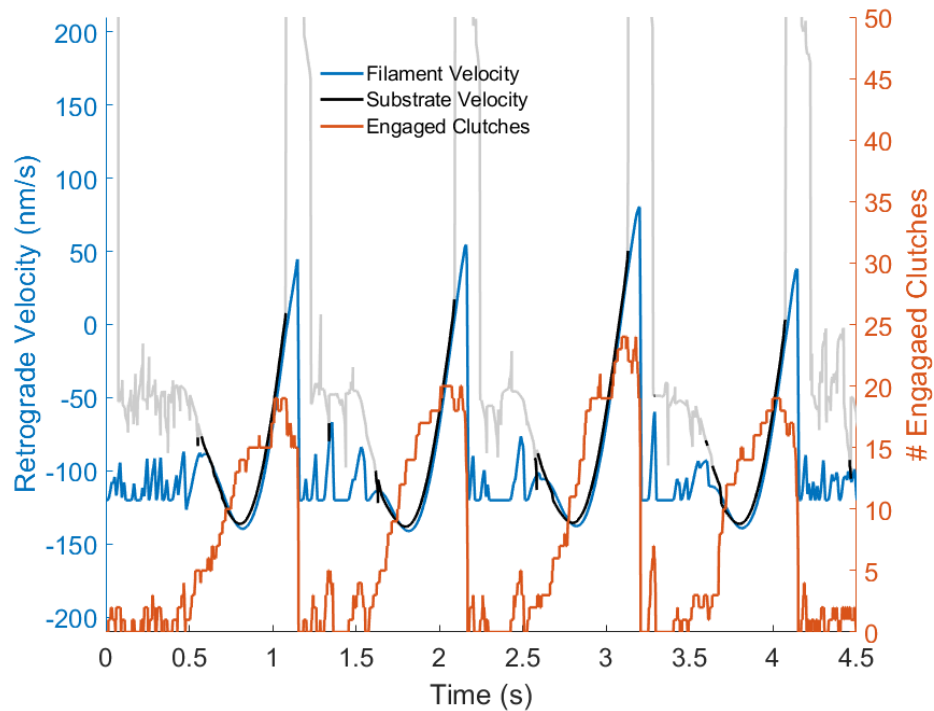


Figure 3-6: Comparison of substrate motion and actin motion for special case of high k_{sub} and low cyclic stretch amplitude.

Substrate velocity (black) and actin velocity (blue) plotted vs. time with corresponding clutch binding profile (orange) for case of $k_{sub} = 10$ pN/nm, and 1% cyclic stretch. Substrate velocity is plotted as a solid, black line while substrate velocity and actin velocity are within 10% of each other. Once the difference between the velocities reaches higher than 10%, substrate velocity is plotted as a gray line.

3.3.5 Inclusion of catch-bond behavior accounts for experimentally observed cell spreading as a function of substrate stiffness and cyclic stretch.

Because the original computational motor-clutch model was created to study neuronal cytoskeletal dynamics, it does not predict the experimental observation of increased cell spreading of many adherent cell types with increasing substrate stiffness (i.e., traction force decreases and retrograde velocity increases as stiffness increases). To first recreate this observation, we introduce the concept of catch-bonds (i.e., bonds that strengthen with increasing force) into our model using a similar approach as Bangasser et al. [71] and by monitoring cell spreading speed. For no stretch conditions, cell spreading speed begins near 0 nm/s and increases with increasing substrate stiffness to a maximum of ~50 nm/s (Figure 3-7, Blue), matching the experimental observation for cell types such as fibroblasts and endothelial cells of increasing cell spread area with increasing substrate stiffness [21]. We then tested whether the catch-bond model can recreate the experimental observation of stretch increasing cell spreading on softer substrates. Cyclic stretch amplitudes of both 10% and 20% increased cell spreading velocity nearly two-fold for all k_{sub} values < 0.2 pN/nm (Figure 3-7 red and yellow lines) which is in agreement with the general trends reported by Cui et al. and Quinlan et al. [47], [54]. Quinlan et al. specifically reports that cell spread area and cell perimeter are doubled for cells exposed to 10% stretch on 0.3 kPa substrates, which is in very good agreement with our computational observation of cell

spreading speed doubling for low values of k_{sub} . Quinlan also observed that cell spread area and cell perimeter decrease for cells exposed to 10% stretch on 50 kPa substrates, which agrees with our observation of decreased cell spreading speed for higher values of k_{sub} for stretch conditions compared to the no stretch condition. Therefore, the preliminary inclusion of catch-bonds in the adapted motor-clutch model accurately recreates cell spreading behavior as a function of substrate stiffness for both no stretch and cyclic stretch conditions.

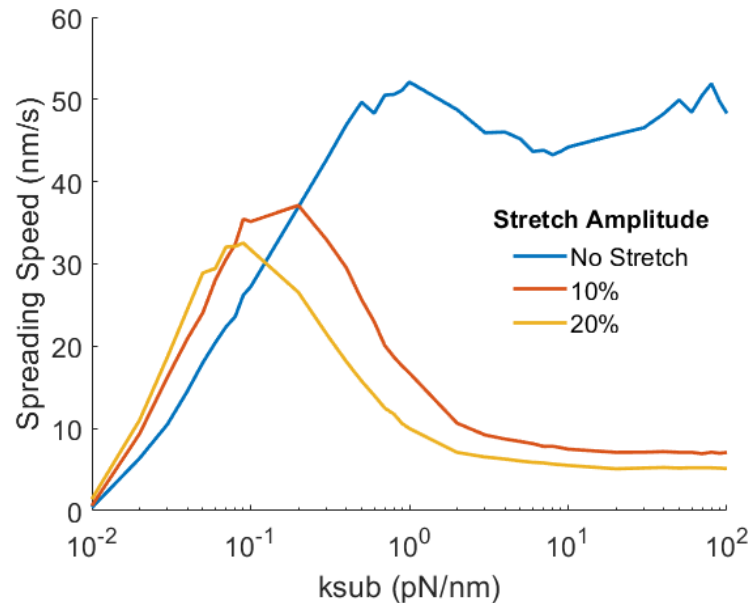


Figure 3-7: Actin spreading speed as a function of substrate stiffness and cyclic stretch amplitude.

Simulated spreading speed (difference between constant polymerization speed and actin retrograde velocity) as a function of k_{sub} for different cyclic stretch amplitudes.

3.4 Discussion

Cyclic stretch studies have interestingly found that stretch alters many of the same cellular processes and functions that substrate stiffness is known to control. Vital processes such as phenotypic differentiation, migration, ECM maintenance, and proliferation are now known to all vary with changes to substrate stiffness or applied cyclic stretch [21], [26], [45], [47], [53], [59], [75], [87], [88]. In their recent study on the role of cyclic stretch and prestress in cellular traction force generation, Cirka et al. demonstrates that force generation is a function of both substrate stiffness and cyclic stretch [89]. Knowing this, we and others have sought to understand whether there is a shared mechanism for sensing changes in both the active and passive mechanical environment. While there are very few studies that successfully vary both applied stretch and substrate stiffness, recent in vitro studies suggest stretching cells on soft substrates generates a response that mimics the response of cells cultured on static, stiff substrates [47], [54], [80]. Using a micropillar substrate where varying pillar height alters perceived substrate stiffness, Cui et al. demonstrate that cells cyclically stretched on “soft” substrates spread to the extent of cells cultured on unstretched polydimethylsiloxane (PDMS, modulus ~ 2MPa) [47]. Perhaps more relevant for our context, they also report the formation and organization of distinct actin stress fibers in cells stretched on “soft” substrates, when cells cultured on soft, static substrates would not typically form stress fibers. Quinlan et al. found similar results, where cell area increases for cells cultured on stretched soft substrates compared to no stretch controls [54]. Interestingly, they also report decreases in cell area for cells stretched on stiff substrates when compared to cells cultured on static stiff substrates.

Our model results show similar trends, where stretch mimics the response to static, more stiff conditions. Traction force generally decreases with increasing k_{sub} over 1 pN/nm for no stretch conditions. For low values of k_{sub} , the introduction of stretch decreases traction force generation that mimics the high k_{sub} , no stretch condition (Figure 3-1). Further analysis in clutch binding dynamics also shows the ability of cyclic stretch to change binding profile type. For moderate values of k_{sub} (1.0 pN/nm), clutch engagement transitions from load and fail like to frictional slippage like with increases in stretch amplitude, eventually nearing the binding behavior typical of higher values of k_{sub} (Figure 3-4). Including catch-bonds in our model also recreates experimental observations of cyclic stretch mimicking the impacts of increased substrate stiffness. Specifically, cyclic stretch increases traction force generation and cell spreading, similar to how increasing substrate stiffness with no stretch does (Figure 3-7). Our data reinforces the proposed hypothesis that a shared mechanism is utilized to sense changes in both substrate stiffness and cyclic stretch. That shared mechanism likely includes key components of the motor-clutch model, specifically actin adhesion through molecular clutches which generate traction by counteracting the force derived from non-muscle myosin contraction.

An interesting caveat to using clutch binding dynamics as an underlying predictor of model behavior is that clutch binding and unbinding does not always match filament traction force generation and flow. For instance, we and Odde and co-workers demonstrate that for no stretch conditions there is a moderate k_{sub} value (~ 1 pN/nm) that is optimal for traction force generation (Figure 3-1) [70]–[72]. However, average bond lifetime and number of engaged clutches decreases monotonically with increasing k_{sub} (Figure 3-3)

(i.e., bond lifetime and number of engaged clutches is maximized for the lowest value of k_{sub} (0.1 pN/nm)). This observation suggests that clutch binding dynamics are important for determination of binding profile classification (load and fail vs. frictional slippage) but do not fully predict force generation. Instead, force generation is clearly a function of clutch dynamics and distinct substrate compliance, where there must be a certain level of substrate resistance to deformation for bound clutches to build force.

3.5 Conclusion

While the distinct responses to altering substrate stiffness and cyclic stretch are well documented, the effects of altering both are more difficult to study and understand. Here we present an adapted motor-clutch model that allows us to finely control both stiffness and cyclic stretch parameters to measure actin dynamics and traction force generation. Typically, the introduction of stretch weakens engaged clutches, decreases traction force generation, and decreases the optimal stiffness for traction force generation. However, there also cases of where clutches are strengthened with the introduction of cyclic stretch, resulting in increased traction force generation compared to the no stretch case. We find that comparing motion of the actin filament with the motion of the substrate describes changes in clutch binding dynamics, explaining how cyclic stretch can alter clutch engagement. Lastly, we introduce catch bond behavior into the adapted motor-clutch model to accurately recreate the experimental observations of increased cell spreading on stiff substrates and cyclically stretched soft substrates. The adapted motor-clutch model demonstrates that it is likely a key part of the shared mechanism that cells utilize to sense and respond to their external mechanical environment.

Chapter 4 The Motor Clutch Model as a Mechanism for the Cellular Morphological Response to Cyclic Force

The contents of this chapter are currently undergoing revisions for re-submission.

Scandling BW, Gou J, Thomas J, Xuan J, Xue C, Gooch KJ. A Motor Clutch Model Predicts and Suggests Mechanisms of Cellular Morphological Response to Cyclic Force. *Molecular Biology of the Cell*. (Under Revision)

4.1 Introduction

4.1.1 Cell alignment in response to cyclic stretch

Many tissues and organs in the body experience cyclic mechanical loading including the cardiovascular systems with the beating of the heart and subsequent pulse wave through the vasculature, the lungs with breathing, the digestive system with peristalsis, and the muscular skeletal system with locomotion. The cyclic mechanical loading and resulting cyclic stretch are thought to impact the structure and functions of these tissues as well as the associated cells in vivo, as summarized in various review articles [87], [90]–[93]. In vitro studies have shown that stretch plays a role in cellular proliferation [26], [42], [43] apoptosis [44], migration [45], [46], extracellular matrix (ECM) maintenance and production [26], [42], [43], and phenotype alteration [47]. Similarly, there is a large amount of experimental evidence detailing the morphological response of cells to cyclic stretch, including spreading, elongation, and alignment [30], [31], [39], [47]. While some cellular and molecular responses to cyclic loading are highly dependent on cell type and alterations in stretch type, many cells tend to alter their orientation similarly in response to cyclic

stretch. Specifically, cells cultured on deformable substrates with initially random orientations align nearly perpendicular to the direction of principal strain, or along an axis of minimal strain, after exposure to cyclic substrate deformation [25]–[33].

4.1.2 Biophysical processes that could potentially lead to cytoskeletal alignment

Several cellular components have been hypothesized to play a role in cellular realignment with most of them focusing on the actin cytoskeleton. Cells under tension from internal (i.e., cellular contraction) [94] or external loads form highly organized actin fiber bundles terminating at substrate linking focal adhesions known as actin stress fibers. [95], [96]. Applied cyclic load reorganizes stress fibers along an axis of minimal strain (roughly perpendicular to the direction of applied stretch) with the whole cell typically also aligning in this direction [25], [97], [98]. When stress fiber formation is inhibited, cells lose the ability to reorient when exposed to cyclic stretching [40]. Similarly, disruption of actin cytoskeletal organization with various pharmacological agents also inhibits cellular reorientation [99]. These observations suggest that the actin cytoskeleton plays a vital role in the cellular morphological response to cyclic stretch. While there exists a wealth of knowledge on the cellular response to cyclic stretch, and data has begun to emerge on potential molecular players, the specific mechanisms behind cellular sensing of cyclic stretch and reorientation of cells remain unknown. On a broad level, one can consider three general processes by which changes in the actin cytoskeleton can result in reorganization of cells in response to cyclic stretch (Figure 4-1) A) Actin bundles can preferentially lengthen and/or shorten depending on their orientation. B) Actin bundles can preferentially

depolymerize or form, again depending on their orientation. C) Intact bundles can change their orientation or rotate within the cells.

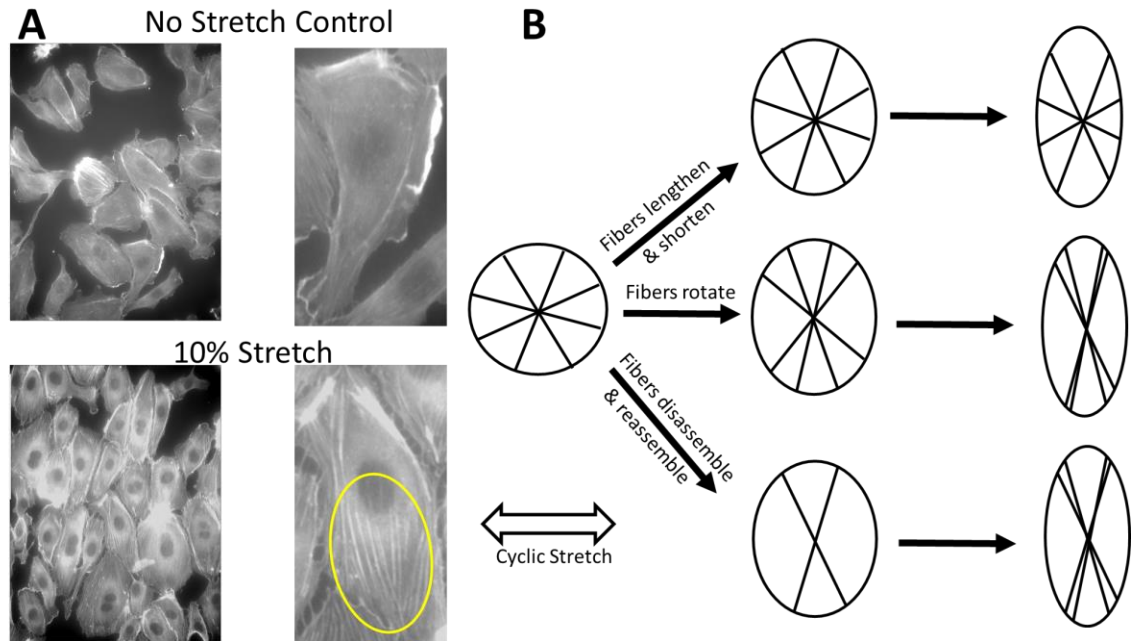


Figure 4-1: Cellular morphological response to applied mechanical stretch.

(A) In vitro HUVEC cells exposed to no stretch control (top) and 10% stretch conditions (bottom). Representative images show overall culture perpendicular realignment (left) and individual cell actin fiber realignment (right, yellow circle). (B) Three general processes by which changes in the actin cytoskeleton (actin fibers) can result in reorganization of cells in response to cyclic stretch. Fibers may lengthen or shorten based on their orientation in respect to the direction of applied stretch. Fibers may rotate as a function of applied strain. Fibers may disassemble in directions where applied strain is greatest, and reassemble in directions where strain is reduced.

4.1.3 Existing mathematical models of fiber and cell alignment

Several mathematical models have been previously developed to predict cellular reorientation in response to cyclic stretch. Generally, models of stress fiber alignment make predictions by focusing on ways that actin bundles are altered by applied cyclic stretch. Many of these models utilize the pivoting of bundles in response to applied cyclic stretch. Models such as the one developed by Wang [100] include pre-existing fibers with initially random orientations. Fibers then change their orientation if their perceived level of stress exceeds a certain threshold value. Fibers continue to sense and change orientation until they reorient in a direction where perceived stress is below the strain threshold. In a similar model, Civelekoglu [101] introduces stress fiber binding with the extracellular substrate as a determinate of final fiber orientation. Fibers initially oriented perpendicular to the direction of stretch are less likely to unbind with the substrate as it is stretched, while fibers oriented parallel to the direction of stretch break their bonds with the substrate and are free to pivot. A separate model developed by De [102] also utilizes fiber pivoting and rotation phenomena, but further describes how cells adjust a force dipole within the cell to maintain constant levels of cellular and matrix stress.

Another commonly modeled phenomena as a means of describing cellular reorientation in response to cyclic stretch is the assembly, disassembly, and subsequent reassembly of actin fibers under stress. Hsu et al. [103], [104] developed a model where stress fibers have a defined rate of turnover dependent on applied stretch, where fibers tend to disassemble in directions with greater amounts of stretch and reassemble in directions where strain is decreased. Similar models, developed by Obbink-Huizer et al. [105], Qian

et al. [106], and Wang et al. [107] also utilize assembly and disassembly of fibers to predict an alignment response.

While previously developed mathematical models can predict certain experimental results, some models are phenomenological in nature, for example assuming fibers exposed to higher stresses rotate without giving an insight into why this might be. Other models do not consider processes likely important for cellular reorientation, the impact of force on the binding and unbinding of the actin fibers via integrins to the substrate, structural alterations to fibers, and the impact of myosin motors on the motion of actin fibers. Therefore, we developed a mechanistic, mathematical model that utilizes specific cell-substrate interactions to examine how cells are linked with their substrate, sense externally applied forces, alter their morphology, and reorient along their substrate as a function of applied cyclic stretch. This model builds upon the work of Odde and coworkers [70]–[72], who developed a computational model of the myosin-actin-integrin motor clutch system hypothesized by Mitchison and Kirschner [69].

4.2 Methods

4.2.1 Cyclic stretch of in vitro cell cultures

Lonza (Lonza, Morristown, NJ) human umbilical vein endothelial cells (HUVEC) were cultured with EGM-2 Bullet Kit media (Lonza, Morristown, NJ) and maintained below passage 8 to ensure constant cellular proliferation. A PDMS substrate was created by mixing a 10:1 mixture of Sylgard® 184 base and curing agent (Dow Corning, Auburn, MI), which was then degassed, poured into molds, and cured at 56°C for 1.5 hours until fully hardened. The stiffness of this substrate is estimated to be about 1 MPa [108]. The

casting was removed from the mold and autoclaved. A solution of $10\mu\text{g/mL}$ of human fibronectin in PBS was added to each well of the sterilized cast and allowed to coat overnight at 4°C and then aspirated. Cells were trypsinized, counted, and seeded on to the cast at a concentration of 4300 cells per well, and incubated for 24h at 37°C with 5% CO_2 to allow for cell adhesion. The casting was then placed in a customized NSC-A1 Single Axis Stepper Motor Controller + Micro-step Driver (Newmark Systems, Inc., Rancho Santa Margarita, CA). The setup was placed in an incubator at 37°C with 5% CO_2 with the stepper motor subjecting the casting and cells to cyclic stretch (Figure 4-2A). The control casting was similarly incubated with no cyclic stretch. After $\sim 24\text{h}$, the castings were removed from the incubator and the cells were fixed with 4% paraformaldehyde.

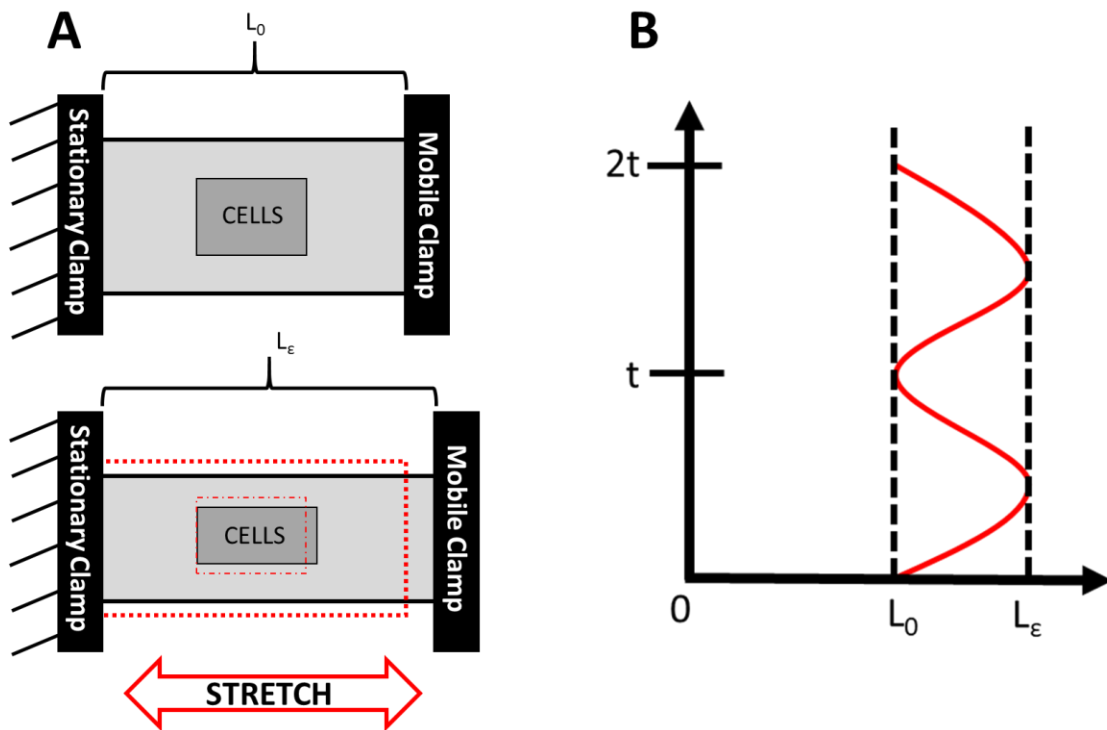


Figure 4-2: Experimental application of mechanical cyclic stretch to culture cells.

(A) Schematic of custom mechanical stretch device capable of applying cyclic strain to cell cultures. Device consist of two clamps attached to a motorized stage, where one clamp moves cyclically to stretch a PDMS slab. The PDMS slab contains wells in which cells are seeded. (B) Graphical representation of cyclic stretch waveform. Cultures are stretched from initial length L_0 to final length L_ϵ according to a sine function with period t .

Cells were permeabilized and stained for actin with 488 AlexaFluor phalloidin, and counterstained for nuclei with DAPI, after which they were imaged for fluorescence and Differential Interference Contrast (DIC). Microscopy images were exported as TIFF images and processed using ImageJ software for cell size, shape, and orientation. Stained actin fibers were analyzed using the ImageJ plug-in FibrilTool [109] for average actin fiber orientation and anisotropy for each cell. 50 – 100 cells were analyzed for each condition and results are presented as means. Independent simultaneous t-tests were performed to determine statistical significance of each stretch condition compared to the no stretch control condition. To control for multiple comparison associated Type I error, the Bonferroni correction [110] was utilized to determine a new statistical significance level. Specifically, the initial significance level of 0.05 was reduced to 0.0125.

4.2.2 Motor-clutch model of cell substrate interactions

Computational simulations utilized the adapted motor-clutch model described in Chapter 2. All simulations were run for a total time of 24 hours unless otherwise noted. Simulation data is presented as an average of 10 individual simulations.

4.3 Results and Discussion

4.3.1 In vitro cell and actin fiber orientation as a function of the amplitude of simple cyclic elongation

Changes in the morphology of cells exposed to cyclic stretch are well-documented [25]–[30], [30]–[33]. The large majority of these studies, however, analyze either cell or actin fiber orientation without quantifying other metrics of cellular morphology such as shape (e.g., aspect ratio) and elongation. Since our computational model can make predictions related to both changes in actin bundle orientation and length, which in turn influence cell shape, it is useful to have experimental data for each of these metrics. Due to differences in the cyclic loading experiments across reports including stretch type, magnitude, and frequency of stretch as well as cell types used, it is difficult to compare the effects of cyclic stretch on different metrics taken from different experiments. Thus, we collected a self-consistent set of experimental data that explored how these metrics changed as amplitude of stretch was varied (Figure 4-3).

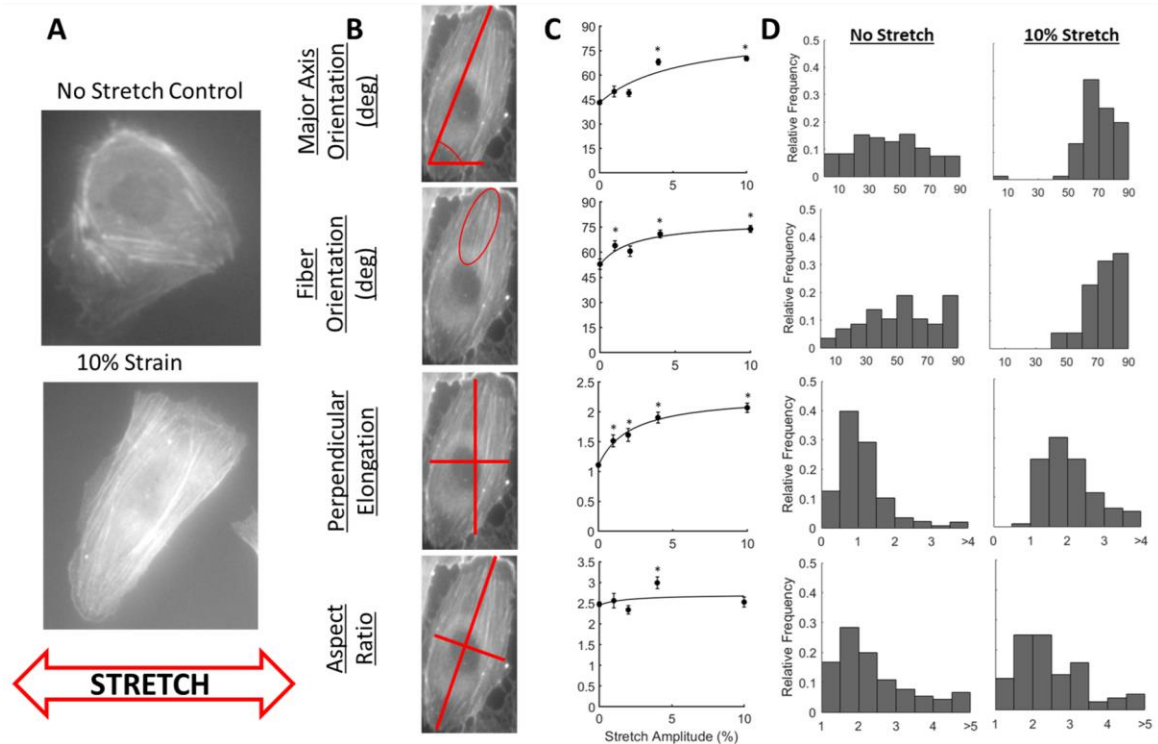


Figure 4-3: In vitro cellular morphology changes as a function of applied cyclic stretch.

(A) Representative images of HUVEC cells exposed to no stretch control and 10% stretch conditions. (B-D) Cellular morphological measurements collected as a function of applied cyclic stretch. From left to right, visual descriptions of each measurement collected, average measurements (* denotes statistical significance with p-value < 0.0125 according to Bonferroni multiple comparisons correction, bars on data points represent SEM), and representative frequency distribution histograms from no stretch control and 10% stretch conditions, n = 50 -100 cells for each condition.

In our experiments, exposing cultured cells to simple uniaxial cyclic elongation, cells reoriented their major axis away from the direction of applied stretch (Figure 4-3B-D row 1). Similar to that reported by others [97], increasing the magnitude of stretch increased the angle (from 49.94 degrees with 1% stretch to 73.88 degrees with 10% stretch) (Figure 4-3B-D row 1). Similarly, actin fibers within the cell tend to realign to a similar angle when exposed to cyclic stretch (Figure 4-3B-D row 2). With increasing stretch

amplitude, cells also tend to be longer along the axis perpendicular to the direction of stretch compared to their length along the axis parallel to stretch (Figure 4-3B-D row 3). However, data suggest that cell shape is not altered by cyclic stretch as cellular aspect ratio (ratio of major axis length to minor axis length) is unchanged, with the exception of the 4% amplitude case (Figure 4-3B-D row4).

4.3.2 Experimental data informs biophysical processes that could potentially lead to actin reorientation.

As noted in section 4.1.2 and Figure 4-1B, there are at least three non-exclusive mechanisms that could lead to changes cellular alignment in response to cyclic stretch. By measuring only changes in cell shape or orientation, it is not possible to exclude any of these three mechanisms. Experimental measurements, however, reveal a change in actin orientation, which can only be accounted for by cyclic stretch preferentially altering fiber rotation (Figure 4-1B) or actin assembly/disassembly (Figure 4-1B). Thus, we explored the case where actin bundles can rotate as a potential mechanism of cellular reorientation in response to applied cyclic stretch.

4.3.3 Type of cyclic stretch and actin reorientation.

To directly compare our model results with our experimental observations of cellular and actin fiber reorientation, we analyzed the effect of cyclic stretch on simulated actin bundle orientation. Under simulation conditions most comparable to our experimental conditions (simple elongation, high substrate stiffness (10 kPa), cyclic stretch frequency of 1 Hz, and 24 hours of stretching), bundles align to an angle of $55.44 \pm 0.12^\circ$ relative to the direction of applied stretch (Figures 4-4A and 4-5A). Notably, this angle is similar to the angle calculated for the axis of minimal strain for simple elongation of an incompressible

material (54.74°) [111], (Figure 4-4A, red dotted line). As noted by others, the calculated angle of minimal strain is similar to the orientation of cells cultured on a substrate subjected to simple cyclic elongation (Figure 4-4A and Table 4-1 Row 1, Type of Stretch) [31], [33], [97].

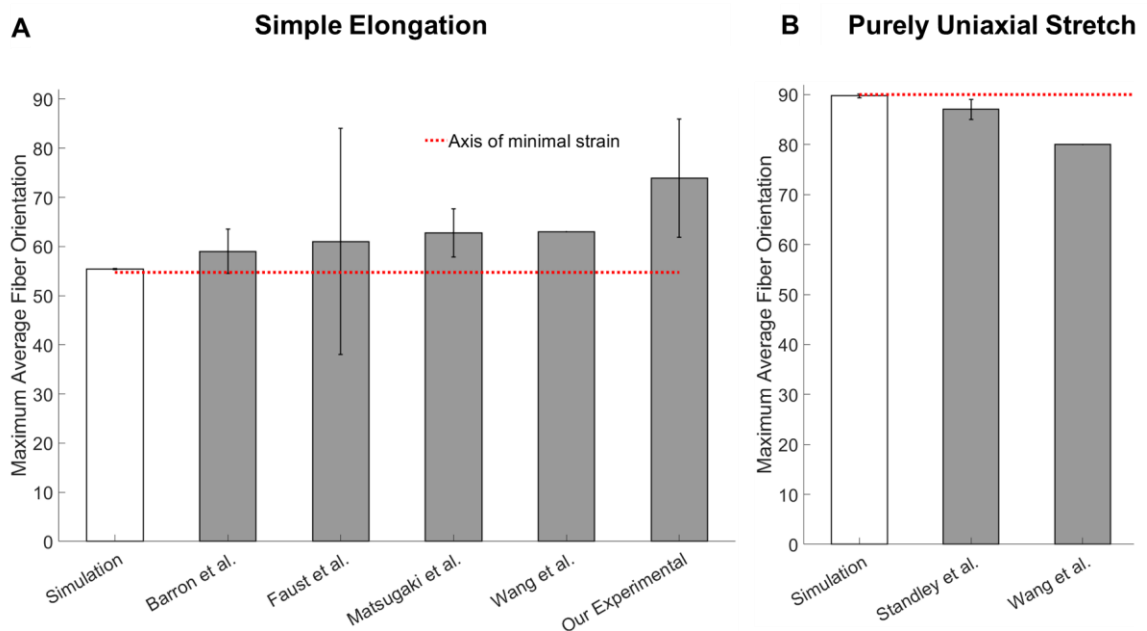


Figure 4-4: Simulated and in vitro maximum reported actin fiber and/or cell orientation.

Relative to the direction of applied stretch, following exposure to cyclic stretch. (A) Actin fiber and/or cell orientation following exposure to simple elongation cyclic stretch. (B) Actin fiber and/or cell orientation following exposure to purely uniaxial cyclic stretch.

In simulations of actin bundles exposed to purely uniaxial stretch (i.e., no deformation of the substrate in the direction perpendicular to the applied stretch), actin bundles align to an

angle of $89.74 \pm 0.38^\circ$ relative to the direction of applied stretch (Figures 4-4B and 4-5B). Again, the direction the actin bundles orient in the simulation is similar to the direction of minimal strain (90 degrees for purely uniaxial strain). This simulation finding is consistent with the experimental results of others that used systems that generated purely uniaxial stretch (Figure 4-4B, Table 4-1 Row 2, Magnitude of Stretch) [26], [27], [29]. Thus, for both simple elongation and purely uniaxial cyclic stretch, the simulations predict that actin bundles reorient to the direction of minimal strain, which is generally consistent with experimental observations (Figure 4-4).

Others have reported that both cells and actin fibers do not align with a preferred orientation following exposure to cyclic equibiaxial stretch [34], [112]. For example, initially randomly oriented cell populations remain randomly oriented following equibiaxial stretch. Following 24 hours of equibiaxial cyclic stretch, simulated actin bundles do not alter their orientation (e.g., a bundle with an initial orientation of 15 degrees remains at 15 degrees following stretching) (Figure 4-5E). Therefore, our adapted model accurately predicts the experimental observation of no preferential realignment of cells or actin fibers following equibiaxial cyclic stretch.

Simulation predictions	In vitro experimental observations
Type of stretch	
Simple Elongation: Actin bundles typically (with many parameters sets) align ~55-60 degrees relative to direction of applied unconfined cyclic stretch (Figure 6A).	In vitro experiments utilizing unconfined cyclic stretch, both ours and others report actin alignment along an axis of minimal strain, ~55-65° relative to direction of applied stretch (Figures 4 and 5B) (Wang et al., 2001; Barron et al., 2007; Faust et al., 2011; Matsugaki et al., 2013).
Purely uniaxial stretch: Actin bundles typically (with many parameters sets) align perpendicular relative to direction of applied purely uniaxial confined cyclic stretch (Figure 6B).	Others report actin realignment ~90° relative to direction of applied cyclic strain (Figures 4 and 5B) (Wang et al., 2001; Standley et al., 2002).
Equibiaxial stretch: Actin bundle orientation is not changed following exposure to equibiaxial cyclic stretch (Figure 6E).	Randomly oriented cell populations remain randomly oriented follow exposure to equibiaxial cyclic stretch (Wang et al., 2001; Kaunas et al., 2006).
Magnitude of stretch	
Dose response: For moderate and high substrate stiffness, final angle of reorientation increases (toward perpendicular) with increasing amplitude of cyclic stretch (Figure 6), until reaching perpendicular.	We and others show increasing cellular and actin fiber reorientation with increasing stretch amplitude (Faust et al., 2011).
For high substrate stiffness, amplitude of cyclic stretch affects rate of actin bundle realignment, where increasing amplitude increases rate of realignment (Supplemental Figure 2).	Rate of reorientation is affected by amplitude of cyclic stretch., where characteristic time of reorientation decreases linearly with increasing stretch amplitude (Jungbauer et al., 2008).
Minimal effective dose: Significant realignment is noticeable with stretch amplitudes as low as 0.1% (Figure 6).	We and others show significant realignment with stretch amplitudes as low as 1% (Faust et al., 2011), while others report minimum stretch amplitudes greater than 1% required for reorientation response (Nava et al., 2020).
Frequency of stretch	
For high substrate stiffness, frequency of cyclic stretch affects rate of actin bundle realignment, where increasing frequency increases rate of realignment exponentially (Figure 7A).	Rate of cellular reorientation is affected by frequency of cyclic stretch, where the characteristic time required for reorientation decreases with increasing frequency. For confluent cell cultures, characteristic time decreases exponentially (Jungbauer et al., 2008).
Frequency has no effect on final angle of orientation (Figure 7).	Frequency affects final angle of orientation, where final angle of reorientation increases with increasing frequency (Jungbauer et al., 2008).
Substrate stiffness	
For low substrate stiffness, actin bundles align parallel to the direction of applied cyclic stretch (Figure 6D).	Others have reported realignment parallel to the direction of applied cyclic stretch on soft collagen substrates (Tondon and Kaunas, 2014).
Myosin motors	
Reducing myosin motor stall force by one order of magnitude completely eradicates actin bundle reorientation in response to cyclic stretch (Figure 8).	Blocking myosin-II function through the use of blebbistatin eliminates perpendicular reorientation of cells in response to cyclic stretch (Goldyn et al., 2010; Greiner et al., 2013).

Table 4-1: Comparison of simulation predictions and in vitro experimental observations.

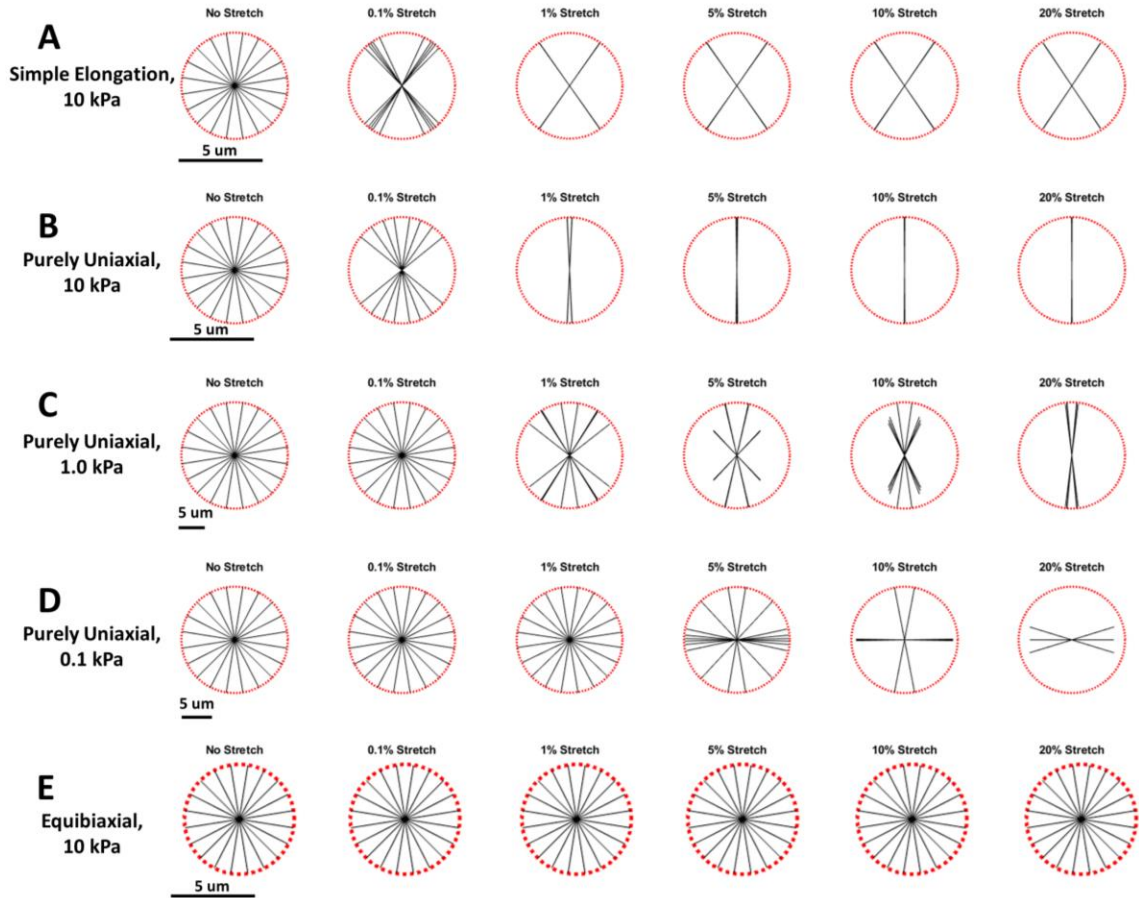


Figure 4-5: Simulated actin bundle reorientation.

Bundles with initial orientations ranging from 0-90 degrees are grouped into cells to create a single figure representing a whole cell. Single bundles in each cell represent the average final orientation and length of ten simulated bundles ($n = 10$). Individual bundles were modeled using the adapted motor-clutch model with an initial length of 5000 nm, orientation ranging 0-90 degrees, and on substrate stiffnesses ranging 0.1-10 kPa. Modeled actin bundles were then exposed to simulated simple substrate elongation (A), purely uniaxial cyclic stretch (B-D), or equibiaxial cyclic stretch (E) with frequency of 1 Hz and variable amplitude following which, bundle length and final orientation was collected. Red circles around bundles represent average size of bundles under no stretch control condition for each substrate stiffness.

4.3.4 Amplitude of stretch and actin reorientation.

In general, simulated actin bundle reorientation increases (towards perpendicular to direction of applied stretch) with increasing stretch amplitude for moderate and high substrate stiffness and towards parallel for low substrate stiffness (Figure 4-5). To compare simulation results to experimental observations, we first focused on the high substrate stiffness case since we and most others used this condition in experiments. For simulations of high substrate stiffness, bundle reorientation begins for stretch amplitudes as small as 0.1% and reaches maximum reorientation at 1% stretch. Interestingly, there is very little difference in final orientation with amplitude increasing from 1 to 20%. Our in vitro studies (Figure 4-3) and the work of others [97] report significant realignment of fibers with stretch amplitudes as small as 1% with further realignment with increasing amplitude. Some have reported no significant realignment with amplitudes lower than 5%, but significant realignment following exposure to 40% stretch [113]. Thus, across various in vitro studies, there is a range of stretch amplitudes required for significant cell and actin alignment, but the amplitude required by our simulations is less than this range (Table 4-1 row 2, Magnitude of Stretch). It is not surprising that we did not see quantitative agreement between the stretch amplitude required to achieve significant alignment in simulation and experimental results since we did not attempt to optimize our model parameters to better fit the experimental data. Odde and coworkers have shown that varying the parameters in a version of the motor clutch model that does not account for cyclic stretch can vary the mechanical stimuli required for a specific response by several orders of magnitude [71],

[72]. Though beyond the scope of this current study, model parameters likely could be optimized to provide better quantitative agreement.

Jungbauer et al. reported that increasing stretch amplitude decreased characteristic time of reorientation [32]. We ran simulations with a range of amplitudes from 1% to 20%, with other parameters held constant. As amplitude was increased, the time it took for actin bundles to reach their final orientation decreased (Figure 4-6, Table 4-1 Row 2 Magnitude of Stretch), consistent with the experimental results. Therefore, the motor clutch model can predict the qualitative effects of stretch amplitude on both the rate and steady-state value of actin alignment in response to cyclic stretch.

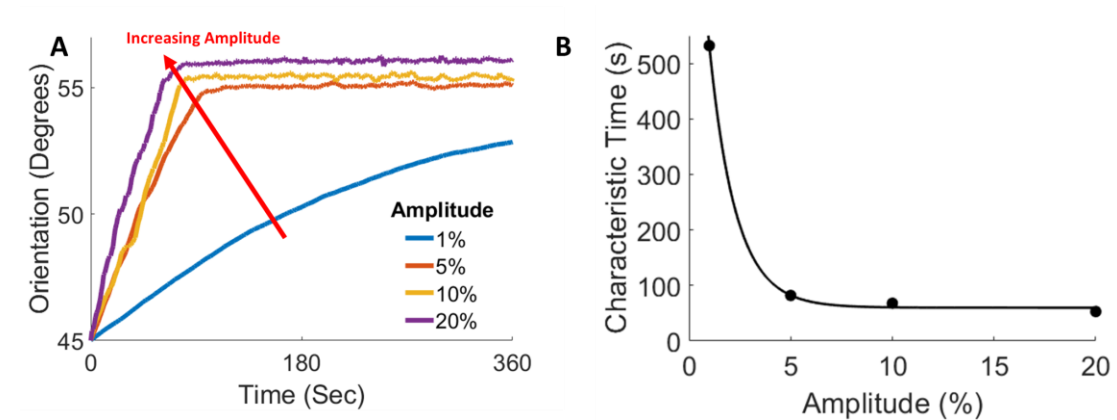


Figure 4-6: Actin bundle reorientation as a function of cyclic stretch amplitude.

Actin bundles are modeled with simple elongation cyclic stretch with a frequency of 1 Hz and variable amplitude for 24 hours on a substrate stiffness of 10 kPa. (A) Reorientation over time with variable cyclic stretch amplitude. (B) Characteristic time required for reorientation as a function of cyclic stretch amplitude.

4.3.5 Frequency of stretch and actin reorientation.

Relative to studies of the effect of stretch amplitude, there have been far fewer experiments studying the impacts of stretch frequency on cell and actin reorientation. Jungbauer et al. reported that increasing the frequency of cyclic stretch of a PDMS substrate decreased the characteristic time required for 2 different types of fibroblasts to reorient [32]. Under simulation conditions most comparable to their experimental conditions (simple elongation, 10% stretch, and high substrate stiffness (10 kPa), 24 hours of stretching), we observed that increasing stretch frequency decreased the characteristic time required for reorientation (Figure 4-7A). However, stretch frequency has no impact on final bundle orientation in simulations, which is in contrast with Jungbauer's observation of increasing final orientation with increasing stretch frequency (Table 4-1 row 3, Frequency of Stretch).

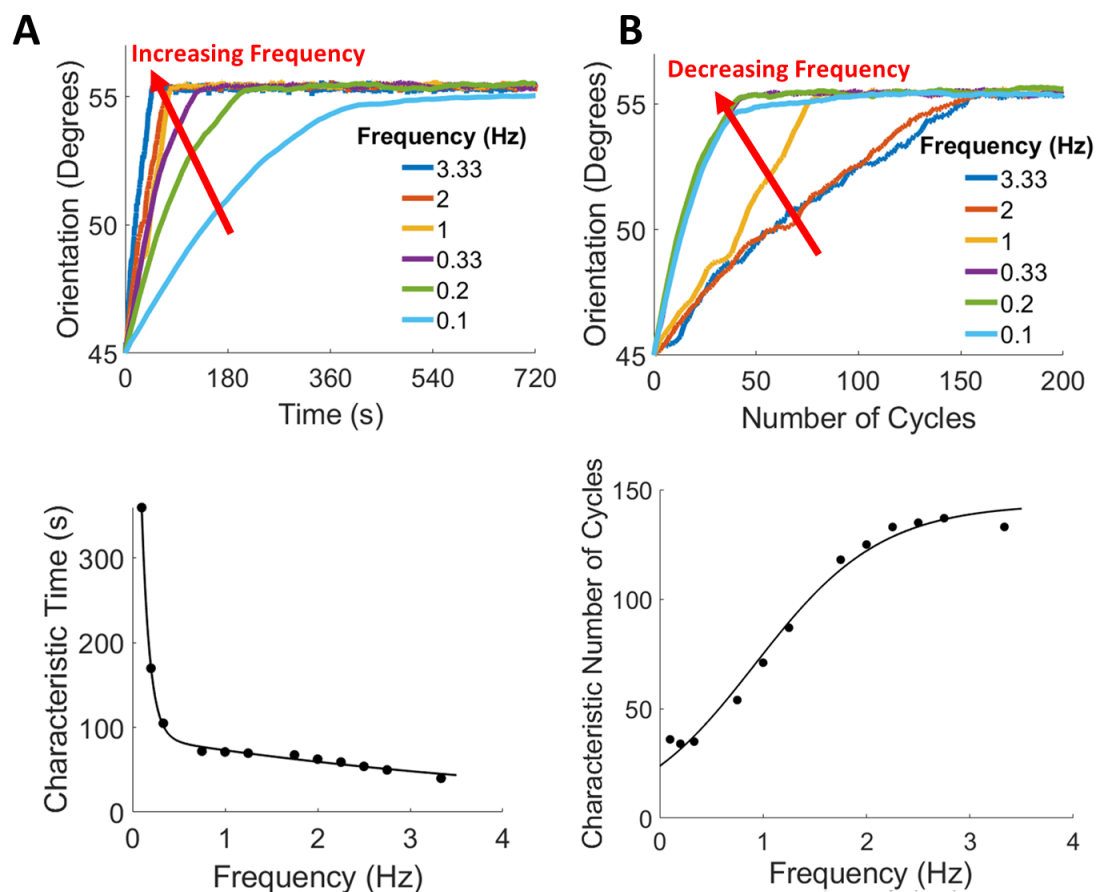


Figure 4-7: Actin bundle reorientation as a function of cyclic stretch frequency. Actin bundles are modeled with 10% simple elongation cyclic stretch for 24 hours on a substrate stiffness of 10 kPa. (A) Reorientation over time with variable cyclic stretch frequency (top) and resultant characteristic time required for reorientation, or time required for a bundle to reach an orientation that is equal to 98% of its steady state orientation (bottom). (B) Reorientation as a function of number of cyclic stretch cycles with variable stretch frequency (top) and resultant characteristic number of cycles required for reorientation, or number of cycles required for a bundle to reach 98% of its steady state orientation (bottom).

We reasoned that one potential explanation for actin bundles aligning more quickly when stretched at higher frequencies is that they simply experience a greater number of stretch cycles over a given time. Plotting the average actin bundle angle as a function of

the number of cycles (Figure 4-7B) reveals that curves that represent lower frequencies (0.1 to 0.33 Hz) largely overlap. Similarly, curves representing higher frequencies (>2 Hz) tended to overlap, but they were clearly distinct from those for lower frequencies. The curve for an intermediate frequency of 1 Hz fell between the two groups of curves. Taken together, these results suggest that the number of cycles is an important but not the only determinant in the extent of fiber reorientation.

4.3.6 Substrate stiffness and actin reorientation.

While holding all other parameters constant, decreasing substrate stiffness by one order of magnitude (from 10 to 1 kPa) diminishes the perpendicular reorientation response to simple elongation (Figure 4-5) and purely uniaxial cyclic stretch (Figure 4-8). That is, at a given stretch amplitude, actin bundles aligned closer to the perpendicular direction with the higher substrate stiffness (Figure 4-5B vs. 4-5C) and a smaller stretch amplitude was required to approach maximal alignment with higher stiffness. However, decreasing substrate stiffness further (from 1 to 0.1 kPa) results in a more complex behavior (Figure 4-5D). At the lowest stretch investigated (0.1% stretch), there was negligible reorientation of actin bundles. With increasing levels of stretch, a greater fraction of the actin bundles aligned parallel to the applied stretch until the highest stretch where all bundles are aligned nearly parallel to the stretch. While we used only a single, relatively stiff, substrate in our *in vitro* cyclic stretch experiments, others have previously reported the *in vitro* parallel alignment of cells on soft extracellular substrates exposed to simple elongation [114]. Thus, our model can reproduce both the perpendicular alignment of fibers when cells are

stretched on relatively stiff substrates and the parallel alignment seen on relatively soft substrates (Table 4-1 row 4, Substrate Stiffness).

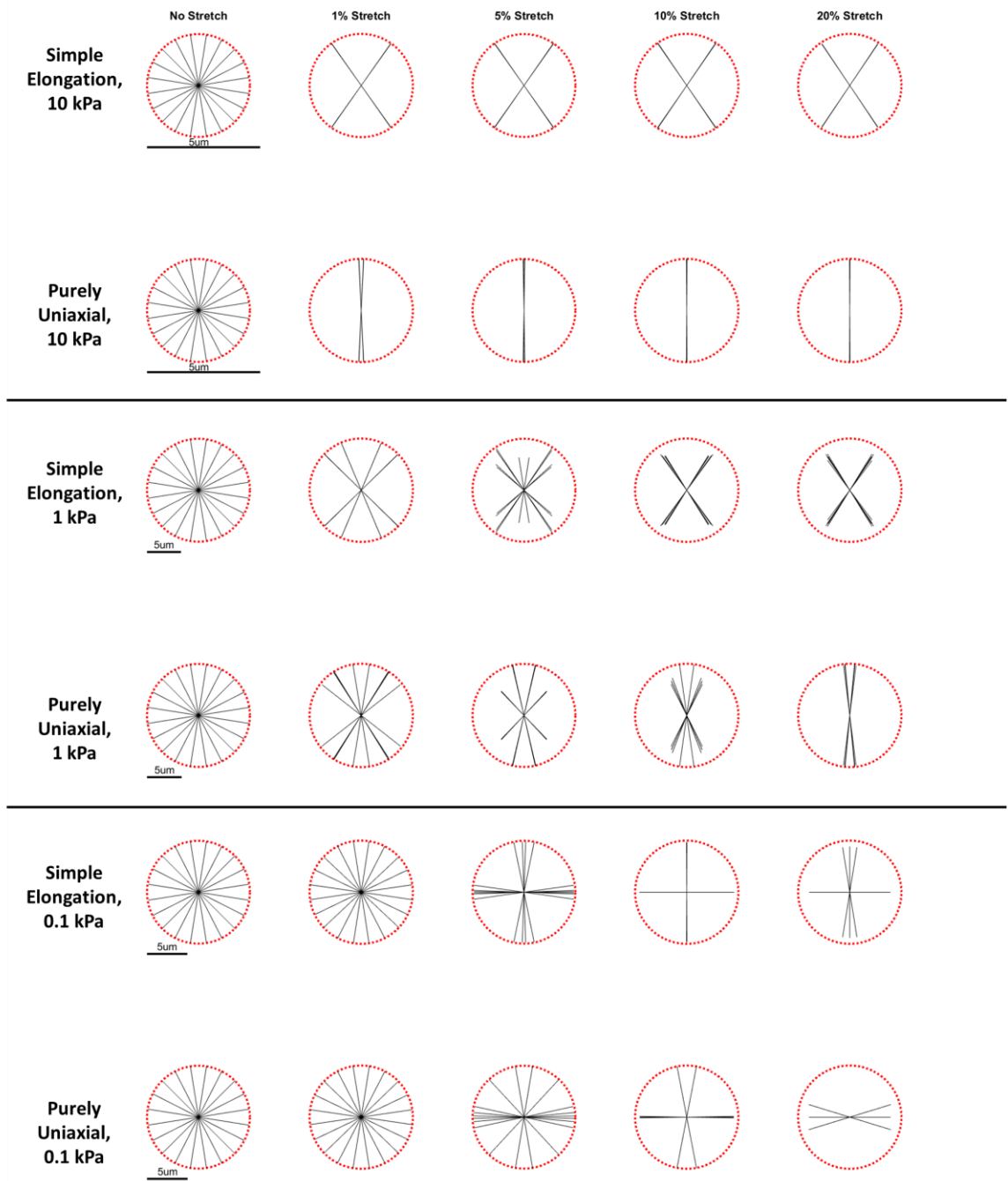


Figure 4-8: Actin bundle reorientation as a function of both substrate stiffness and cyclic stretch type.

4.3.7 Myosin motor function is required for actin bundle reorientation response.

Blocking myosin motor function with the myosin II muscle and non-muscle myosin ATPase inhibitor blebbistatin significantly reduces or eliminates the reorientation response to cyclic stretch in vitro [39], [99]. Blebbistatin alters myosin motor function by binding to the myosin complex at the actin binding interface, effectively blocking any myosin-actin interaction [115].

We interpret the effects of blebbistatin to be incorporated in the motor clutch model through alterations to the myosin motor stall force parameter, F_m . As blebbistatin decouples actin-myosin bonds, the actin bundle is free to move without influence from the myosin motors. In the model, decreasing F_m decreases the amount of force required to stall myosin motors and, therefore, allow the actin bundle to move independently. Reducing F_m on level of a single order of magnitude nearly eradicates reorientation response, especially when analyzing stretch amplitudes comparable to those utilized in in vitro experiments (Figure 4-9). Specifically, a stall force of 0.1 pN results in no changes in actin bundle reorientation on any substrate stiffness, even with increased levels of stretch amplitude, up to 10% stretch (Figure 4-9B). Final average orientation also decreases with decreasing F_m (Figure 4-9B), suggesting a potential dose response to myosin motor function. Thus, our model accurately predicts the effects of blebbistatin and proper myosin motor function on the reorientation response to cyclic stretch through alterations to myosin motor stall force (F_m).

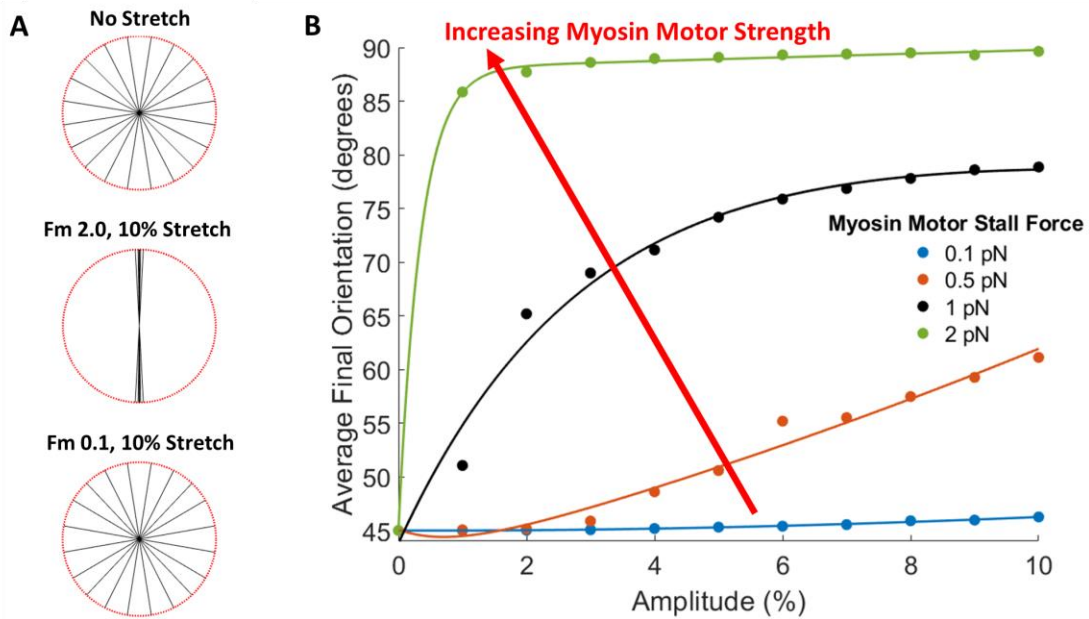


Figure 4-9: Simulated actin bundle reorientation as a function of motor-clutch model myosin motor function.

(A) Actin bundle final orientation as a function of cyclic stretch and myosin motor stall force, F_m . (B) Average final bundle orientation as a function of stretch amplitude and myosin motor stall force, F_m .

4.3.8 Mechanism by which cyclic stretch causes changes in actin bundle orientation.

Experimental (Figure 4-3) and computational results (Figure 4-5) show that cells and/or actin bundles within cells alter their orientation in response to applied cyclic stretch. While most conditions result in perpendicular reorientation, under certain conditions (Figure 4-5D) bundles may align parallel to the direction of applied stretch. Factors such as initial bundle orientation, type of cyclic stretch, cyclic stretch frequency, stretch magnitude, and extracellular substrate stiffness all impact direction of bundle realignment (Figures 4-5 and 4-7). We considered whether these factors work through a common mechanism. We reasoned that during the relative rare times when there were no clutched bound to the

substrate, a condition we called a cell-substrate detachment event, both the actin bundle and the extracellular substrate are free to move independent of one another. Independent movement then allows for large changes in the relative position between the bundle and the substrate resulting in changes in overall fiber orientation. Moreover, as illustrated in Figure 4-10, we anticipated that timing of the detachment event in relation to the cyclic stretch cycle will influence how the angle of the bundle will change, where failure during stretching of the substrate will increase the angle between the bundle (i.e., toward perpendicular) and substrate and failure during relaxing will decrease the angle between the bundle and substrate (toward parallel). Thus, we hypothesized that conditions that lead to a greater chance for bond failure to occur during the stretching phase will favor perpendicular alignment while conditions that lead to a greater chance for bond failure to occur during the relaxing phase will favor parallel alignment.

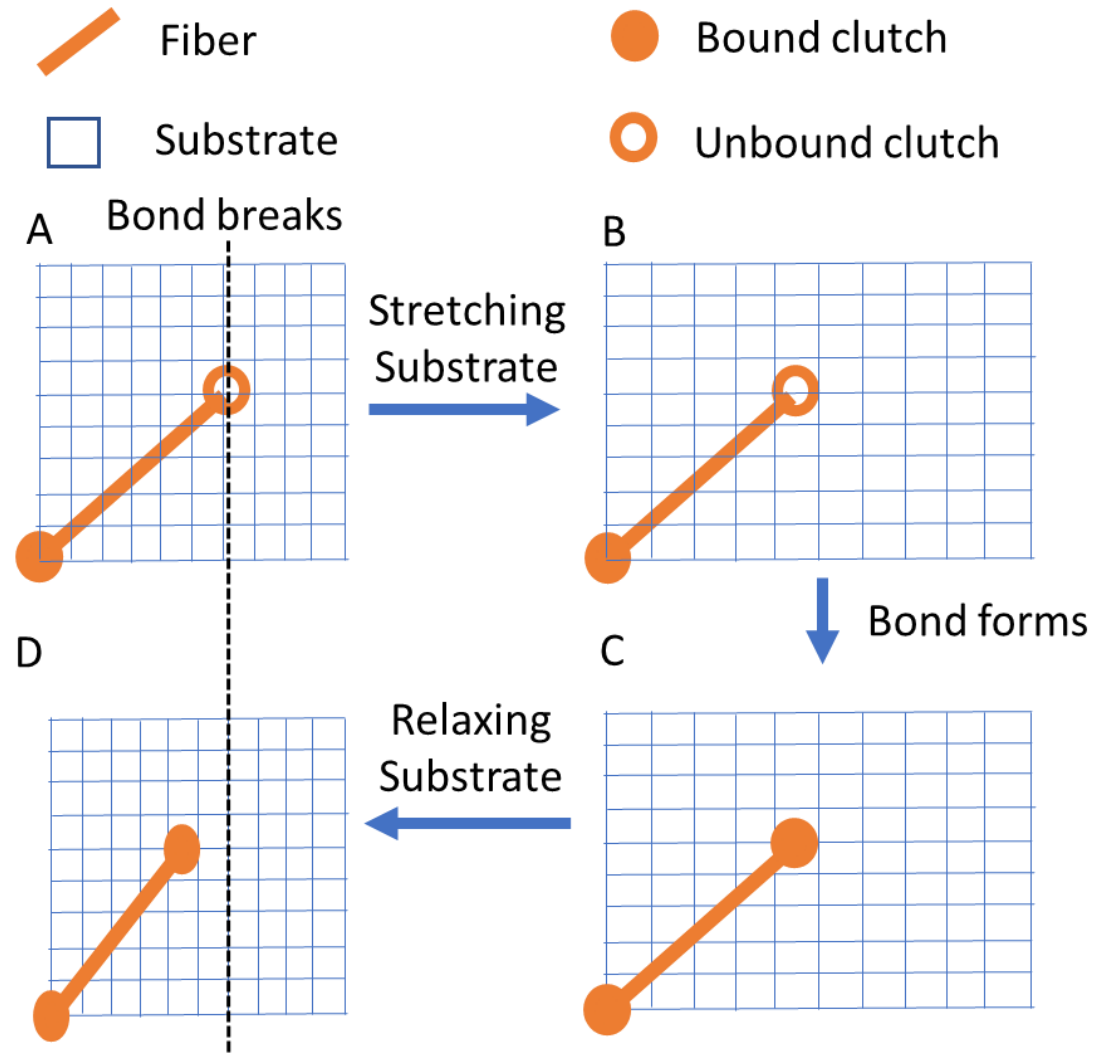


Figure 4-10: Clutch bond failure timing.

Timing of clutch bond failure influences direction of fiber alignment. A clutch unbinds as the substrate is stretching (A) allowing the substrate to move relative to the fiber (B). The clutch bond reforms (C), allowing the fiber and substrate to move together where (D) the final position of the fiber has rotated relative to its initial position (dotted line).

To test this hypothesis, we first calculated how often detachment events (i.e., no bound clutches) occurred during the stretching and relaxing phases of cyclic stretch of the substrate (Figure 4-11, top row). In some stretch conditions, the number of detachment

events is consistently greater during the stretching phase (Figure 4-11A) while other stretching conditions tend to have more detachment events during the relaxing phase (Figure 4-11, middle row). For some stretching conditions, however (Figure 4-11C), whether more detachment events occur during stretching or relaxing is dependent on the initial orientation of the actin bundle. Since our hypothesis focuses on whether detachment events were more likely during the stretching or relaxing phase, we calculated the difference between the two (Figure 4-11, middle row). A difference greater than 0 corresponds with a greater number of detachment events occurring during the stretching phase, and a difference less than 0 corresponds with a greater number of detachment events occurring during the relaxing phase. Therefore, a positive difference would predict perpendicular reorientation while a negative difference would predict parallel reorientation. An analysis of bundle reorientation over time shows that, consistent with our hypothesis, conditions that caused more detachment events during stretching of the substrate (blue line, Figure 4-11A) than during relaxing of the substrate (red line, Figure 4-11A) occur as the bundles rotated toward perpendicular to the direction of applied stretch (Figure 4-11A, bottom). Conversely, conditions that caused more detachment events during relaxation lead to parallel realignment (Figure 4-11B).

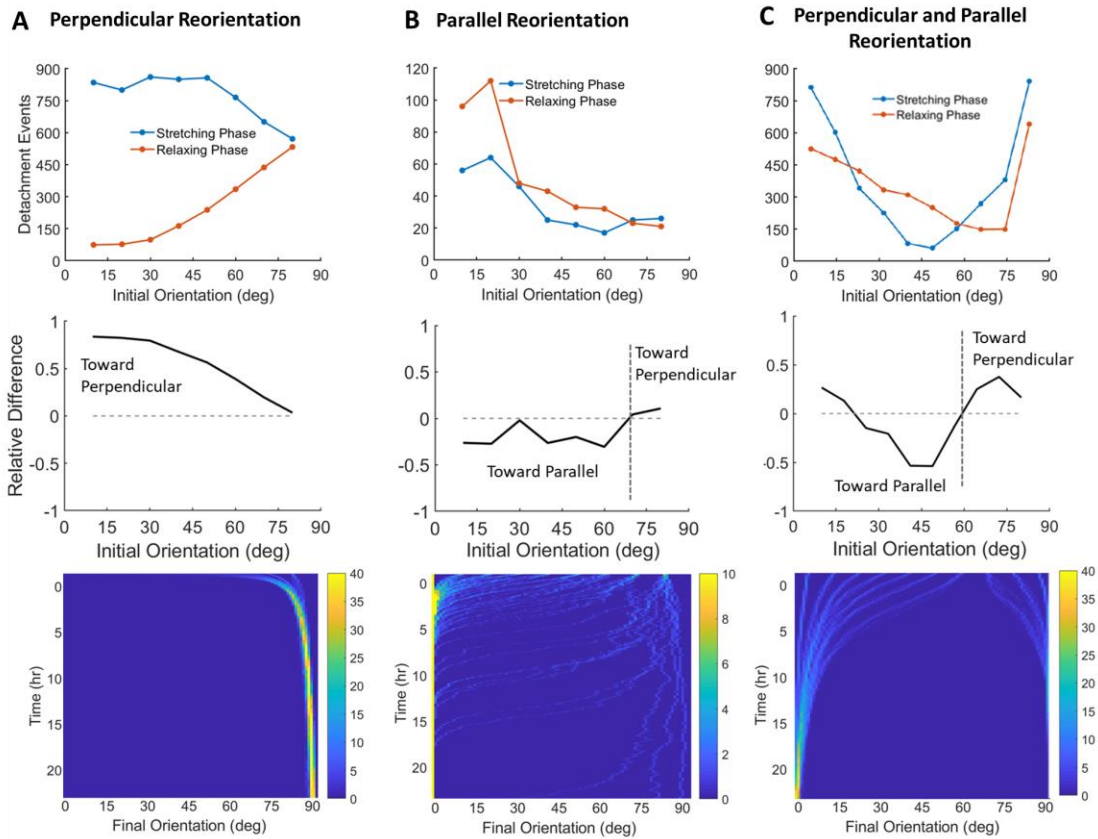


Figure 4-11: Proposed mechanism for changes in actin bundle orientation.

Detachment events, moments where the actin bundle is completely detached from the substrate (i.e., no bound clutches), are counted during both the stretching and relaxing phase of the cyclic stretch regime for bundles with initial orientations (Top). Differences in stretching phase events and relaxing phase events are plotted, where differences > 0 predict perpendicular reorientation and differences < 0 predict parallel reorientation (middle). Simultaneously, actin bundle reorientation is tracked over a course of 24 hours of cyclic stretch (Bottom). (A) Perpendicular realignment of all actin bundles on stiff substrates (10 kPa). Detachment events are significantly increased during the stretching phase compared to relaxing phase, which corresponds with rapid perpendicular realignment. (B) Parallel realignment of actin bundles on soft substrates (0.1 kPa). For many bundles, detachment events are increased during the relaxing phase of stretching, which corresponds to parallel realignment. (C) Increased detachment events fluctuate between the stretching and relaxing phase corresponding with both parallel and perpendicular realignment of actin bundles for cases with decreased frequency and stiffness (0.5 kPa, 0.5 Hz). Bundles with initial orientations < 65 degrees align parallel to stretch while bundles initially oriented > 65 degrees orient perpendicular to stretch. Color bars represent number of bundles at each data location.

Interestingly, bundles exposed to the same extracellular conditions (stiffness, frequency and amplitude of stretch) can experience changes in reorientation based solely on their initial orientations. For example, this behavior is seen in the simulation results for 10% stretch on soft substrate (Figure 4-5). Other conditions lead to more pronounced changes where bundles align either parallel or perpendicular to that applied stretch, depending on the initial angle of the bundle (Figure 4-11C). Again, consistent with our hypothesis, relative number of detachment events in the stretching and relaxing phase correctly predicts the direction of fiber rotation.

While these observations support the hypothesis relating timing of detachment events to direction of bundle rotation, not all observations can be explained solely by this hypothesis. For example, in Figure 4-11C, for initial angles from 10° to 25° , the relative number of detachment events predicts bundle rotation perpendicular to the direction of stretch, when the bundles actually reorient parallel to the direction of stretch (i.e., difference between detachment events is greater than 0 which would typically correspond to perpendicular realignment). The ability of the relative number of detachment events to explain the direction of bundle rotation in most but not all cases suggests that other factors also play a role. Other potential factors could be related to the stretch rate during detachment events (which varies through the sinusoidal cyclic stretch) or where within either the stretching or relaxing phase detachment occurs (e.g., detaching at the beginning of a stretch phase could have a different effect than detaching at the end of the same stretching phase even though stretch rates are the same).

4.3.9 Model capabilities, limitations, and opportunities for improvements.

The motor clutch model is based on established molecular processes and has been shown to describe previously known cell-substrate interactions, and make specific predictions, which were subsequently observed experimentally [70]–[72]. Our modifications to the model to account for exogenously applied substrate stretch predicts and gives mechanistic insights into changes in actin bundle orientation as well as cellular morphology in response to cyclic stretch. Despite these accomplishments, the model has several limitations. As with other computational models of the motor-clutch, the equations used to describe specific behaviors are reasonable but simplified descriptions and not all potentially relevant processes are modeled. For example, in our model, each bundle is considered independent of others. In cells, however, one would expect steric interactions between fibers preventing one to move independent of its neighbors. The ability of the modeled bundles, but not ones in real cells, to rotate independently of one another is likely why the model can predict two different preferred orientations of bundles within a given cell (Figure 4-5D) while experimental observations reveal that most actin bundles within a given stretched cell have similar alignment (Figure 4-3). One can envision a model of multiple actin bundles that considers steric interactions between fibrils, but this is beyond the scope of the work here. As a simpler alternative, we suggest that the *probability* of an experimental cell will have most of its bundles in a given direction after exposure to cyclic stretch is the *percentage* of bundles in that direction at the end of a model simulation where the bundles were originally uniformly distributed.

In addition to predicting bundle orientation, this model also can predict the effects of cyclic stretch on bundle length, another potential mechanism by which cyclic stretch alters cellular morphology (Figure 4-1). Examples of this can be seen in Figure 6, where simulating 5 and 10% stretch for 24 hours changed the initially uniform bundle lengths to different lengths. Notably, bundles oriented more parallel to applied stretch were shorter than those oriented more perpendicular, which is consistent with cells aligning away from the direction of applied stretch. The ability of this model to explore how cyclic stretch alters bundle lengths merits further investigation but is beyond the scope of this study.

The parameters used in our adapted model are the same selected by Odde and coworkers in their investigation of how substrate stiffness alters clutch binding and actin bundle motion [70]–[72]. The parameters selected were often chosen from a range of experimental values and could be considered as useful for a generic cell. As they showed in their later work, altering model parameters can be used to better match model predictions for experimental data from specific cell types [71], [72]. Similarly, there is an opportunity in future work to improve the agreement between our model predictions and experimental results by altering model parameters.

4.4 Conclusions

A computational simulation of the motor clutch system that accounts for cyclic stretch of the substrate was developed. The major findings from the computational model are 1) actin bundles align roughly perpendicular to the direction of the applied stretch, $\sim 90^\circ$ for pure uniaxial stretch and $\sim 56^\circ$ for simple elongation stretch. In both cases these directions coincide with the direction of minimal strain. 2) Under specific conditions, such as low

substrate stiffness, actin bundles are predicted to align parallel to the direction of stretch.

3) Increasing stretch amplitude tends to promote a greater degree of predicted actin bundle alignments while increasing the stretch frequency tends to increase the rate at which fibers reorient. 4) Myosin motor function is critical in the perpendicular reorientation response.

All these model predictions are generally in good agreement with the experimental data (Table 4-1). The model suggests that though a number of factors including stretch amplitude, stretch frequency, substrate stiffness and initial bundle orientation can influence the reorientation of bundles, the impact of all of these factors can largely be understood in light of their impact on cell-substrate detachments events. Conditions that lead to more detachment events occurring when the substrate is stretching than when the substrate is relaxing cause the bundles to orient away from the direction of applied stretch. Conversely, conditions that lead to more detachment events when the substrate is relaxing cause alignment toward the direction of applied stretch.

Chapter 5 Discussion and Future Directions

5.1 Volume overload heart failure mechanics and impacts on cell function

Heart failure is a progressive disease resulting from initial changes in hemodynamic load. Our group has spent time studying a specific altered hemodynamic load referred to as volume overload (VO) which if pathophysiologic, can result in heart failure. VO is defined as an increase in cardiac pre-load (end-diastolic volume), or filling of the heart, which can be physiologic (e.g., during exercise) [116] or pathophysiologic often as a result of septal defects or mitral valve regurgitation. As pre-load increases to VO levels, the heart dilates, stretching the myocardium and cells embedded within. While this initial structural change increases contractility due to the Frank-Starling mechanism, eventually the chambers are stretched beyond optimal amounts for increased contractility. Beyond this optimum strain level, the chambers distend and progressively weaken, eventually leading to HF. In both initial and compensatory stages of VO HF, ECM maintenance and production is decreased [117]. Our group has also shown that myocardial tissue from VO hearts is less stiff (i.e., decreased modulus) than normal myocardial tissue (Figure 5-1) [118], [119].

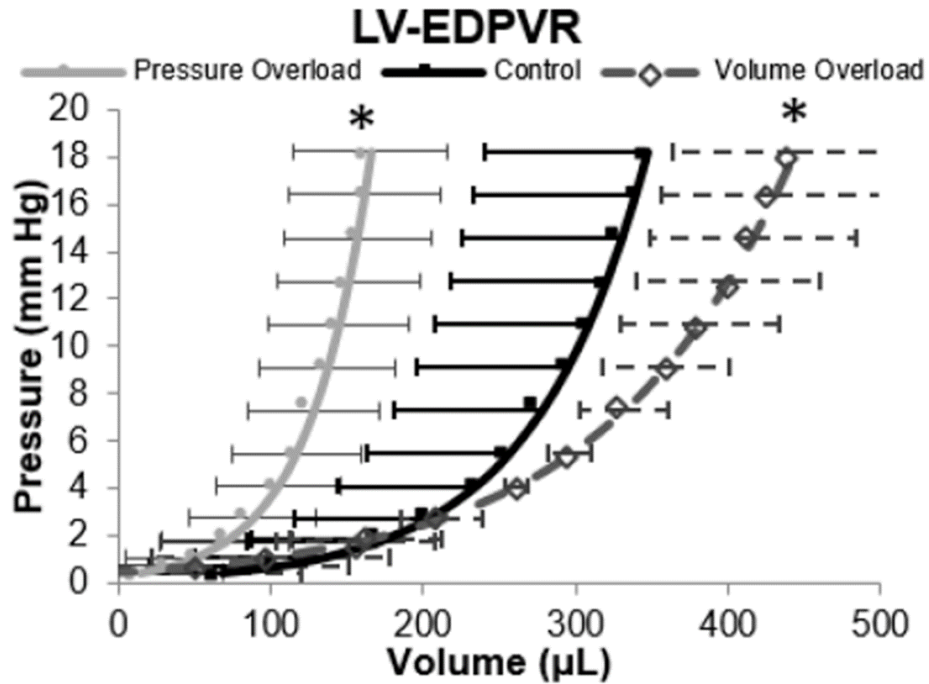


Figure 5-1: Myocardial stiffness in various HF disease states.

Left ventricular end-diastolic pressure-volume relationship for normal, pressure overload, and volume overload hearts. The shift to the right of the VO curve demonstrates decreases myocardial stiffness associated with VO. Recreated from Childers et al. 2021 [119] with permission.

Cardiac fibroblasts (CFs) are responsible for ECM maintenance through production of matrix proteins and matrix metalloproteinases (MMPs). In a healthy environment CFs maintain a constant balance of matrix deposition through production of additional proteins and matrix degradation through secretion of MMPs. There are several external cellular cues that alter CF ECM maintenance such as inflammation, hormonal regulation, mechanical stress, and cellular crosstalk [120]. CFs are also known to be dynamic plastic cells, meaning they can activate between phenotypes characterized by their fibrotic function. For instance, fibroblasts are known to be phenotypically responsive to their mechanical environments. Specifically, fibroblasts (and CFs) are known to activate to a profibrotic myofibroblast

state as a result of increases in substrate stiffness or mechanical strain characterized by increased production of ECM proteins [121] (Figure 5-2). Interestingly, our group has recently demonstrated that decreased substrate stiffness associated with VO HF drives CFs to a hypofibrotic phenotype, where ECM production is decreased and MMP secretion is increased [118], [119], [122] (Figure 5-3). Therefore, we suggested that changes in the cardiac mechanical environment are related to changes in CF phenotype.

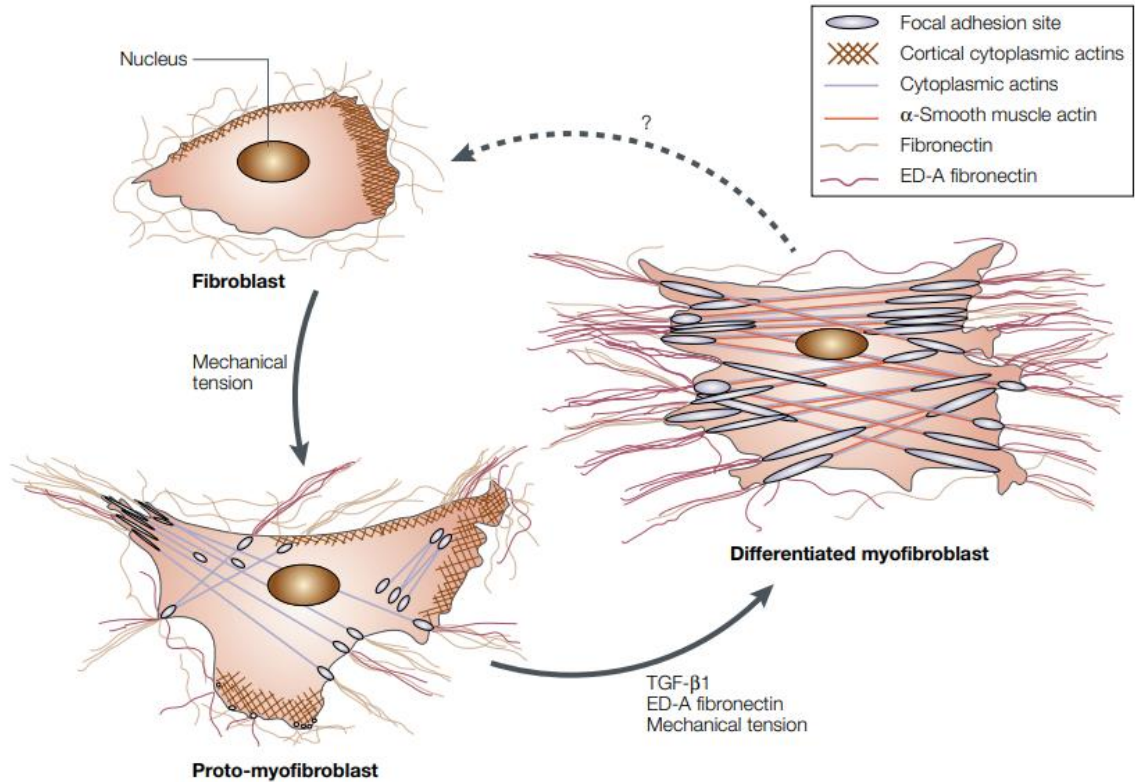


Figure 5-2: Fibroblast classification.

Fibroblast activation to a myofibroblast phenotype as a function of the mechanical and chemical environment. Figure reproduced from Tomasek et al. 2002 [121] with permission.

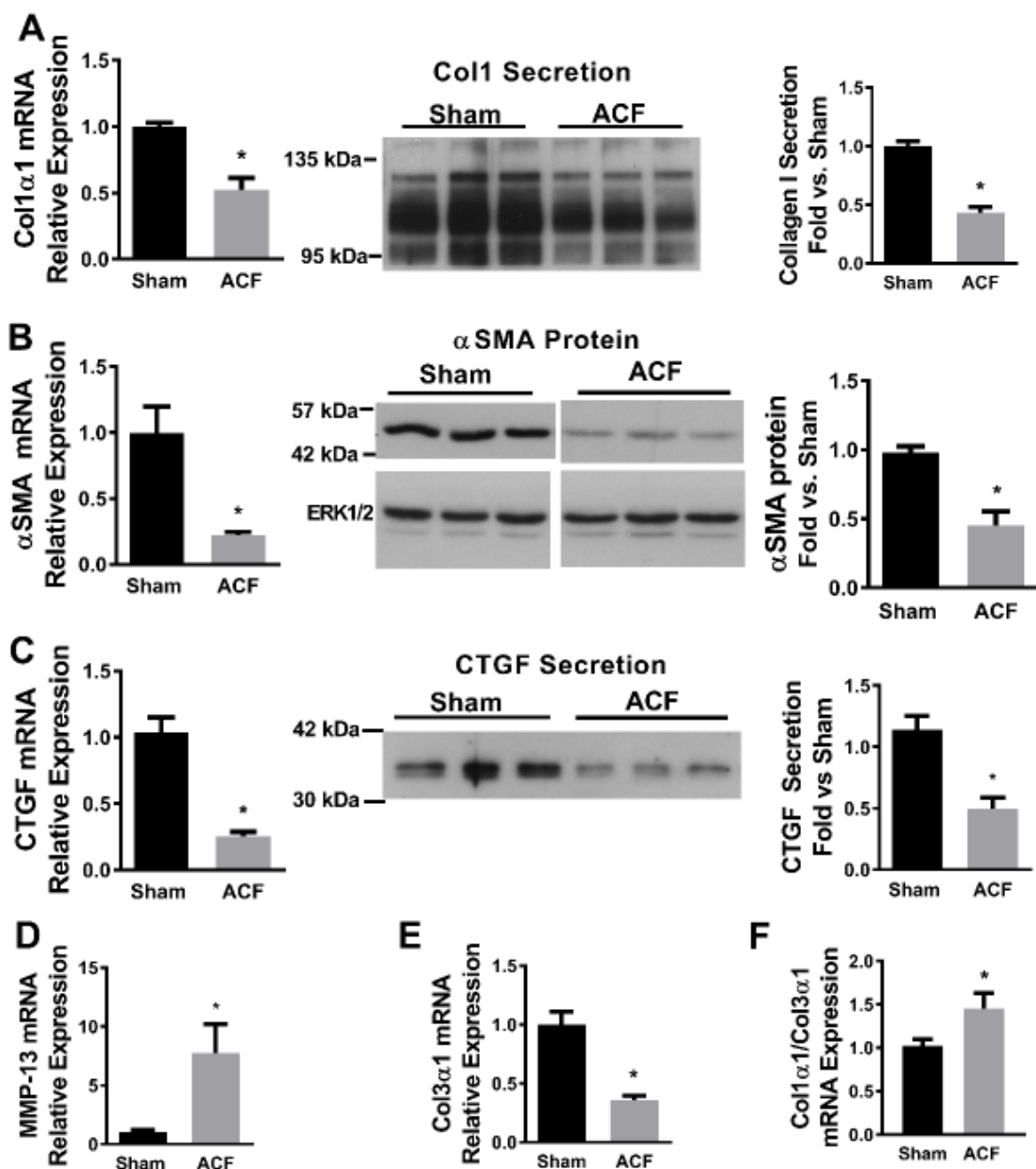


Figure 5-3: Hypofibrotic CF phenotype associated with VO HF.

mRNA expression and relative fluorescent expression of several proteins associated with an activated myofibroblast phenotype in two animal models (sham = control, ACF = aortocaval fistula (VO HF model)). Proteins such as collagen (A) and α SMA (B) are noticeably decreased in VO HF, while MMP expression (D) is increased. Recreated from Childers 2019 [122] with permission.

5.2 Utilizing the adapted motor-clutch model to further study CF function in the VO HF environment.

5.2.1 Why the adapted motor-clutch model is useful to study the VO HF environment.

As discussed in section 5.1, VO HF is the result of a complex hemodynamic environment exposing myocardial cells to increased strain and decreased substrate stiffness. Although there have been recent advances in experimental techniques, combining the effects of altered substrate stiffness and mechanical substrate deformation is very challenging. Quinlan et al. and Herum et al. both successfully adhered PA gels to PDMS deformable substrates prior applying cyclic substrate stretch [54], [80], but there have been very few experiments that have been able to alter both components of the mechanical environment. The adapted motor-clutch model includes parameters for controlling both substrate stiffness and cyclic stretch amplitude and frequency. Therefore, the adapted model presents a simulation tool that can accurately recreate an in vivo environment which experimental tools cannot.

VO HF also consists of a dynamic mechanical environment, where substrate stiffness and stretch are constantly changing with time and disease progression. Following an initial insult, increased myocardial stretch contributes to a compensatory remodeling stage where the heart undergoes structural changes to maintain wall stress. At the same time, hypofibrotic CFs remodel the ECM to decrease tissue modulus, further contributing to maintenance of normal wall stress. While initial changes maintain proper cardiac mechanics, changes in tissue modulus contribute to a CF vicious cycle, where changes in

stiffness result in a hypofibrotic phenotype that further decreases tissue modulus. While compensatory remodeling is critical for maintaining proper heart mechanics, it introduces a mechanical environment of constantly changing forces. As it is already very difficult to experimentally alter both substrate stiffness and substrate stretch, altering both parameters with time during an ongoing experiment only increases the difficulty of simulating the true *in vivo* environment. The adapted motor-clutch model allows for fine tuning of all mechanical properties as a function of time, eliminating difficult challenges associated with accurately simulating an *in vivo* mechanical environment.

The complex mechanical environment associated with VO HF discussed previously brings about several questions regarding how the mechanical environment alters CF form and function. Specifically, I propose addressing questions about the initial alterations in cardiac mechanics that begin VO HF related structural changes, how cyclic stretch impacts CF function, the combined effects of stretch and altered stiffness on CF function, and how alterations in heartrate associated with common cardiac diseases affect CF function.

The most important question to first address is how motor-clutch model outputs (mainly traction force generation and actin flow) can be used to inform and predict CF phenotype and function. Fibroblast activation to a myofibroblast phenotype is triggered by increased tension within the cytoskeletal framework and activation of the transforming growth factor beta (TGF- β) pathway. Myofibroblasts are typically identified by the presence of defined α -smooth muscle actin (α SMA) fibers that generate high levels of contractile force within the cell [2]. Increases in contraction also play a role in releasing and activating latent TGF- β 1 from cell-generated stores [123], which is a key regulator of

myofibroblast activation [2], [6], [121], [124]. These known phenotype characterizations point to traction force generation and retrograde velocity as good predictors of CF phenotype. Therefore, increased traction force generation and decreased retrograde velocity within the motor-clutch model would coincide with increased likelihood of myofibroblast activation. By monitoring the two main model outputs as a function of substrate stiffness and cyclic stretch, one can confidently predict CF behavior.

5.2.3 How does cyclic stretch impact CF behavior, and can the adapted motor-clutch model provide insight into the initial insult that fuels the cascade into VO HF?

While the specific hemodynamic and mechanical alterations associated with VO HF are now known and understood, there is some uncertainty about the initial insult and initial mechanical alteration that begins disease progression. Logically, the hemodynamic change resulting in increased myocardial stretch would precede any changes to CF phenotype and myocardial ECM content. However, many groups have demonstrated that CFs typically respond to increased stretch by activating to a myofibroblast phenotype and by increasing production of ECM proteins such as collagen and alpha smooth muscle actin [88], [125]–[127]. Therefore, if increased stretch were acting on CFs alone initially, according to experimental evidence presented in the literature, ECM synthesis would be increased instead of decreased as we typically see in VO HF progression. This data suggests that either increased stretch is not the sole initial driver of changes in CF phenotype, or that experimental data is not accurately recreating the VO environment.

One issue with current experimental data is that studies that report CF behavior in response to cyclic stretch utilize cell culture substrates such as plastic and PDMS that are several orders of magnitude stiffer than typical myocardial tissue. In an attempt to bypass

this issue, Herum et al. utilized a PA gel and cyclic stretch system to alter both stretch and substrate stiffness to more accurately recreate the myocardial mechanical environment [80]. They report that collagen production is increased with stretch at lower substrate stiffness values (3 and 8 kPa) suggesting stretch activates fibroblasts to a myofibroblast phenotype at any stiffness, but they utilize relatively small stretch amplitudes (maximum stretch amplitude of 6%). Typical healthy myocardial longitudinal strain calculated by echocardiography is reported to be somewhere between 18-25% [128], suggesting strains lower than this range may not recreate pathological or even physiological conditions. While this new data improves upon a previously poorly studied experimental parameter space, the question of effects of initial mechanical changes in VO still exists.

Although it is difficult to equate in vivo myocardial longitudinal strain with in vitro applied uniaxial or equibiaxial stretch amplitude, comparing the two gives insight into the importance of choosing experimental conditions. For instance, in vitro stretch amplitudes lower than 10% may be recreating an environment where CF response will not be typical of those in normal conditions. The adapted motor-clutch model allows for systematic studies of a wide range of stretch amplitudes that would more accurately represent both physiological and pathological stretch. Therefore, it is possible to alter stretch to pathophysiological levels associated with VO to examine impacts on cell form and function. This new insight would be valuable in determining whether increased stretch begins the transition of CFs to a hypofibrotic state, or if there is some interplay between stiffness and stretch that is responsible. As discussed in Chapter 3, there are specific combinations of stretch and stiffness that exceed optimal conditions for proper cell

function, perhaps suggesting that increased levels of stretch associated with VO may inhibit CF ECM production and maintenance. Similarly, the adapted motor-clutch model demonstrates that cellular response is a function of the distinct combination of stiffness and stretch where certain combinations may mimic other combinations (i.e., soft and high stretch can mimic stiff and low stretch). Therefore, the model can give new insight into the effects of changing either component of the mechanical environment that can help to answer the question of how VO HF disease progression initiates.

5.2.4 Why does cyclic stretch not revert fibroblasts back quiescent phenotype following initial structural changes?

Following the initial insult that leads to VO, CFs remain in a hypofibrotic state further contributing to disease progression. According to previous experimental studies, cyclic stretch would be predicted to activate myofibroblasts and increase ECM production [80]. Therefore, an important question to ask is why do CFs maintain a hypofibrotic phenotype throughout progression of VO HF? The unique ability to finely control both substrate stiffness and cyclic stretch as a function of time (i.e., disease progression) makes the adapted motor-clutch model an effective tool for monitoring CF phenotype during different disease states. For instance, it is known that healthy myocardial tissue typically has a stiffness of roughly 10-25 kPa and will increase or decrease significantly during HF [121], [124], [129]–[132]. Similarly, cyclic strain in the myocardial wall will change as a function of compensatory stage. Following initial VO insult, strain will be high, and the heart will structurally compensate to reduce strain to physiological levels. Further progression in VO will again increase stretch until compensation can no longer maintain physiological strains. These constant changes in strain as a function of compensation presents an interesting and

difficult to recreate mechanical environment for experimental analysis. I propose that the maintenance of the CF hypofibrotic phenotype is a function of constantly decreasing substrate stiffness, and fluctuations between physiologic and increased pathophysiologic amounts of myocardial stretch.

Recent experimental evidence has shed light on possible CF response to pathological levels of cyclic strain. Waxman et al. and Gould et al. demonstrated that valve interstitial cells (VICs) exposed to cyclic stretch amplitudes of 15-20% favor a quiescent phenotype without expressing profibrotic markers [133], [134]. Typically, VICs maintain the ECM of the valve leaflets and express myofibroblast like α -SMA stress fibers [19]. Therefore, the VIC fibrotic response to stretch may likely be similar to that of CFs. Using the adapted motor-clutch model to simultaneously decrease substrate stiffness and increase cyclic stretch amplitude may also provide critical information to help determine what drives and maintains a hypofibrotic CF phenotype.

5.2.5 What are the effects of changes in heart rate and contractility waveform on CF function?

Heart rate is a common metric for determining overall cardiac health as it is strongly correlated with cardiac related mortality [135], [136]. Specifically, heart rate is typically elevated in HF patients [137], which may contribute to further disease progression. Although heart rate is an increasingly popular metric of study, the specific effects of heart rate variability on CF function is poorly studied. In fact, effects of changes in cyclic stretch frequency are rarely studied in any cell type. The fact that heart rate is strongly correlated with cardiac related death, any study of the effects of heart rate on CF function may be very important. Data presented in Chapters 3 and 4 demonstrate that altering cyclic stretch

frequency has significant impacts on actin traction force generation and overall cytoskeletal organization. Others have demonstrated similar impacts experimentally, where stretch frequency plays a role in final cell orientation [32], [97], [103]. Based on the simulated and experimental effects of stretch frequency on overall cell form and function, one may assume that heart rate-based changes in myocardial stretch frequency likely impact CF function.

Perhaps the most apparent fluctuation in heart rate and stretch frequency results from non-uniform heart beats (i.e., arrhythmias). Typically, HF related compensatory remodeling is thought of as a pre-cursor to ventricular arrhythmias, where changes in the myocardial structure creates an ideal environment for the generation of ventricular arrhythmias. However, recent evidence points to ventricular arrhythmias accelerating disease progression, typically as a function of changes in metabolic function [138], [139]. Knowing what we know about stretch and organization and function of cytoskeletal elements, it is possible that non-uniform asynchronous contraction may be altering CF function. Whatever the timeline of altered myocardial strain frequency and disease progression, arrhythmias are known to be very common and fatal in patients with HF and at least deserve further study.

A second interesting application for changes in stretch frequency is related to the specific stretch waveform associated with cardiac contraction. Cardiac myograms report force development within the myocardial tissue as a function of time and can be used to determine the general stretch waveform experienced by cells within the tissue. Typical myocardial force development curves have similarities with the cosine waveform used in

the first version of the adapted motor-clutch model but developing a waveform that exactly mimics a cardiac myogram would be the first step in recreating the true cyclic stretch environment. Next, the waveform can be altered to match contraction-relaxation kinetics associated with different disease conditions. Others have shown that while force development curves remain similar in shape during different disease states, there are significant alterations in contraction force generation and kinetics in failing hearts (Figure 5-4) [140]. On an individual cell level, Tondon et al. previously demonstrated the profound impacts altering stretch waveform has on cytoskeletal organization and stress fiber formation [141]. Specifically, they found that stress fiber formation and tension generation is strictly a function of the rate of substrate lengthening. This observation suggests that the altered muscle contraction kinetics associated with HF may play a role in altering CF phenotype as a function of cytoskeletal organization and function. Experimental observations such as these further demonstrate the potential importance of changes in cyclic stretch frequency associated with HF and their potential impacts on overall disease progression.

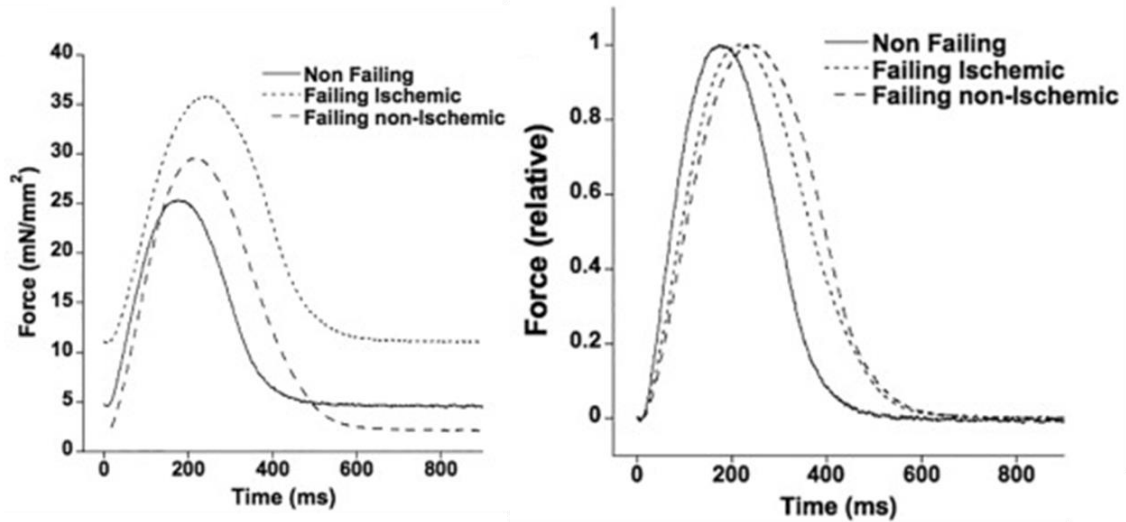


Figure 5-4: Force generation and kinetics in normal and failing hearts.

Unmodified (left) and relative (right) twitch contractions from ex vivo human myocardial tissue. Reproduced from Chung et al. 2018 [140].

5.3 Future Directions

Several significant updates to the adapted motor-clutch model are required to accurately utilize the model to study the complex mechanical environment associated with VO HF. As discussed in previous chapters, the motor clutch hypothesis was initially intended to describe neuronal cell extension as a function of adhesion and actin dynamics. In their initial presentation of the computational motor-clutch model, Chan and Odde demonstrate that their solution to the model accurately captures true in vitro neuronal cell behavior [72], [142]. However, fibroblasts are known to exhibit a very different behavior than the model predicted for neuronal cells, where fibroblasts generate high levels of tension and increase their spread area as substrate stiffness increases (Figure 5-5) [53], [80], [123], [124], [143], [144]. Chapter 3 introduces the concept of catch bonds into the adapted motor-clutch model that generally begin to recreate the true in vitro observation for adhesive cell types such as

fibroblasts. Specifically, Figure 3-7 shows that spreading velocity (the inverse of actin retrograde velocity) increases with increasing substrate stiffness. Extension of the adapted motor-clutch model to study VO HF would require further development of model characteristics that mimic the results presented in Figure 3-7. A second alteration to the model that may assist in re-creating proper cell behavior is the inclusion of focal adhesion maturation and reinforcement. Shenoy et al. initially include the concept of clutch reinforcement in the motor-clutch model [145] where the rate of clutch binding increases as a function of force within bound clutches. This simple, but important, update to the motor-clutch model replicates experimental observations of increasing cell binding site density with increases in traction force generation. Focal adhesion maturation and the ability for CFs to form focal adhesions is known to play an important role in typical fibroblast sensing of the mechanical environment [146]–[149], pointing to the importance of including this type of behavior in any model that attempts to study fibroblast like cell behavior.

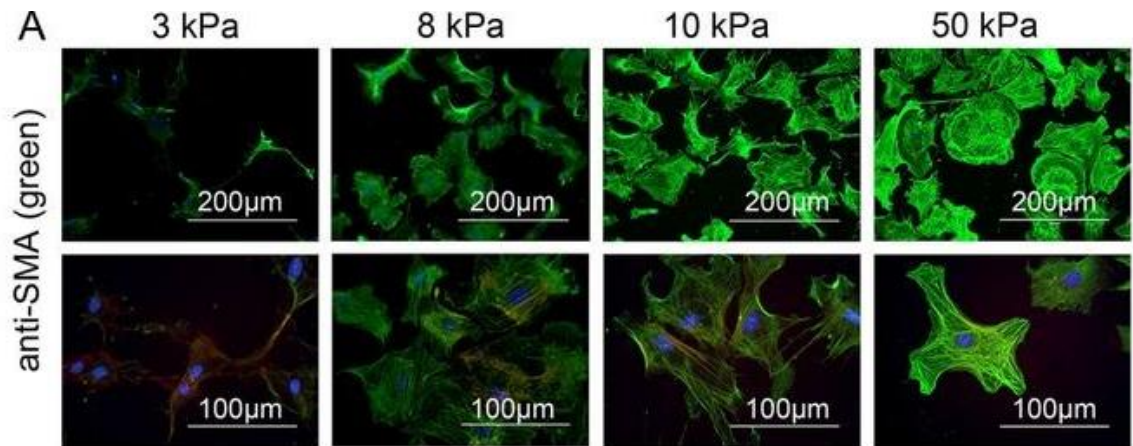


Figure 5-5: CF morphology as a function of substrate stiffness.

In vitro CF cultured on PA gels of variable stiffnesses. Smooth muscle actin (SMA) is stained in green, F-actin in red, and nuclei in blue. CFs increase spread area and expression of SMA with increasing substrate stiffness. Figure reproduced from Herum et al. 2017 [80].

Future usage of the adapted motor-clutch model will focus on the VO HF problem discussed in Chapter 5. Following the addition of proper cell adhesion and spreading into the model, the specific effects of varying cyclic stretch and substrate stiffness on CF behavior will be studied. These simulations will prove critical in determining the role of the mechanical environment in cardiac disease progression, as it has been very difficult to experimentally re-create the dynamic cardiac mechanical environment.

Chapter 6 Summary and Concluding Remarks

In summary, the work presented here describes a computational model that can be used to study complex mechanical environments and their effects on cell behavior. While specific functional responses to cyclic stretch are well-studied at this point, the mechanism by which cells sense changes in the mechanical environment is not known. The motor-clutch biophysical model has been used to predict neuronal cell adhesion behavior in response to changes in substrate stiffness in the past, which suggests the model can be used to further study cell behavior as a function of a more complex mechanical environment. Here, the motor-clutch model is adapted to include cyclic motion of the substrate to study the effects of cyclic stretch on cell behavior.

Chapter 3 discusses use of the adapted motor-clutch model to study the impacts of cyclic stretch on actin traction force generation. Model results provide novel insight into a poorly studied experimental space (changing both substrate stiffness and cyclic stretch) and provide predictions for how cells will respond to alterations in the external mechanical environment. Next, Chapter 4 presents a further modified version of the adapted model to study the impacts of stretch and stiffness on actin organization. Model results match experimentally observed cell reorientation in response to applied cyclic stretch and detail the mechanisms for how cells alter their morphology in response to changes in stiffness

and stretch. Importantly, the adapted motor-clutch model strongly suggests that components of the model (cytoskeletal related adhesion proteins and force generating myosin) play a critical role in cell sensing of the mechanical environment.

Perhaps most importantly, the adapted motor-clutch model allows for fine tuning of mechanical environment components that are difficult to alter experimentally. Most cyclic stretch experiments utilize silicone deformable substrates that must be a certain stiffness to withstand applied strain. This allows for future use of the model to study disease environments that also include complex substrate mechanics, such as heart failure. Volume overload heart failure is known to include significant changes in myocardial stiffness and strain that alter cell behavior that further contributes to disease progression.

Bibliography

- [1] M. Akhmanova, E. Osidak, S. Domogatsky, S. Rodin, and A. Domogatskaya, “Physical, Spatial, and Molecular Aspects of Extracellular Matrix of *In Vivo* Niches and Artificial Scaffolds Relevant to Stem Cells Research,” *Stem Cells Int.*, vol. 2015, pp. 1–35, 2015, doi: 10.1155/2015/167025.
- [2] B. Hinz, “Matrix mechanics and regulation of the fibroblast phenotype,” *Periodontol. 2000*, vol. 63, no. 1, pp. 14–28, Oct. 2013, doi: 10.1111/prd.12030.
- [3] S. E. Mutsaers, J. E. Bishop, G. McGrouther, and G. J. Laurent, “Mechanisms of tissue repair: from wound healing to fibrosis,” *Int. J. Biochem. Cell Biol.*, vol. 29, no. 1, pp. 5–17, Jan. 1997, doi: 10.1016/S1357-2725(96)00115-X.
- [4] R. Raghov, “The role of extracellular matrix in postinflammatory wound healing and fibrosis,” *FASEB J.*, vol. 8, no. 11, pp. 823–831, Aug. 1994, doi: 10.1096/fasebj.8.11.8070631.
- [5] F. Liu *et al.*, “Feedback amplification of fibrosis through matrix stiffening and COX-2 suppression,” *J. Cell Biol.*, vol. 190, no. 4, pp. 693–706, Aug. 2010, doi: 10.1083/jcb.201004082.
- [6] B. Hinz, “Tissue stiffness, latent TGF- β 1 Activation, and mechanical signal transduction: Implications for the pathogenesis and treatment of fibrosis,” *Curr. Rheumatol. Rep.*, vol. 11, no. 2, pp. 120–126, Apr. 2009, doi: 10.1007/s11926-009-0017-1.
- [7] K. W. Yong *et al.*, “Mechanoregulation of cardiac myofibroblast differentiation: implications for cardiac fibrosis and therapy,” *Am. J. Physiol.-Heart Circ. Physiol.*, vol. 309, no. 4, pp. H532–H542, Aug. 2015, doi: 10.1152/ajpheart.00299.2015.
- [8] P. C. Georges *et al.*, “Increased stiffness of the rat liver precedes matrix deposition: implications for fibrosis,” *Am. J. Physiol.-Gastrointest. Liver Physiol.*, vol. 293, no. 6, pp. G1147–G1154, Dec. 2007, doi: 10.1152/ajpgi.00032.2007.
- [9] B. Piersma, M. K. Hayward, and V. M. Weaver, “Fibrosis and cancer: A strained relationship,” *Biochim. Biophys. Acta BBA - Rev. Cancer*, vol. 1873, no. 2, p. 188356, Apr. 2020, doi: 10.1016/j.bbcan.2020.188356.
- [10] A. Harvey, A. C. Montezano, R. A. Lopes, F. Rios, and R. M. Touyz, “Vascular Fibrosis in Aging and Hypertension: Molecular Mechanisms and Clinical Implications,” *Can. J. Cardiol.*, vol. 32, no. 5, pp. 659–668, May 2016, doi: 10.1016/j.cjca.2016.02.070.
- [11] L. Henaó-Murillo, K. Ito, and C. C. van Donkelaar, “Collagen Damage Location in Articular Cartilage Differs if Damage is Caused by Excessive Loading Magnitude or Rate,” *Ann. Biomed. Eng.*, vol. 46, no. 4, pp. 605–615, Apr. 2018, doi: 10.1007/s10439-018-1986-x.
- [12] M. N. Pathria, C. B. Chung, and D. L. Resnick, “Acute and Stress-related Injuries of Bone and Cartilage: Pertinent Anatomy, Basic Biomechanics, and Imaging Perspective,” *Radiology*, vol. 280, no. 1, pp. 21–38, Jul. 2016, doi: 10.1148/radiol.16142305.

- [13] L. G. E. Cox, B. van Rietbergen, C. C. van Donkelaar, and K. Ito, "Analysis of bone architecture sensitivity for changes in mechanical loading, cellular activity, mechanotransduction, and tissue properties," *Biomech. Model. Mechanobiol.*, vol. 10, no. 5, pp. 701–712, Oct. 2011, doi: 10.1007/s10237-010-0267-x.
- [14] C. H. Turner, T. A. Woltman, and D. A. Belongia, "Structural Changes in Rat Bone Subjected to Long-Term, in Vivo Mechanical Loading," *Bone*, vol. 13, pp. 417–422, 1992.
- [15] K. Balachandran, P. Sucusky, and A. P. Yoganathan, "Hemodynamics and Mechanobiology of Aortic Valve Inflammation and Calcification," *Int. J. Inflamm.*, vol. 2011, pp. 1–15, 2011, doi: 10.4061/2011/263870.
- [16] B. F. Stewart *et al.*, "Clinical Factors Associated With Calcific Aortic Valve Disease," *J. Am. Coll. Cardiol.*, vol. 29, no. 3, pp. 630–634, Mar. 1997, doi: 10.1016/S0735-1097(96)00563-3.
- [17] E. R. Mohler, F. Gannon, C. Reynolds, R. Zimmerman, M. G. Keane, and F. S. Kaplan, "Bone Formation and Inflammation in Cardiac Valves," *Circulation*, vol. 103, no. 11, pp. 1522–1528, Mar. 2001, doi: 10.1161/01.CIR.103.11.1522.
- [18] A. C. Liu, V. R. Joag, and A. I. Gotlieb, "The Emerging Role of Valve Interstitial Cell Phenotypes in Regulating Heart Valve Pathobiology," *Am. J. Pathol.*, vol. 171, no. 5, pp. 1407–1418, Nov. 2007, doi: 10.2353/ajpath.2007.070251.
- [19] P. M. Taylor, P. Batten, N. J. Brand, P. S. Thomas, and M. H. Yacoub, "The cardiac valve interstitial cell," *Int. J. Biochem. Cell Biol.*, vol. 35, no. 2, pp. 113–118, Feb. 2003, doi: 10.1016/S1357-2725(02)00100-0.
- [20] R. J. Pelham and Y.-L. Wang, "Cell Locomotion and Focal Adhesions are Regulated by Substrate Flexibility," *Proc. Natl. Acad. Sci.*, vol. 94, pp. 13661–13665, Dec. 1997.
- [21] P. A. Janmey, "Stiffness Sensing by Cells," *Phys. Rev. E*, vol. 100, no. 2, pp. 695–724, Apr. 2020.
- [22] M. Guo *et al.*, "Cell volume change through water efflux impacts cell stiffness and stem cell fate," *Proc. Natl. Acad. Sci.*, vol. 114, no. 41, pp. E8618–E8627, Oct. 2017, doi: 10.1073/pnas.1705179114.
- [23] M. Gupta *et al.*, "Adaptive rheology and ordering of cell cytoskeleton govern matrix rigidity sensing," *Nat. Commun.*, vol. 6, no. 1, p. 7525, Nov. 2015, doi: 10.1038/ncomms8525.
- [24] C. L. Ives, S. G. Eskin, and L. V. McIntire, "Mechanical effects on endothelial cell morphology: In vitro assessment," *In Vitro Cell. Dev. Biol.*, vol. 22, no. 9, pp. 500–507, Sep. 1986, doi: 10.1007/BF02621134.
- [25] P. C. Dartsch and E. Betz, "Response of cultured endothelial cells to mechanical stimulation," *Basic Res. Cardiol.*, vol. 84, no. 3, pp. 268–281, May 1989, doi: 10.1007/BF01907974.
- [26] B. E. Sumpio, A. J. Banes, G. W. Link, and T. Iba, "Modulation of endothelial cell phenotype by cyclic stretch: Inhibition of collagen production," *J. Surg. Res.*, vol. 48, no. 5, pp. 415–420, May 1990, doi: 10.1016/0022-4804(90)90005-M.

- [27] T. Iba and B. E. Sumpio, "Morphological response of human endothelial cells subjected to cyclic strain in vitro," *Microvasc. Res.*, vol. 42, no. 3, pp. 245–254, Nov. 1991, doi: 10.1016/0026-2862(91)90059-K.
- [28] K. Kada, K. Yasui, K. Naruse, K. Kamiya, I. Kodama, and J. Toyama, "Orientation Change of Cardiocytes Induced by Cyclic Stretch Stimulation: Time Dependency and Involvement of Protein Kinases," *J. Mol. Cell. Cardiol.*, vol. 31, no. 1, pp. 247–259, Jan. 1999, doi: 10.1006/jmcc.1998.0865.
- [29] P. R. Standley, A. Camaratta, B. P. Nolan, C. T. Purgason, and M. A. Stanley, "Cyclic stretch induces vascular smooth muscle cell alignment via NO signaling," *Am. J. Physiol.-Heart Circ. Physiol.*, vol. 283, no. 5, pp. H1907–H1914, Nov. 2002, doi: 10.1152/ajpheart.01043.2001.
- [30] M. Moretti, A. Prina-Mello, A. J. Reid, V. Barron, and P. J. Prendergast, "Endothelial cell alignment on cyclically-stretched silicone surfaces," *J. Mater. Sci. Mater. Med.*, vol. 15, no. 10, pp. 1159–1164, Oct. 2004, doi: 10.1023/B:JMSM.0000046400.18607.72.
- [31] V. Barron *et al.*, "The effect of physiological cyclic stretch on the cell morphology, cell orientation and protein expression of endothelial cells," *J. Mater. Sci. Mater. Med.*, vol. 18, no. 10, pp. 1973–1981, Sep. 2007, doi: 10.1007/s10856-007-3125-3.
- [32] S. Jungbauer, H. Gao, J. P. Spatz, and R. Kemkemer, "Two Characteristic Regimes in Frequency-Dependent Dynamic Reorientation of Fibroblasts on Cyclically Stretched Substrates," *Biophys. J.*, vol. 95, no. 7, pp. 3470–3478, Oct. 2008, doi: 10.1529/biophysj.107.128611.
- [33] A. Matsugaki, N. Fujiwara, and T. Nakano, "Continuous cyclic stretch induces osteoblast alignment and formation of anisotropic collagen fiber matrix," *Acta Biomater.*, vol. 9, no. 7, pp. 7227–7235, Jul. 2013, doi: 10.1016/j.actbio.2013.03.015.
- [34] J. H. Wang, P. Goldschmidt-Clermont, J. Wille, and F. C. Yin, "Specificity of endothelial cell reorientation in response to cyclic mechanical stretching," *J. Biomech.*, vol. 34, no. 12, pp. 1563–1572, Dec. 2001, doi: 10.1016/s0021-9290(01)00150-6.
- [35] M. Gupta *et al.*, "Cell shape and substrate stiffness drive actin-based cell polarity," *Phys. Rev. E*, vol. 99, no. 1, p. 012412, Jan. 2019, doi: 10.1103/PhysRevE.99.012412.
- [36] A. Jannatbabaie, M. Tafazzoli-Shadpour, E. Seyedjafari, and N. Fatourae, "Cytoskeletal remodeling induced by substrate rigidity regulates rheological behaviors in endothelial cells: Cytoskeletal remodeling regulates rheological behaviors in EC s," *J. Biomed. Mater. Res. A*, vol. 107, no. 1, pp. 71–80, Jan. 2019, doi: 10.1002/jbm.a.36533.
- [37] S. Tojkander, G. Gateva, and P. Lappalainen, "Actin stress fibers - assembly, dynamics and biological roles," *J. Cell Sci.*, vol. 125, no. 8, pp. 1855–1864, Apr. 2012, doi: 10.1242/jcs.098087.
- [38] D. E. Discher, "Tissue Cells Feel and Respond to the Stiffness of Their Substrate," *Science*, vol. 310, no. 5751, pp. 1139–1143, Nov. 2005, doi: 10.1126/science.1116995.

- [39] A. M. Greiner, H. Chen, J. P. Spatz, and R. Kemkemer, “Cyclic Tensile Strain Controls Cell Shape and Directs Actin Stress Fiber Formation and Focal Adhesion Alignment in Spreading Cells,” *PLoS ONE*, vol. 8, no. 10, p. e77328, Oct. 2013, doi: 10.1371/journal.pone.0077328.
- [40] R. Kaunas, P. Nguyen, S. Usami, and S. Chien, “Cooperative effects of Rho and mechanical stretch on stress fiber organization,” *Proc. Natl. Acad. Sci.*, vol. 102, no. 44, pp. 15895–15900, Nov. 2005.
- [41] C.-F. Lee, C. Haase, S. Deguchi, and R. Kaunas, “Cyclic stretch-induced stress fiber dynamics – Dependence on strain rate, Rho-kinase and MLCK,” *Biochem. Biophys. Res. Commun.*, vol. 401, no. 3, pp. 344–349, Oct. 2010, doi: 10.1016/j.bbrc.2010.09.046.
- [42] S. F. Gorfien, F. K. Winston, L. E. Thibault, and E. J. Macarak, “Effects of biaxial deformation on pulmonary artery endothelial cells,” *J. Cell. Physiol.*, vol. 139, no. 3, pp. 492–500, Jun. 1989, doi: 10.1002/jcp.1041390307.
- [43] R. P. Butt and J. E. Bishop, “Mechanical Load Enhances the Stimulatory Effect of Serum Growth Factors on Cardiac Fibroblast Procollagen Synthesis,” *J. Mol. Cell. Cardiol.*, vol. 29, no. 4, pp. 1141–1151, Apr. 1997, doi: 10.1006/jmcc.1996.0347.
- [44] M. Sotoudeh *et al.*, “Induction of apoptosis in vascular smooth muscle cells by mechanical stretch,” *Am. J. Physiol.-Heart Circ. Physiol.*, vol. 282, no. 5, pp. H1709–H1716, May 2002, doi: 10.1152/ajpheart.00744.2001.
- [45] N. A. Hasaneen, S. Zucker, J. Cao, C. Chiarelli, R. A. Panettieri, and H. D. Foda, “Cyclic mechanical strain-induced proliferation and migration of human airway smooth muscle cells: role of EMMPRIN and MMPs,” *FASEB J.*, vol. 19, no. 11, pp. 1507–1509, Sep. 2005, doi: 10.1096/fj.04-3350fje.
- [46] B. Zhang *et al.*, “Cyclic mechanical stretching promotes migration but inhibits invasion of rat bone marrow stromal cells,” *Stem Cell Res.*, vol. 14, no. 2, pp. 155–164, Mar. 2015, doi: 10.1016/j.scr.2015.01.001.
- [47] Y. Cui *et al.*, “Cyclic stretching of soft substrates induces spreading and growth,” *Nat. Commun.*, vol. 6, no. 1, p. 6333, May 2015, doi: 10.1038/ncomms7333.
- [48] S. R. Peyton and A. J. Putnam, “Extracellular matrix rigidity governs smooth muscle cell motility in a biphasic fashion,” *J. Cell. Physiol.*, vol. 204, no. 1, pp. 198–209, Jul. 2005, doi: 10.1002/jcp.20274.
- [49] I. V. Dokukina and M. E. Gracheva, “A Model of Fibroblast Motility on Substrates with Different Rigidities,” *Biophys. J.*, vol. 98, no. 12, pp. 2794–2803, Jun. 2010, doi: 10.1016/j.bpj.2010.03.026.
- [50] L. A. Flanagan, Y.-E. Ju, B. Marg, M. Osterfield, and P. A. Janmey, “Neurite branching on deformable substrates:,” *NeuroReport*, vol. 13, no. 18, pp. 2411–2415, Dec. 2002, doi: 10.1097/00001756-200212200-00007.
- [51] P. C. Bridgman, S. Dave, C. F. Asnes, A. N. Tullio, and R. S. Adelstein, “Myosin IIB Is Required for Growth Cone Motility,” *J. Neurosci.*, vol. 21, no. 16, pp. 6159–6169, Aug. 2001, doi: 10.1523/JNEUROSCI.21-16-06159.2001.
- [52] A. Engler, L. Bacakova, C. Newman, A. Hategan, M. Griffin, and D. Discher, “Substrate Compliance versus Ligand Density in Cell on Gel Responses,” *Biophys. J.*, vol. 86, no. 1, pp. 617–628, Jan. 2004, doi: 10.1016/S0006-3495(04)74140-5.

- [53] T. Yeung *et al.*, “Effects of substrate stiffness on cell morphology, cytoskeletal structure, and adhesion,” *Cell Motil. Cytoskeleton*, vol. 60, no. 1, pp. 24–34, Jan. 2005, doi: 10.1002/cm.20041.
- [54] A. M. Throm Quinlan, L. N. Sierad, A. K. Capulli, L. E. Firstenberg, and K. L. Billiar, “Combining Dynamic Stretch and Tunable Stiffness to Probe Cell Mechanobiology In Vitro,” *PLoS ONE*, vol. 6, no. 8, p. e23272, Aug. 2011, doi: 10.1371/journal.pone.0023272.
- [55] D. E. Ingber, “Cellular tensegrity: defining new rules of biological design that govern the cytoskeleton,” *J. Cell Sci.*, vol. 104, pp. 613–627, 1993.
- [56] D. E. Ingber, “Tensegrity I. Cell structure and hierarchical systems biology,” *J. Cell Sci.*, vol. 116, no. 7, pp. 1157–1173, Apr. 2003, doi: 10.1242/jcs.00359.
- [57] D. Stamenović, Z. Liang, J. Chen, and N. Wang, “Effect of the cytoskeletal prestress on the mechanical impedance of cultured airway smooth muscle cells,” *J. Appl. Physiol.*, vol. 92, no. 4, pp. 1443–1450, Apr. 2002, doi: 10.1152/jappphysiol.00782.2001.
- [58] N. Wang *et al.*, “Cell prestress. I. Stiffness and prestress are closely associated in adherent contractile cells,” *Am. J. Physiol.-Cell Physiol.*, vol. 282, no. 3, pp. C606–C616, Mar. 2002, doi: 10.1152/ajpcell.00269.2001.
- [59] A. J. Engler, S. Sen, H. L. Sweeney, and D. E. Discher, “Matrix Elasticity Directs Stem Cell Lineage Specification,” *Cell*, vol. 126, no. 4, pp. 677–689, Aug. 2006, doi: 10.1016/j.cell.2006.06.044.
- [60] S. Even-Ram, A. D. Doyle, M. A. Conti, K. Matsumoto, R. S. Adelstein, and K. M. Yamada, “Myosin IIA regulates cell motility and actomyosin–microtubule crosstalk,” *Nat. Cell Biol.*, vol. 9, no. 3, pp. 299–309, Mar. 2007, doi: 10.1038/ncb1540.
- [61] Y. Cai *et al.*, “Nonmuscle Myosin IIA-Dependent Force Inhibits Cell Spreading and Drives F-Actin Flow,” *Biophys. J.*, vol. 91, no. 10, pp. 3907–3920, Nov. 2006, doi: 10.1529/biophysj.106.084806.
- [62] B. L. Doss *et al.*, “Cell response to substrate rigidity is regulated by active and passive cytoskeletal stress,” *Proc. Natl. Acad. Sci.*, vol. 117, no. 23, pp. 12817–12825, Jun. 2020, doi: 10.1073/pnas.1917555117.
- [63] B. Geiger and A. Bershadsky, “Exploring the neighborhood: Adhesion-coupled cell mechanosensors,” *Cell*, vol. 110, no. 2, pp. 139–142, Jul. 2002.
- [64] G. Giannone and M. P. Sheetz, “Substrate rigidity and force define form through tyrosine phosphatase and kinase pathways,” *Trends Cell Biol.*, vol. 16, no. 4, pp. 213–223, Apr. 2006, doi: 10.1016/j.tcb.2006.02.005.
- [65] A. Katsumi *et al.*, “Effects of cell tension on the small GTPase Rac,” *J. Cell Biol.*, vol. 158, no. 1, pp. 153–164, Jul. 2002, doi: 10.1083/jcb.200201105.
- [66] Y. Sawada, “Rap1 and cell stretching-initiated p38 activation,” *J. Cell Sci.*, vol. 114, no. 6, pp. 1221–1227, Mar. 2001.
- [67] P. Defilippi, P. Di Stefano, and S. Cabodi, “p130Cas: a versatile scaffold in signaling networks,” *Trends Cell Biol.*, vol. 16, no. 5, pp. 257–263, May 2006, doi: 10.1016/j.tcb.2006.03.003.

- [68] Y. Sawada *et al.*, “Force Sensing by Mechanical Extension of the Src Family Kinase Substrate p130Cas,” *Cell*, vol. 127, no. 5, pp. 1015–1026, Dec. 2006, doi: 10.1016/j.cell.2006.09.044.
- [69] T. Mitchison and M. Kirschner, “Cytoskeletal dynamics and nerve growth,” *Neuron*, vol. 1, no. 9, pp. 761–772, Nov. 1988, doi: 10.1016/0896-6273(88)90124-9.
- [70] C. E. Chan and D. J. Odde, “Traction Dynamics of Filopodia on Compliant Substrates,” *Science*, vol. 322, no. 5908, pp. 1687–1691, Dec. 2008, doi: 10.1126/science.1163595.
- [71] B. L. Bangasser, S. S. Rosenfeld, and D. J. Odde, “Determinants of Maximal Force Transmission in a Motor-Clutch Model of Cell Traction in a Compliant Microenvironment,” *Biophys. J.*, vol. 105, no. 3, pp. 581–592, Aug. 2013, doi: 10.1016/j.bpj.2013.06.027.
- [72] B. L. Bangasser *et al.*, “Shifting the optimal stiffness for cell migration,” *Nat. Commun.*, vol. 8, no. 1, p. 15313, Aug. 2017, doi: 10.1038/ncomms15313.
- [73] G. P. O’Hara, “Mechanical Properties of Silicone Rubber in a Closed Volume,” ARMY ARMAMENT RESEARCH AND DEVELOPMENT CENTER WATERVLIET NY LARGE CALIBER WEAPON SYSTEMS LAB, Dec. 1983. Accessed: Nov. 20, 2020. [Online]. Available: <https://apps.dtic.mil/sti/citations/ADA138129>.
- [74] E. G. Rens and R. M. H. Merks, “Cell Shape and Durotaxis Explained from Cell-Extracellular Matrix Forces and Focal Adhesion Dynamics,” *iScience*, vol. 23, no. 9, p. 101488, Sep. 2020, doi: 10.1016/j.isci.2020.101488.
- [75] P. A. Janmey, J. P. Winer, M. E. Murray, and Q. Wen, “The hard life of soft cells,” *Cell Motil. Cytoskeleton*, vol. 66, no. 8, pp. 597–605, Aug. 2009, doi: 10.1002/cm.20382.
- [76] T. Svitkina, “The Actin Cytoskeleton and Actin-Based Motility,” *Cold Spring Harb. Perspect. Biol.*, vol. 10, no. 1, p. a018267, Jan. 2018, doi: 10.1101/cshperspect.a018267.
- [77] B. Li and J. H.-C. Wang, “Fibroblasts and myofibroblasts in wound healing: Force generation and measurement,” *J. Tissue Viability*, vol. 20, no. 4, pp. 108–120, Nov. 2011, doi: 10.1016/j.jtv.2009.11.004.
- [78] C. A. Lemmon, C. S. Chen, and L. H. Romer, “Cell Traction Forces Direct Fibronectin Matrix Assembly,” *Biophys. J.*, vol. 96, no. 2, pp. 729–738, Jan. 2009, doi: 10.1016/j.bpj.2008.10.009.
- [79] L. Trichet *et al.*, “Evidence of a large-scale mechanosensing mechanism for cellular adaptation to substrate stiffness,” *Proc. Natl. Acad. Sci.*, vol. 109, no. 18, pp. 6933–6938, May 2012, doi: 10.1073/pnas.1117810109.
- [80] K. M. Herum, J. Choppe, A. Kumar, A. J. Engler, and A. D. McCulloch, “Mechanical regulation of cardiac fibroblast profibrotic phenotypes,” *Mol. Biol. Cell*, vol. 28, no. 14, pp. 1871–1882, Jul. 2017, doi: 10.1091/mbc.e17-01-0014.
- [81] A. S. Mao, J.-W. Shin, and D. J. Mooney, “Effects of substrate stiffness and cell-cell contact on mesenchymal stem cell differentiation,” *Biomaterials*, vol. 98, pp. 184–191, Aug. 2016, doi: 10.1016/j.biomaterials.2016.05.004.

- [82] B. Bhana *et al.*, “Influence of substrate stiffness on the phenotype of heart cells,” *Biotechnol. Bioeng.*, p. n/a-n/a, 2010, doi: 10.1002/bit.22647.
- [83] Y. Wang, G. Wang, X. Luo, J. Qiu, and C. Tang, “Substrate stiffness regulates the proliferation, migration, and differentiation of epidermal cells,” *Burns*, vol. 38, no. 3, pp. 414–420, May 2012, doi: 10.1016/j.burns.2011.09.002.
- [84] M. Y. M. Chiang, Y. Yangben, N. J. Lin, J. L. Zhong, and L. Yang, “Relationships among cell morphology, intrinsic cell stiffness and cell–substrate interactions,” *Biomaterials*, vol. 34, no. 38, pp. 9754–9762, Dec. 2013, doi: 10.1016/j.biomaterials.2013.09.014.
- [85] N. D. Leipzig and M. S. Shoichet, “The effect of substrate stiffness on adult neural stem cell behavior,” *Biomaterials*, vol. 30, no. 36, pp. 6867–6878, Dec. 2009, doi: 10.1016/j.biomaterials.2009.09.002.
- [86] J. Huang, X. Peng, C. Xiong, and J. Fang, “Influence of substrate stiffness on cell–substrate interfacial adhesion and spreading: A mechano-chemical coupling model,” *J. Colloid Interface Sci.*, vol. 355, no. 2, pp. 503–508, Mar. 2011, doi: 10.1016/j.jcis.2010.12.055.
- [87] V. Gupta and K. J. Grande-Allen, “Effects of static and cyclic loading in regulating extracellular matrix synthesis by cardiovascular cells,” *Cardiovasc. Res.*, vol. 72, no. 3, pp. 375–383, Dec. 2006, doi: 10.1016/j.cardiores.2006.08.017.
- [88] B. Husse, W. Briest, L. Homagk, G. Isenberg, and M. Gekle, “Cyclical mechanical stretch modulates expression of collagen I and collagen III by PKC and tyrosine kinase in cardiac fibroblasts,” *Am. J. Physiol.-Regul. Integr. Comp. Physiol.*, vol. 293, no. 5, pp. R1898–R1907, Nov. 2007, doi: 10.1152/ajpregu.00804.2006.
- [89] H. Cirka, M. Monterosso, N. Diamantides, J. Favreau, Q. Wen, and K. Billiar, “Active Traction Force Response to Long-Term Cyclic Stretch Is Dependent on Cell Pre-stress,” *Biophys. J.*, vol. 110, no. 8, pp. 1845–1857, Apr. 2016, doi: 10.1016/j.bpj.2016.02.036.
- [90] K. G. Birukov, “Cyclic stretch, reactive oxygen species, and vascular remodeling,” *Antioxid. Amp Redox Signal.*, vol. 11, no. 7, pp. 1651–1668, Jul. 2009.
- [91] N. Morita, S. Takada, and K. Okita, “Influence of stretch and pressure as mechanical stresses on skeletal muscle,” *J. Phys. Fit. Sports Med.*, vol. 2, no. 3, pp. 347–350, 2013, doi: 10.7600/jpfsm.2.347.
- [92] J. Qiu *et al.*, “Biomechanical regulation of vascular smooth muscle cell functions: from *in vitro* to *in vivo* understanding,” *J. R. Soc. Interface*, vol. 11, no. 90, p. 20130852, Jan. 2014, doi: 10.1098/rsif.2013.0852.
- [93] Hye-Sun Yu, Jung-Ju Kim, Hae-Won Kim, M. P. Lewis, and I. Wall, “Impact of mechanical stretch on the cell behaviors of bone and surrounding tissues,” *J. Tissue Eng.*, vol. 7, pp. 1–24, Jan. 2016, doi: 10.1177/2041731415618342.
- [94] M. Chrzanowska-Wodnicka and K. Burridge, “Rho-stimulated contractility drives the formation of stress fibers and focal adhesions,” *J. Cell Biol.*, vol. 133, no. 6, pp. 1403–1415, Jun. 1996, doi: 10.1083/jcb.133.6.1403.
- [95] K. Burridge, K. Fath, T. Kelly, G. Nuckolls, and C. Turner, “Focal Adhesions: Transmembrane Junctions Between the Extracellular Matrix and the Cytoskeleton,” *Annu. Rev. Cell Biol.*, vol. 4, no. 1, pp. 487–525, 1988.

- [96] S. Pellegrin and H. Mellor, “Actin stress fibres,” *J. Cell Sci.*, vol. 120, no. 20, pp. 3491–3499, Oct. 2007, doi: 10.1242/jcs.018473.
- [97] U. Faust *et al.*, “Cyclic Stress at mHz Frequencies Aligns Fibroblasts in Direction of Zero Strain,” *PLoS ONE*, vol. 6, no. 12, p. e28963, Dec. 2011, doi: 10.1371/journal.pone.0028963.
- [98] M. Ghibaudo *et al.*, “Traction forces and rigidity sensing regulate cell functions,” *Soft Matter*, vol. 4, no. 9, p. 1836, 2008, doi: 10.1039/b804103b.
- [99] A. M. Goldyn, P. Kaiser, J. P. Spatz, C. Ballestrem, and R. Kemkemer, “The kinetics of force-induced cell reorganization depend on microtubules and actin,” *Cytoskeleton*, pp. 241–250, 2010, doi: 10.1002/cm.20439.
- [100] H. Wang and E. S. Grood, “Cell Orientation Response to Cyclically Deformed Substrates: Experimental Validation of a Cell Model,” *J. Biomech.*, vol. 28, no. 12, pp. 1543–1552, 1992.
- [101] Civelekoglu, G., Y. Tardy, and J-J. Meister, “Modeling actin filament reorganization in endothelial cells subjected to cyclic stretch,” *Bull. Math. Biol.*, vol. 60, no. 6, pp. 1017–1037, 1998.
- [102] R. De, A. Zemel, and S. A. Safran, “Dynamics of cell orientation,” *Nat. Phys.*, vol. 3, no. 9, pp. 655–659, Sep. 2007, doi: 10.1038/nphys680.
- [103] H.-J. Hsu, C.-F. Lee, and R. Kaunas, “A Dynamic Stochastic Model of Frequency-Dependent Stress Fiber Alignment Induced by Cyclic Stretch,” *PLoS ONE*, vol. 4, no. 3, p. e4853, Mar. 2009, doi: 10.1371/journal.pone.0004853.
- [104] R. Kaunas and H.-J. Hsu, “A kinematic model of stretch-induced stress fiber turnover and reorientation,” *J. Theor. Biol.*, vol. 257, no. 2, pp. 320–330, Mar. 2009, doi: 10.1016/j.jtbi.2008.11.024.
- [105] C. Obbink-Huizer, C. W. J. Oomens, S. Loerakker, J. Foolen, C. V. C. Bouten, and F. P. T. Baaijens, “Computational model predicts cell orientation in response to a range of mechanical stimuli,” *Biomech. Model. Mechanobiol.*, vol. 13, no. 1, pp. 227–236, Jan. 2014, doi: 10.1007/s10237-013-0501-4.
- [106] J. Qian, H. Liu, Y. Lin, W. Chen, and H. Gao, “A Mechanochemical Model of Cell Reorientation on Substrates under Cyclic Stretch,” *PLoS ONE*, vol. 8, no. 6, p. e65864, Jun. 2013, doi: 10.1371/journal.pone.0065864.
- [107] J. H.-C. Wang, “Substrate Deformation Determines Actin Cytoskeleton Reorganization: A Mathematical Modeling and Experimental Study,” *J. Theor. Biol.*, vol. 202, no. 1, pp. 33–41, Jan. 2000, doi: 10.1006/jtbi.1999.1035.
- [108] Palchesko, R. N., Zhang, L., Sun, Y., & Feinberg, A. W., “Development of polydimethylsiloxane substrates with tunable elastic modulus to study cell mechanobiology in muscle and nerve,” *PloS ONE*, no. 7, p. 12, 2012.
- [109] Boudaoud, A., Burian, A., Borowska-Wykręć, D., Uyttewaal, M., Wrzalik, R., Kwiatkowska, D., & Hamant, O., “FibrilTool, an ImageJ plug-in to quantify fibrillar structures in raw microscopy images,” *Nat. Protoc.*, vol. 9, no. 2, pp. 457–463, Feb. 2014.
- [110] R. G. J. Miller, *Simultaneous Statistical Inference*, 2nd ed. New York: Springer-Verlag, 1981.

- [111] A. Livne, E. Bouchbinder, and B. Geiger, “Cell reorientation under cyclic stretching,” *Nat. Commun.*, vol. 5, no. 1, p. 3938, May 2014, doi: 10.1038/ncomms4938.
- [112] R. Kaunas, S. Usami, and S. Chien, “Regulation of stretch-induced JNK activation by stress fiber orientation,” *Cell. Signal.*, vol. 18, no. 11, pp. 1924–1931, Nov. 2006, doi: 10.1016/j.cellsig.2006.02.008.
- [113] M. M. Nava *et al.*, “Heterochromatin-Driven Nuclear Softening Protects the Genome against Mechanical Stress-Induced Damage,” *Cell*, vol. 181, no. 4, pp. 800–817.e22, May 2020, doi: 10.1016/j.cell.2020.03.052.
- [114] A. Tondon and R. Kaunas, “The Direction of Stretch-Induced Cell and Stress Fiber Orientation Depends on Collagen Matrix Stress,” *PLoS ONE*, vol. 9, no. 2, p. e89592, Feb. 2014, doi: 10.1371/journal.pone.0089592.
- [115] M. Kovács, J. Tóth, C. Hetényi, A. Málnási-Csizmadia, and J. R. Sellers, “Mechanism of blebbistatin inhibition of myosin II,” *J. Biol. Chem.*, vol. 279, no. 34, pp. 35557–35563, Aug. 2004, doi: 10.1074/jbc.M405319200.
- [116] T. R. Kimball, W. A. Mays, P. R. Khoury, R. Mallie, and R. P. Claytor, “Echocardiography determination of left ventricular preload, afterload, and contractility during and after exercise,” *J. Pediatr.*, vol. 122, no. 6, pp. S89–S94, Jun. 1993, doi: 10.1016/S0022-3476(09)90050-6.
- [117] K. R. Hutchinson *et al.*, “Temporal pattern of left ventricular structural and functional remodeling following reversal of volume overload heart failure,” *J. Appl. Physiol.*, vol. 111, no. 6, pp. 1778–1788, Dec. 2011, doi: 10.1152/jappphysiol.00691.2011.
- [118] R. C. Childers, “The Role of Tissue Modulus and Cardiac Fibroblast Phenotype in Volume Overload Induced Heart Failure.” PhD Dissertation, The Ohio State University, 2016.
- [119] R. Childers, A. Trask, J. Liu, P. Lucchesi, and K. Gooch, “Paired PV Loop Analysis and Biaxial Mechanical Testing Characterize Differences in Left Ventricular Tissue Stiffness of Volume Overload and Angiotensin-Induced Pressure Overload Hearts,” *J. Biomech. Eng.*, Mar. 2021, doi: 10.1115/1.4050541.
- [120] C. A. Souders, S. L. K. Bowers, and T. A. Baudino, “Cardiac Fibroblast: The Renaissance Cell,” *Circ. Res.*, vol. 105, no. 12, pp. 1164–1176, Dec. 2009, doi: 10.1161/CIRCRESAHA.109.209809.
- [121] J. J. Tomasek, G. Gabbiani, B. Hinz, C. Chaponnier, and R. A. Brown, “Myofibroblasts and mechano-regulation of connective tissue remodelling,” *Nat. Rev. Mol. Cell Biol.*, vol. 3, no. 5, pp. 349–363, May 2002, doi: 10.1038/nrm809.
- [122] R. C. Childers, I. Sunyecz, T. A. West, M. J. Cismowski, P. A. Lucchesi, and K. J. Gooch, “Role of the cytoskeleton in the development of a hypofibrotic cardiac fibroblast phenotype in volume overload heart failure,” *Am. J. Physiol.-Heart Circ. Physiol.*, vol. 316, no. 3, pp. H596–H608, Mar. 2019, doi: 10.1152/ajpheart.00095.2018.
- [123] P.-J. Wipff, D. B. Rifkin, J.-J. Meister, and B. Hinz, “Myofibroblast contraction activates latent TGF- β 1 from the extracellular matrix,” *J. Cell Biol.*, vol. 179, no. 6, pp. 1311–1323, Dec. 2007, doi: 10.1083/jcb.200704042.

- [124] S. van Putten, Y. Shafieyan, and B. Hinz, "Mechanical control of cardiac myofibroblasts," *J. Mol. Cell. Cardiol.*, vol. 93, pp. 133–142, Apr. 2016, doi: 10.1016/j.yjmcc.2015.11.025.
- [125] Y. Guo *et al.*, "Extracellular Matrix of Mechanically Stretched Cardiac Fibroblasts Improves Viability and Metabolic Activity of Ventricular Cells," *Int. J. Med. Sci.*, vol. 10, no. 13, pp. 1837–1845, 2013, doi: 10.7150/ijms.6786.
- [126] J. Wang, H. Chen, A. Seth, and C. A. McCulloch, "Mechanical force regulation of myofibroblast differentiation in cardiac fibroblasts," *Am. J. Physiol.-Heart Circ. Physiol.*, vol. 285, no. 5, pp. H1871–H1881, Nov. 2003, doi: 10.1152/ajpheart.00387.2003.
- [127] G. E. Lindahl *et al.*, "Activation of Fibroblast Procollagen α 1(I) Transcription by Mechanical Strain Is Transforming Growth Factor- β -dependent and Involves Increased Binding of CCAAT-binding Factor (CBF/NF-Y) at the Proximal Promoter," *J. Biol. Chem.*, vol. 277, no. 8, pp. 6153–6161, Feb. 2002, doi: 10.1074/jbc.M108966200.
- [128] O. A. Smiseth, H. Torp, A. Opdahl, K. H. Haugaa, and S. Urheim, "Myocardial strain imaging: how useful is it in clinical decision making?," *Eur. Heart J.*, vol. 37, no. 15, pp. 1196–1207, Apr. 2016, doi: 10.1093/eurheartj/ehv529.
- [129] M. F. Berry *et al.*, "Mesenchymal stem cell injection after myocardial infarction improves myocardial compliance," vol. 290, p. 8, 2006.
- [130] A. J. Engler *et al.*, "Embryonic cardiomyocytes beat best on a matrix with heart-like elasticity: scar-like rigidity inhibits beating," *J. Cell Sci.*, vol. 121, no. 22, pp. 3794–3802, Nov. 2008, doi: 10.1242/jcs.029678.
- [131] J. M. Goffin, P. Pittet, G. Csucs, J. W. Lussi, J.-J. Meister, and B. Hinz, "Focal adhesion size controls tension-dependent recruitment of α -smooth muscle actin to stress fibers," *J. Cell Biol.*, vol. 172, no. 2, pp. 259–268, Jan. 2006, doi: 10.1083/jcb.200506179.
- [132] J. F. Williams and R. D. Potter, "Passive stiffness of pressure-induced hypertrophied cat myocardium.," *Circ. Res.*, vol. 49, no. 1, pp. 211–215, Jul. 1981, doi: 10.1161/01.RES.49.1.211.
- [133] A. S. Waxman, B. G. Kornreich, R. A. Gould, N. Sydney Moïse, and J. T. Butcher, "Interactions between TGF β 1 and cyclic strain in modulation of myofibroblastic differentiation of canine mitral valve interstitial cells in 3D culture," *J. Vet. Cardiol.*, vol. 14, no. 1, pp. 211–221, Mar. 2012, doi: 10.1016/j.jvc.2012.02.006.
- [134] R. A. Gould *et al.*, "Cyclic strain anisotropy regulates valvular interstitial cell phenotype and tissue remodeling in three-dimensional culture," *Acta Biomater.*, vol. 8, no. 5, pp. 1710–1719, May 2012, doi: 10.1016/j.actbio.2012.01.006.
- [135] M. Hori and H. Okamoto, "Heart rate as a target of treatment of chronic heart failure," *J. Cardiol.*, vol. 60, no. 2, pp. 86–90, Aug. 2012, doi: 10.1016/j.jjcc.2012.06.013.
- [136] P. Palatini and S. Julius, "Elevated Heart Rate: A Major Risk Factor for Cardiovascular Disease," *Clin. Exp. Hypertens.*, vol. 26, no. 7–8, pp. 637–644, Jan. 2004, doi: 10.1081/CEH-200031959.

- [137] D. Nanchen *et al.*, “Resting Heart Rate and the Risk of Heart Failure in Healthy Adults: The Rotterdam Study,” *Circ. Heart Fail.*, vol. 6, no. 3, pp. 403–410, May 2013, doi: 10.1161/CIRCHEARTFAILURE.112.000171.
- [138] N. Boyle, “A Clinical Review of Ventricular Arrhythmias in Patients with Congestive Heart Failure,” *EMJ Cardiol.*, Sep. 2019, doi: 10.33590/emjcardiol/18-00058R1.
- [139] P. Santangeli, J. E. Rame, E. Y. Birati, and F. E. Marchlinski, “Management of Ventricular Arrhythmias in Patients With Advanced Heart Failure,” *J. Am. Coll. Cardiol.*, vol. 69, no. 14, pp. 1842–1860, Apr. 2017, doi: 10.1016/j.jacc.2017.01.047.
- [140] J.-H. Chung *et al.*, “Etiology-dependent impairment of relaxation kinetics in right ventricular end-stage failing human myocardium,” *J. Mol. Cell. Cardiol.*, vol. 121, pp. 81–93, Aug. 2018, doi: 10.1016/j.yjmcc.2018.07.005.
- [141] A. Tondon, H.-J. Hsu, and R. Kaunas, “Dependence of cyclic stretch-induced stress fiber reorientation on stretch waveform,” *J. Biomech.*, vol. 45, no. 5, pp. 728–735, Mar. 2012, doi: 10.1016/j.jbiomech.2011.11.012.
- [142] C. E. Chan and D. J. Odde, “Traction Dynamics of Filopodia on Compliant Substrates,” *Science*, vol. 322, no. 5908, pp. 1687–1691, Dec. 2008, doi: 10.1126/science.1163595.
- [143] Z. Li, J. A. Dranoff, E. P. Chan, M. Uemura, J. Sévigny, and R. G. Wells, “Transforming growth factor- β and substrate stiffness regulate portal fibroblast activation in culture,” *Hepatology*, vol. 46, no. 4, pp. 1246–1256, Oct. 2007, doi: 10.1002/hep.21792.
- [144] J. Solon, I. Levental, K. Sengupta, P. C. Georges, and P. A. Janmey, “Fibroblast Adaptation and Stiffness Matching to Soft Elastic Substrates,” *Biophys. J.*, vol. 93, no. 12, pp. 4453–4461, Dec. 2007, doi: 10.1529/biophysj.106.101386.
- [145] Z. Gong *et al.*, “Matching material and cellular timescales maximizes cell spreading on viscoelastic substrates,” *Proc. Natl. Acad. Sci.*, vol. 115, no. 12, pp. E2686–E2695, Mar. 2018, doi: 10.1073/pnas.1716620115.
- [146] S. Balasubramanian *et al.*, “ β 3 Integrin in Cardiac Fibroblast Is Critical for Extracellular Matrix Accumulation during Pressure Overload Hypertrophy in Mouse,” *PLoS ONE*, vol. 7, no. 9, p. e45076, Sep. 2012, doi: 10.1371/journal.pone.0045076.
- [147] J.-J. Santiago *et al.*, “Cardiac fibroblast to myofibroblast differentiation in vivo and in vitro: Expression of focal adhesion components in neonatal and adult rat ventricular myofibroblasts,” *Dev. Dyn.*, vol. 239, no. 6, pp. 1573–1584, Jun. 2010, doi: 10.1002/dvdy.22280.
- [148] A. M. Manso *et al.*, “Cardiac fibroblasts require focal adhesion kinase for normal proliferation and migration,” *Am. J. Physiol.-Heart Circ. Physiol.*, vol. 296, no. 3, pp. H627–H638, Mar. 2009, doi: 10.1152/ajpheart.00444.2008.
- [149] J. Zhang *et al.*, “Targeted inhibition of Focal Adhesion Kinase Attenuates Cardiac Fibrosis and Preserves Heart Function in Adverse Cardiac Remodeling,” *Sci. Rep.*, vol. 7, no. 1, p. 43146, Mar. 2017, doi: 10.1038/srep43146.

Appendix A: Adapted motor-clutch model MATLAB function

Function used to simulate cyclic stretch in adapted motor-clutch model.

```

for i = 1:length(t)-1
    % update clutch binding
    clutch_state(:,1) = clutch_state(:,2);
    xi(:,1) = xi(:,2);

    r_on = kon*(1-clutch_state(:,1));
    ion = find(rand(nc,1)<r_on*dt); % Find unbound clutches that have a
    randomly associated tag less than 0.01

    r_off = koff_star.*clutch_state(:,1);
    ioff = find(rand(nc,1)<r_off*dt);

    clutch_state(ion,2) = 1;      % update states
    clutch_state(ioff,2) = 0;

    % calculate filament length
    vpoly = vpmx*((lmax-L)/lmax); % Variable polymerization rate
    L = L + ((vflm+vpoly) * dt);
    %L_all(i) = L;

    % Set anchor position and calculate substrate position
    if non == 0 && any(clutch_state(:,2)) == 1
        X = L/(0.5*(1-cos(2*pi*t(i)/pd))*(rt-1)
        vfilament= vu;
        koff_star(1,:) = koff;
        Fclutch_total = 0;
    elseif non == 0
        vfilament= vu;
        Fclutch_total = 0;
    elseif non > 0
        %xanc(i) = X*((1-cos(2*pi*t(i)/pd))/2*(rt-1)+1);
        xanc = X*((1-cos(2*pi*t(i)/pd))/2*(rt-1)+1);

        % calculate xsub
        xeng = xi(clutch_state(:,1)==1,1);
        %xsub(i+1) = (kclutch*sum(xeng)+ksub*xanc(i))/(ksub +
kclutch*length(xeng));

```

```

        xsub = (kclutch*sum(xeng)+ksub*xanc)/(ksub +
kclutch*length(xeng));

        Fclutch = kclutch*(xi(:,1)-xsub);
        Fclutch_total = sum(Fclutch);           % for plotting, analysis
        koff_star = koff*exp(abs(Fclutch/Fb)); % Bound clutch off-rate
including only slip bond behavior

        % calculate velocity
        vfilament = vu*(1 - ksub*(xsub-xanc)/Fstall);
end

        % update clutch position
        xi(clutch_state(:,1)==1,2) = xi(clutch_state(:,1)==1,1) +
vfilament*dt;
        %xi(clutch_state(:,i)==0,i+1) = xsub(i);
        xi(clutch_state(:,1)==0,2) = xsub;
end

```